UNIVERSIDADE FEDERAL DE MINAS GERAIS

Curso de Pós-Graduação em Engenharia Metalúrgica, Materiais e de Minas

Leandro Augusto Viana Teixeira

SULFATAÇÃO E USTULAÇÃO SELETIVA DE ELEMENTOS DE TERRAS RARAS CONTIDOS EM MINÉRIOS COMPLEXOS

Orientadora: Professora Virginia Sampaio Teixeira Ciminelli

Belo Horizonte

2020

Leandro Augusto Viana Teixeira

SULFATAÇÃO E USTULAÇÃO SELETIVA DE ELEMENTOS DE TERRAS RARAS CONTIDOS EM MINÉRIOS COMPLEXOS

SULFATION AND SELECTIVE ROASTING OF RARE EARTH ELEMENTS IN COMPLEX, IRON-RICH ORES

Tese de doutorado apresentada ao Curso de Pós-Graduação em Engenharia Metalúrgica, Materiais e de Minas da Universidade Federal de Minas Gerais como requisito parcial para obtenção do grau de Doutor em Engenharia Metalúrgica, Materiais e de Minas.

Área de concentração: Tecnologia Mineral

Orientadora: Profª Virginia Sampaio Teixeira Ciminelli

Belo Horizonte

2020

T266s

Teixeira, Leandro Augusto Viana.
Sulfatação e ustulação seletiva de elementos de terras raras contidos em minérios complexos ricos em ferro [recurso eletrônico] = Sulfation and selective roasting of rare Earth elements in complex, Iron-rich Ores / Leandro Augusto Viana Teixeira. – 2020.
1 recurso online (xx, 117 f.: il., color.): pdf.

Orientadora: Virgínia Sampaio Teixeira Ciminelli.

Tese (doutorado) - Universidade Federal de Minas Gerais, Escola de Engenharia.

Anexo: f. 108-117.
Inclui bibliografia.

Exigências do sistema: Adobe Acrobat Reader.

1. Engenharia de Minas - Teses. 2. Tecnologia mineral - Teses. 3. Minérios – Teses. 4. Pirometalurgia – Teses. 5. Separação (Tecnologia) Teses. 6. Terras Raras – Teses. I. Ciminelli, V.S.T. (Virgínia Sampaio Teixeira). II. Universidade Federal de Minas Gerais. Escola de Engenharia. III. Título.

CDU: 622(043)

Ficha catalográfica elaborada pela Bibliotecária Letícia Alves Vieira - CRB-6/2337
Biblioteca Prof. Mário Werneck - Escola de Engenharia da UFMG

UNIVERSIDADE FEDERAL DE MINAS GERAIS
ESCOLA DE ENGENHARIA
Programa de Pós-Graduação em Engenharia Metalúrgica, Materiais e de Minas

PPGEM

Tese intitulada **"Sulfation and Selective Roasting of Rare Earth Elements in Complex Ores"**, área de concentração: Tecnologia Mineral, apresentada pelo candidato **Leandro Augusto Viana Teixeira**, para obtenção do grau de Doutor em Engenharia Metalúrgica, Materiais e de Minas, aprovada pela comissão examinadora constituída pelos seguintes membros:

Profª Virginia Sampaio Teixeira Ciminelli
Orientadora - PhD (UFMG)

Prof. Daniel Majuste
Dr. (UFMG)

Prof. Maurício Covcevich Bagatini
Dr. (UFMG)

Prof. Kazuki Morita
Dr. (The University of Tokyo)

Prof. Takeshi Yoshikawa
Dr. (The University of Tokyo)

Prof. Rodrigo Lambert Oréfice
Coordenador do Programa de Pós-Graduação em Engenharia Metalúrgica, Materiais e de Minas/UFMG

Belo Horizonte, 26 de junho de 2020

Dedication

Dedicated to my parents, Mary and José Eustáquio, for the constant encouragement in pursuing further education. It is also dedicated to professor Kazuki Morita, for believing in a foreign student; incentivizing him to do better; teaching how exciting science can be and for being a guide, inside and outside the university walls.

AGRADECIMENTOS

Este trabalho só foi possível com a ajuda de vários colegas, amigos e família. Gostaria de agradecer a minha esposa Natália, por compreender as dificuldades de realizar um doutorado em paralelo ao trabalho, por vezes muito conturbado. Obrigado pela paciência e carinho. Agradeço ao meu pai, José Eustáquio que, por sempre ter acreditado que o aprendizado é contínuo e que ser mestre e doutor seriam essenciais na minha vida, me transmitiu o seu apreço pelo conhecimento e sua relevância na sociedade. A minha mãe Mary e irmã Lílian que, apesar de não participarem diretamente do processo, sempre me suportaram com seu carinho incondicional.

Um agradecimento muito especial ao Professor Daniel Majuste e a minha orientadora Professora Virgínia Ciminelli. Esse trabalho poderia ter tomado uma direção bem diferente, mas foi graças a vocês que acreditaram no meu potencial e na relevância do tema que conseguimos produzir um bom trabalho. O importante para mim não era apenas fazer um doutorado, mas estudar com profissionais que pudessem me servir de inspiração e que tivessem um ambiente de produção tão bom quanto em qualquer lugar do exterior. A excelência de vocês permitiu isso; saibam que possuem meu agradecimento, admiração e apreço. À Professora Virgínia, meu obrigado pelas longas sessões de discussão, pelo alto rigor exigido no trabalho e por ser um exemplo de profissionalismo, uma professora que consegue unir excelência na educação, na pesquisa, na parceria com a indústria e com a sociedade. Ao Professor Daniel, obrigado pelas várias discussões de corredor e laboratório. A energia e empolgação com que fala da pesquisa inspira todos ao seu redor.

Obrigado as gestoras da Vale Keila Gonçalves e Patrice Mazzoni por permitirem e suportarem esse trabalho. Um obrigado muito especial a Cássia Souza e Ruberlan Silva. Cássia foi grande incentivadora desse trabalho e forneceu todos os recursos necessários para que os estudos acontecessem. Obrigado Ruberlan, pela parceria nos trabalhos e pelo seu auxílio nos momentos de dificuldade. A sua amizade, parceria e dedicação ao trabalho são dignos de reconhecimento e admiração.

Meu muito obrigado a todos do laboratório de processos do Centro de Desenvolvimento Mineral da Vale, em Santa Luzia, liderados pelo Wagner Soares. Os resultados e conclusões desse estudo só foram possíveis graças ao

suporte, zelo e altíssima qualidade nos testes realizados por vocês. Agradeço também a todos do laboratório químico, liderados pela Luzia Chaves. Um centro de referência nacional e internacional em análises minerais, que possibilitaram resultados precisos mesmo em químicas tão desafiadoras, como das Terras Raras. Obrigado também ao geólogo Rogério Kwitko, por sua ajuda nas mais diversas análises mineralógicas. Agradeço também aos colegas do Centro de Tecnologia de Ferrosos da Vale, a Doutora Valdirene Resende e o Doutor Fabrício Parreira. Doutora Valdirene, por seu apoio em análises bem especiais de mineralogia e termogravimetria. Doutor Fabrício, por sua liderança junto ao laboratório metalúrgico, permitindo que os testes sob atmosfera redutora pudessem ser realizados. Meu agradecimento especial a engenheira Maria Carolina Dona Peterle, por sua ajuda incondicional na formatação final do documento. Obrigado pela paciência e disposição.

Agradeço ao Programa de Pós-Graduação em Engenharia Metalúrgica, Materiais e de Minas, às agências financiadoras: CNPq, INCT-Acqua, Fapemig, e CAPES pelo suporte e apoio na realização de pesquisa no país.

RESUMO

Os elementos de terras raras (ETR) são insumos essenciais utilizados em várias tecnologias contemporâneas, principalmente de equipamentos relacionados à tecnologia verde. O mineral monazita é a principal fonte de ETR no Brasil, mas geralmente contêm impurezas que consomem grandes quantidades de ácidos, como o ferro e fosfatos, podendo também conter níveis proibitivos de elementos radioativos (e. g. tório). Este trabalho discute os fundamentos de uma rota de processo seletivo para extração de terras raras de minérios monazíticos com alto teor de ferro. O processo consiste na sulfatação por meio de ácido sulfúrico concentrado e a ustulação à elevadas temperaturas. Foram obtidas extrações de terras raras de até 80%, enquanto extrações de ferro e tório permaneceram inferiores a 1%, sendo o consumo de ácido abaixo de 0,34 kg de ácido sulfúrico por kg de minério. Houve ótima concordância entre a simulação termodinâmica e os resultados de TGA obtidos para sulfatos de ferro e lantânio, que indicam a decomposição de sulfato. Os resultados também mostram que o sulfato de lantânio se decompõe em duas etapas sob atmosfera oxidante, havendo a formação de $La_2O_2SO_4$ como um composto intermediário, fato que não pode ser previsto por avaliação termodinâmica. Observou-se uma queda de extração de ETR a 800°C, apesar da previsão baseada nos resultados de TGA e avaliação termodinâmica indicarem que essa queda devesse ocorrer a 1100°C. Esse comportamento foi atribuído a conversão de sulfatos de ETR em fosfatos. Foi demonstrado que essa conversão depende do excesso de fósforo presente no sistema em compostos menos estáveis que a monazita. Propõe-se que a presença de altas pressões parciais de P_2O_5 no sistema promova a conversão dos sulfatos de ETR em polifosfatos insolúveis - $ETR(PO_3)_3$. O ácido fosfórico, por sua vez, levou à formação de compostos do tipo monazita. A reação por meio gás-sólido é o modelo mais adequado devido ao fácil acesso da fase gasosa às partículas de sulfato de ETR, causando assim a queda drástica na extração de ETR observada a 800°C. Observou-se que o emprego de atmosfera redutora durante a ustulação apresenta grande efeito na temperatura ótima de extração, sendo reduzida de 700°C (ar) para 400°C, sob atmosfera redutora. As condições redutoras não alteraram a extração de ETR (80%), favoreceu a seletividade frente ao tório, mas não houve mudança com relação ao ferro. Outra opção do pré-tratamento com monazita é o processo de cloração, no qual o $ETRPO_4$ é transformado em $ETRCl_3$ solúvel. Não foi confirmada a reação de dupla troca entre sulfato (Fe, Mg e Ca) e fosfato (Nd, Ce) e entre $MgCl_2$ e os fosfatos de Ce e Nd em atmosfera inerte. Entretanto, foi confirmada a reação entre os fosfatos e $MgCl_2$ sob atmosfera oxidante (ar). Os produtos foram CeO_2 e NdOCl.

ABSTRACT

Rare earth elements (REE) are essential for the manufacture of modern life products and the increasing applications of green technologies. Monazite-type ores, the predominant REE carrying in Brazil, often occur in association with high acid consumption impurities, such as iron, phosphates, and prohibitive levels of radioactive elements (e.g., thorium). These features result in high operational costs of the extraction units, thus becoming a barrier to making the mineral deposit economically feasible. This work discusses the fundamentals of a selective process route for rare earth extraction from monazite ores with high iron content. The process involves sulfation by addition of concentrated sulfuric acid and roasting at high temperatures. Rare earth extractions as high as 80% were achieved, while iron and thorium extractions were lower than 1%, and acid consumption lower than 0.34 kg of sulfuric acid per kg of ore. There was very good agreement between thermodynamic simulation and TGA results for the decomposition of iron and lanthanum sulfates. Lanthanum sulfate decomposed in a two-step process, likely forming $La_2O_2SO_4$ as an intermediate compound, which could not be predicted from thermodynamics. The expected drop in REE extraction at 1100°C was seen at 800°C. This behavior was attributed to the conversion of REE sulfates into phosphates, by the excess phosphorus made available from compounds less stable than monazite, such as monocalcium phosphates and phosphoric acid generated by the addition of sulfuric acid. The presence of high partial pressures of P_2O_5 in the system reconverted REE sulfates into insoluble REE polyphosphates – $REE(PO_3)_3$. Phosphoric acid in turn led to the formation of monazite-like compounds. The gas-solid mechanism was considered the most suitable due to the easier access of the gas phase to the REE sulfate particles, thus drastically decreasing the REE extraction at 800°C. It was observed that the atmosphere within the furnace has a significant effect on the optimal roasting temperature to achieve maximum REE extraction. This temperature decreased from 700°C (air) to 400°C, under reducing atmosphere. The reducing conditions did not affect the REE extraction (80% in both cases) and favored selectivity against thorium. There was no significant impact on iron extraction. Another option of pre-treatment with monazite is the chlorination process, in which $REEPO_4$ is transformed into soluble $REECl_3$. The double exchange reaction between sulfate (Fe, Mg and Ca) and phosphate (Nd, Ce) and between $MgCl_2$ and the phosphates of Ce and Nd in an inert atmosphere has not been confirmed. The reaction between phosphates and $MgCl_2$ took place under an oxidizing atmosphere (air). The products were CeO_2 and NdOCl.

LIST OF FIGURES

LIST OF TABLES

LIST OF ACRONYMS

BSE: Backscattered Electrons

CAT: Computerized Axial Tomography

CAPEX: Capital Expenditure

DBS: Duplicates, Blanks and Standards

DSC: Differential Scanning Calorimetry

DTA: Differential Thermal Analyses

EDS: Energy Dispersive X-ray Spectrometry

EPMA: Electron Probe Micro Analyzer

ETR: Elementos de Terras Raras

FCC: Fluid Crack Catalyst

GGG: Gadolinium Gallium Garnet

HDD: Hard Disk Drive

HREE: Heavy Rare Earth Element

HREO: Heavy Rare Earth Oxide

ICDD: Internacional Center for Diffraction Data

ICP: Inductively Coupled Plasma

ICP-MS: Inductively Coupled Plasma Mass Spectrometry

ICP-OES: Inductively Coupled Plasma Optical Emission Spectrometry

LED: Light Emitting Diode

LREE: Light Rare Earth Elements

LREO: Light Rare Earth Oxides

MRI: Magnetic Resonance Image

ME: Mean Error

NMR: Nuclear Magnet Resonance

OPEX: Operacional Expenditures

OTR: Óxido de Terras Raras

PET: Positron Emission Tomography

QEMSCAN: Quantitative Evaluation of Minerals by Scanning Electron microscopy

QMS: Quadrupole Mass Spectroscopy

REE: Rare Earth Elements

REO: Rare Earth Oxides

SEM: Scanning Electron Microscope

SX: Solvent Extraction

TGA: Thermal Gravimetric Analysis

TG-DSC: Thermogravimetry - Differential Scanning Calorimetry

TG-DTA: Termogravimetria - Análise Térmica Diferencial

TR: Terras Raras

UV: Ultra Violet

XRD: X-ray Diffraction

YAG: Yttrium Aluminum Garnet

SUMMARY

1 CONSIDERAÇÕES INICIAIS

Os elementos de terras raras (ETR) podem ser definidos como os 15 elementos que compõem a série dos lantanídeos (compreendendo desde o lantânio até o lutécio) acrescidos do ítrio e o escândio. Apesar dos dois últimos não pertencerem a série de lantanídeos, estes são considerados ETR devido à similaridade do comportamento químico, no caso do (Y) e coocorrência natural (Sc). As principais aplicações e direcionadores de consumo de terras raras são: catálise (principalmente para FCC, *Fluid Crack Catalist*), a indústria petrolífera, a produção de imãs permanentes, a indústria eletrônica e de energia eólica, material de polimento para a indústria eletrônica (vidros e monitores) e a composição de catodos em baterias recarregáveis (Roskill, 2019).

Desde os anos 90, a China é o maior produtor e exportador de REE do mundo, sendo responsável por mais de 90% da produção mundial. O aumento da produção de ETR na China está associado a grandes danos ambientais e, juntamente com questões de contrabando de ETR, levou a China a lançar uma série de políticas rigorosas para regular a mineração de terras raras e atividades comerciais relacionadas. Entre estas estão o licenciamento de produção e exportação, o sistema de cotas, a introdução de imposto sobre recursos e taxas de exportação. Essas ações levaram ao aumento nos preços que atingiram o seu pico em 2011 e reduziram em mais da metade a produção ilegal de terras raras em 2016 (Roskill, 2019). O novo cenário econômico atraiu o interesse da indústria em estabelecer fontes alternativas de abastecimento, o que levou à descoberta de vários novos depósitos e gerou centenas de projetos minerais em todo o mundo. Também resultou em intensa pesquisa tecnológica em novas formas alternativas para o processamento e separação de terras raras. Os preços começaram a ceder em 2015 e agora estão no nível anterior ao da implementação do sistema de cotas, exceto no caso do neodímio e do praseodímio os quais, apoiados pelo desenvolvimento de tecnologias verdes, ainda apresentam preços elevados.

Os ETR são mais abundantes em rochas graníticas do que em variedades ígneas básicas, embora as concentrações mais altas sejam encontradas em rochas ígneas alcalinas e carbonatitos. Os ETR são encontrados em mais de 160 minerais, mas 95% de todos os recursos de terras raras do mundo ocorrem em apenas quatro minerais: bastnaesite (Ce, La, Y) (CO_3) F, monazita (Ce,

Argilas de La, Pr, Nd, Th, Y) PO_4, xenotima YPO_4 e argilas iônicas. Bastnaesite e monazita são minerais ricos em ETR leves, enquanto xenomita e argilas de adsorção iônicas são mais ricas em ETR pesadas. O recente aumento nos preços mencionados no parágrafo anterior, levou as mineradoras juniores a iniciarem vários projetos de ETR ao redor de todo o mundo, na sua grande maioria direcionados ao aproveitamento de depósitos contendo monazitas e bastenasitas. As rotas de tratamento e extração de minérios de terras raras são compostas basicamente de quatro grandes estágios: concentração física, extração, purificação e separação, sendo a etapa de extração geralmente feita por lixiviação do concentrado (Gupta and Krishnamurthy, 2005). As características dos minérios são um fator importante na definição da rota de processo.

O Brasil abriga quantidades significativas de ETR em seu território, quase 75% destes presentes como monazitas. Os principais depósitos monazíticos estão localizados no sudeste do país, muitos dos quais são depósitos ígneos que sofreram forte intemperismo. Devido a essas características, a monazita encontra-se finamente disseminada no minério e frequentemente associada a minerais de ferro. A disseminação dificulta os processos de concentração física (como flotação, concentração magnética e gravítica). A etapa de extração das monazitas é geralmente realizada com a utilização de ácido sulfúrico (Zhang et al, 2015). Entretanto, a presença de grandes quantidades de ferro e álcalis leva a um aumento no consumo desse ácido, aumentando a complexidade dos licores obtidos após a etapa de extração e os custos de produção. Existem outros elementos que estão frequentemente associados às monazitas, como tório e urânio, assim como os seus decaimentos radioativos. Esses elementos não podem acompanhar as terras raras na forma de produto final, precisando ser removidos do processo. Entretanto, essa remoção precisa ser cuidadosa, pois se forem concentrados durante essa etapa, trarão grandes problemas de disposição ou armazenamento. A monazita ocorre frequentemente de forma associada a outros minerais fosfatados, como a apatita. O efeito do fosfato na extração dos elementos terras raras ainda é pouco explorado.

O presente trabalho propoem a introdução de uma etapa de ustulação previamente à etapa de lixiviação (ambas dentro do estágio de extração) com o

intuito de criar condições para uma lixiviação mais seletiva dos ETR frente ao ferro e ao tório. A maior seletividade irá resultar na obtenção de um licor mais puro para alimentar a etapa de purificação, reduzindo gastos com reagentes e melhorando a recuperação de ETR no processo. Espera-se que os conhecimentos gerados possam contribuir para melhorar a viabilidade econômica de novos projetos para a extração e produção de ETR no Brasil e no mundo.

O texto está dividido em oito capítulos. O presente capítulo corresponde a uma breve introdução, em língua portuguesa, contextualizando o trabalho realizado. O segundo capítulo discute de forma mais abrangente as principais aplicações dos elementos de terras raras, o mercado, as ocorrências naturais além de uma breve descrição do processo de extração, purificação e separação desses elementos. Este capítulo também abrigados principais objetivos desse estudo, assim como a relevância do mesmo para o meio acadêmico, industrial e sociedade são também apresentados.

O terceiro capítulo investiga um novo processo de ustulação seletiva de terras raras, baseado na suposta decomposição seletiva do sulfato de terras raras frente à decomposição dos sulfatos de ferro e tório. As suposições baseadas em simulações termodinâmicas do sistema são confrontadas com dados de experimentos utilizando sulfato de lantânio.

O quarto capítulo aprofunda o entendimento do mecanismo envolvido na seletividade identificada nos trabalhos realizados com a decomposição de sulfatos. Neste capítulo, o efeito da presença de elevadas concentrações de fósforo é estudado e um mecanismo é proposto para explicar sua influência no processo de ustulação seletiva. Simulações termodinâmicas são novamente o guia para o entendimento do sistema.

O quinto capítulo se propõe a estudar o efeito da atmosfera controlada na ustulação seletiva, especificamente, o efeito de uma atmosfera redutora na temperatura de decomposição dos ETR e das principais impurezas presentes no sistema. O impacto desse novo processo na solubilidade dos elementos alvo em lixiviação aquosa também é avaliado.

O sexto capítulo avalia a possibilidade de realizar a ustulação seletiva sem a necessidade de uma etapa anterior de sulfatação. Ao invés disso, a dupla troca

entre fosfatos e sulfatos é estudada. Na mesma linha de investigação, a possibilidade de se realizar a dupla troca entre fosfatos e cloretos também é abordada, com a intenção de produção de cloretos de terras raras solúveis.

O sétimo capítulo abriga as conclusões gerais, os pontos mais relevantes obtidos do estudo, a lista de publicações geradas desse estudo e outras publicações relacionadas. O oitavo capítulo compreende o fechamento do trabalho, com as conclusões obtidas.

O apêndice A reúne o material gerado durante estudos de geometalurgia com o intuito de se elaborar um diagnóstico rápido da suscetibilidade de uma dada amostra ao novo processo de ustulação. Este se baseia apenas na análise de TGA de uma amostra sulfatada e tem o intuito de economizar tempo e recursos que seriam gastos em ensaios de bancada para as etapas de sulfatação e lixiviação.

1.1 Referências

Gupta, C. K.; Krishnamurthy, N. (2005) Extractive metallurgy of rare earths, CRC Press, Nova York.

Roskill Information Service, Rare Earth: Market Outlook to 2029 (2019), Sample Page, 19th Edition, London.

Teixeira LAV, Silva RG (2014) System and process for selective rare earth extraction with sulphur recovery. Patent US 2015/0329940 A1.

Zhang J., Zhao B. and Schereiner B. (2016) Separation hydrometallurgy of rare earth elements, Springer, Switzerland

2 INTRODUCTION

The rare earth elements (REE) can be defined as the 15 elements of the lanthanide series (ranging from lanthanum to lutetium) plus yttrium and scandium. Although yttrium and scandium do not belong to the lanthanides series, they are treated as rare earth elements due to their similar chemical behaviour and their natural co-occurrence with the other 15 elements (Figure 2.1). Those 17 elements can be divided in 2 groups - the light rare earth elements group (LREE) and the heavy rare earth elements (HREE) group. This division is based on the double salt solubility (Zhang et al, 2016). In this case, elements ranging from lanthanum to europium belong to the LREE group and elements ranging from gadolinium to lutetium belong to the HREE group. Yttrium and scandium may be included in the HREE group.

In chemistry, electron configuration is the distribution of electrons of an atom or molecule in atomic or molecular orbitals. The rare earth unique properties lie on its electron configuration. As one moves from left to right along the rare earth elements in the periodic table, the 4f orbitals are usually being filled. The effect of 4f orbitals on the chemistry of the rare earths is the key factor that distinguishes these from other elements. As there are seven 4f orbitals, the number of unpaired electrons can be as high as 7, which gives rise to the very large magnetic moments observed for some rare earths. The phenomenon called lanthanide contraction is the decrease in the atomic radius with increase of atomic number. This occurs because of the weak shielding effect of the 4f electrons. Although chemically similar, the rare earth elements have individual physical qualities; for example, they have very different responses to light, electricity, and magnetism. The properties that make REE special for some industrial applications are: Most REE metals exhibit strong magnetism; fluorescence under UV light; Ignite and burn vigorously at high temperatures; reacts with water to liberate hydrogen gas; and have high melting and boiling point (Roskill, 2015).

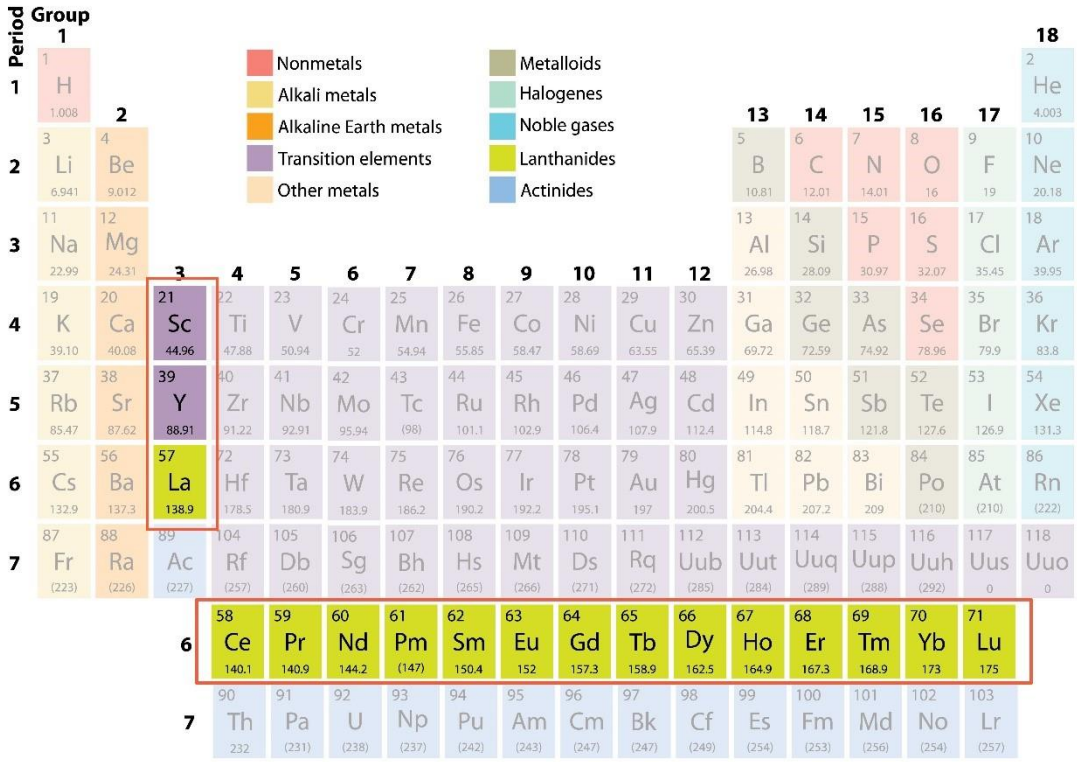

Figure 2.1 - Rare Earth Elements position in the periodic table of elements (http://www.rareelementresources.com)

2.1 REE Applications and Global Market

The main drivers for rare earth consumption are the catalyst, magnets, polishing powders and rechargeable batteries electrodes. The contribution of each segment is shown in Figure 2.2. Other relevant industries are metallurgical, ceramics, phosphors and pigments and the glass industry (Lucas et al, 2015). The catalyst industry uses mainly Ce, La and Nd in process such as the FCC (Fluid Crack Catalyst) for petroleum cracking. The magnets industry, which is showing a strong growth due to the increased relevance of green technologies, uses manly Nd, Pr and Dy for permanent magnets. These magnets are used in several modern applications, such as wind turbines, cell phone speakers and Computerized Axial Tomography (CAT) scans. The metallurgical industry uses Ce and La as mischmetal or in more advanced applications, as lightweight, formable alloys (Hosseinifar, 2009). Cerium is also largely employed as glass polishing powder. The glass industry also uses La and Ce as components for several types of glasses, including optical glasses for cameras. The phosphor and pigment industry use several REE, including Y, Sc, Ce, La and Eu. Specific

REE elements grant specific colors to LED lights. The proportion of each application to each element is shown on Figure 2.3. The dependence of modern technology on REE make them part of the so-called critical elements.

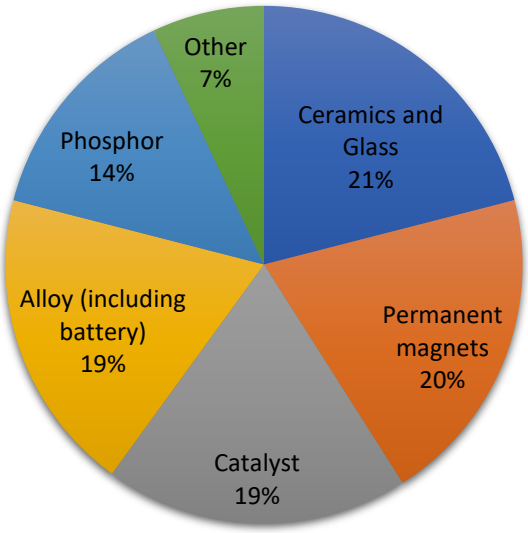

Figure 2.2 - The main drivers for industrial application of rare earth elements (Lucas et al 2015)

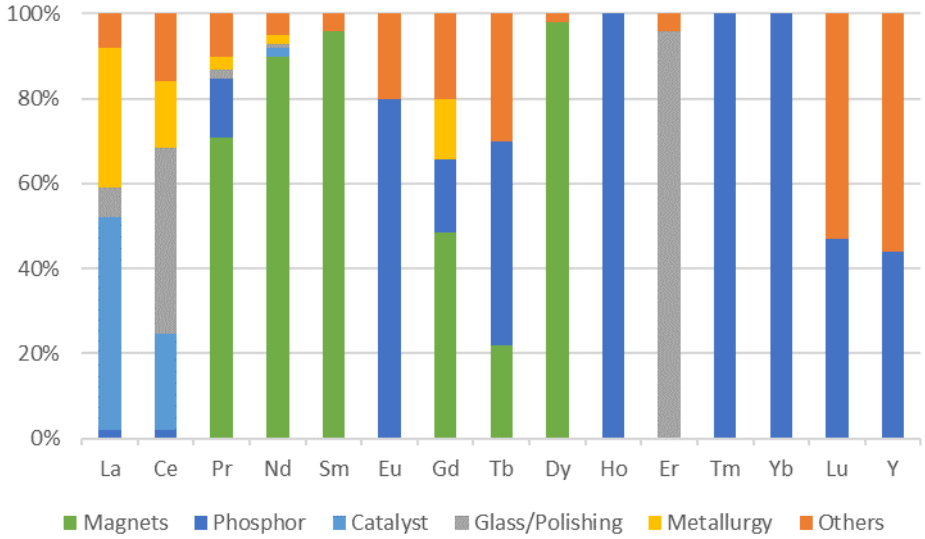

Figure 2.3 - REE application by element (Illustration prepared with data from Roskill, 2015)

Since the 1990's, China is the largest REE producer and exporter in the world (Figure 2.4). The increase in production is associated with a heavy environmental burden and, together with REE smuggling issues and other reasons, made China to launch a series of stringent policies to regulate rare earth mining and commercial activities. Amongst these is the production and export licensing, the quota system and the introduction of resource tax and export duty (Liu et al, 2016). In 2010 China was responsible for 92% of the world's total production. In the same year, China reduced the exportation quotas by 22.5% leading to a shortage worldwide and to the very high spike in prices, which reached maximum values in 2011. The spike in prices drove the discovery of several new deposits and generated hundreds of mineral projects around the world. It also resulted in very intense technological research for new alternatives for rare earth processing and separation. The prices started to fall in 2015 and are now at the level it was before the implementation of the quota system, except for neodymium and praseodymium which, supported by green technology development, are still displaying high price levels. The illegal rare earth mining in China fell more than 50% by 2016 (Roskill, 2019).Figure 2.5 shows the price change for some rare earth oxides (REO) since 2004, the drive force for recent intensive technology development. In 2014, China was responsible for 70% of demand and Japan and other Asian countries a further 15% (Figure 2.6).

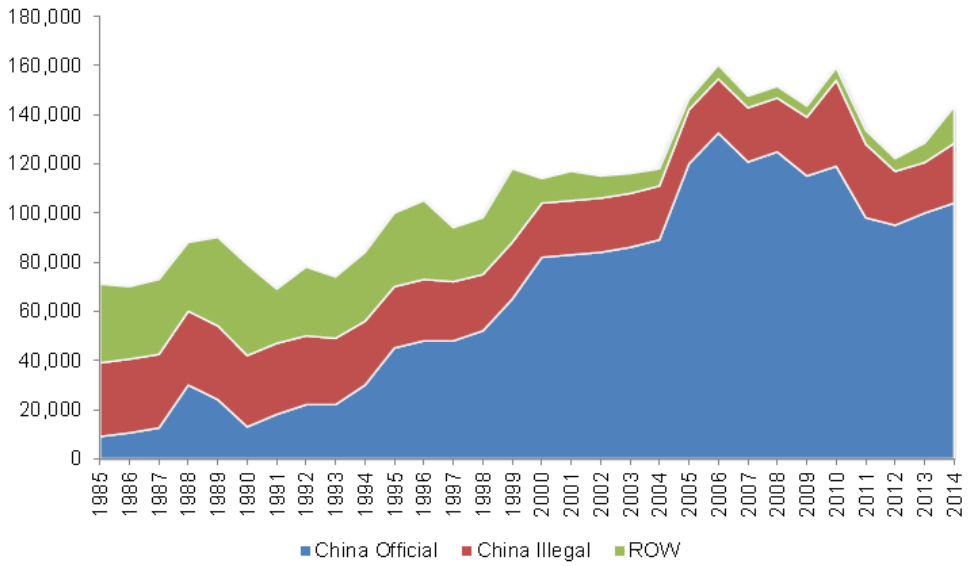

Figure 2.4 - World production of REE (tREO) divided between China legal, illegal and rest of the world -ROW (Roskill, 2015)

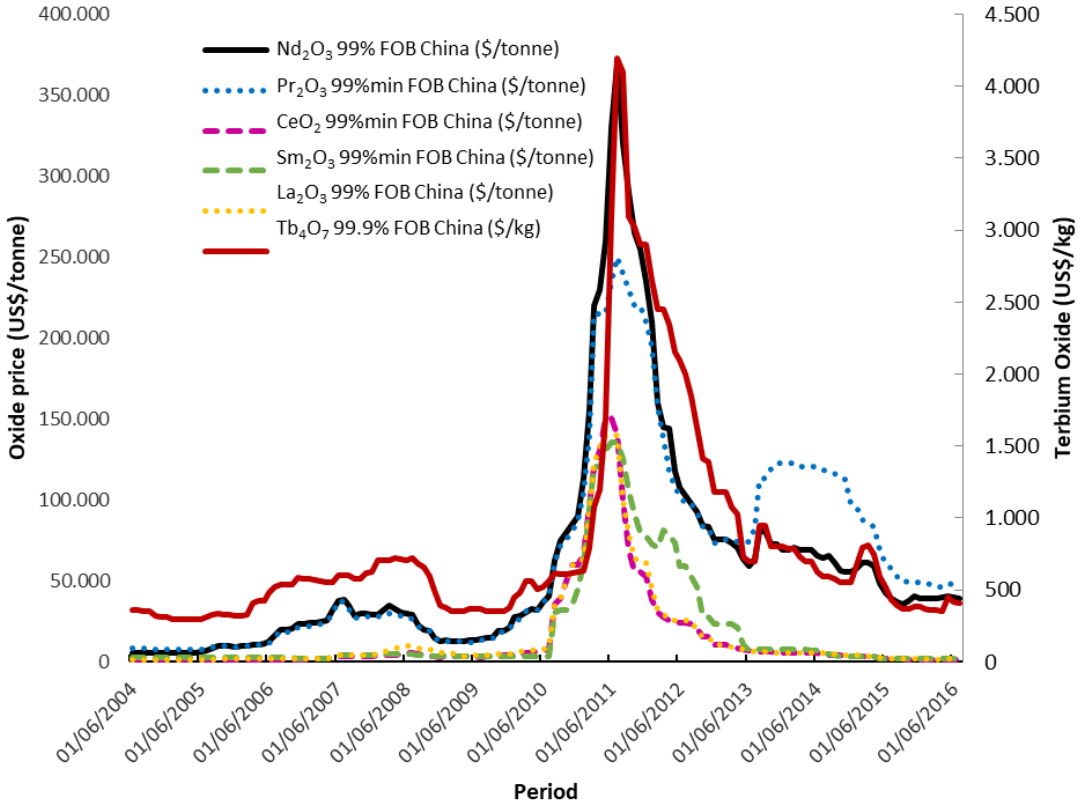

Figure 2.5 - Price change for rare earth oxides of praseodymium, neodymium, cerium, samarium, lanthanum (to the left) and terbium (to the right). Illustration prepared with data from SNL/S&P Global (2017)

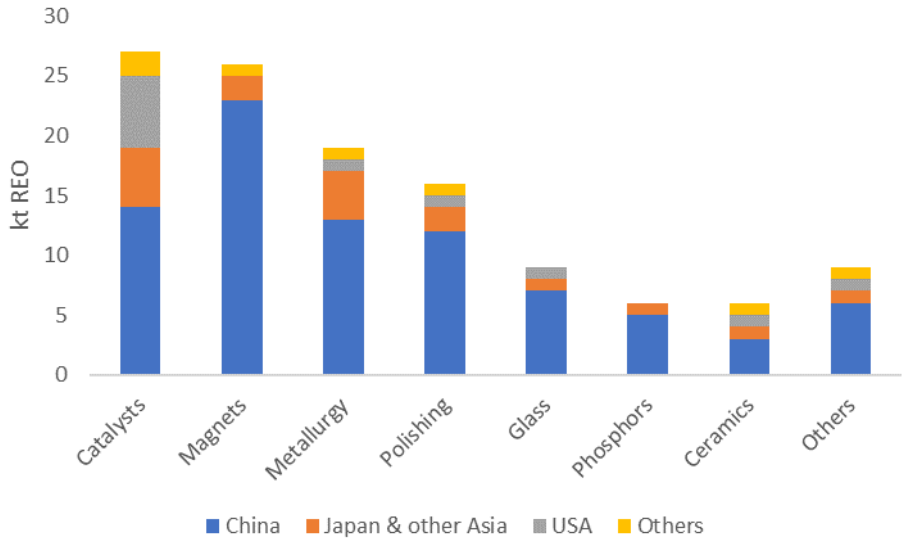

Figure 2.6 - Estimated rare earths market by application and region in 2014 (Illustration prepared with data from Roskill 2015)

The three largest end use sectors were catalysts, magnets and metallurgy, which together accounted for 60% of demand, as shown in Figure 2.6. Detailed information on each element application is described in Table 2.1. The items directly related to environmental applications and increase in energy efficiency are underlined. There are other several indirect applications that can lead to energy and environmental improvements.

These applications help to understand why neodymium and dysprosium are often in short supply. It is because they are critical components in Fe-(Nd, Dy)-B high-strength permanent magnets, and the demand for such magnets is growing rapidly as hybrid, electric vehicles and wind energy markets grow.

Dysprosium, especially, is often in short supply because (i) it is present in low concentration in most ores and (ii) it is indispensable for improving the high-temperature strength (i.e., near internal combustion engines and other heat sources) of Fe-(Nd, Dy)-B magnets. Cerium and samarium are often in excess supply, as are holmium, erbium, thulium, and ytterbium. However, lanthanum is likely to be in short supply because of its large use in petroleum refining catalysis.

Table 2.1 - Market application for individual rare earth element (Roskill, 2015)

Lanthanum	• Fluid Catalytic cracking (FCC) • To produce lanthanum-nickel alloys used in a variety of applications to assimilate hydrogen. Alloy is used to manufacture nickel metal hydride (NiMH) batteries* • Lighter flints • Component of glassmaking to produce glass with high refractive index • To boost some superalloys performance • A dopant in ceramic capacitors • Green color phosphors production
Cerium	• Catalytic – to mitigate automobile emissions and fuel additive for diesel particular filters • Elevation of thermal stability of zeolite and reduction of sulphur and nitrogen oxide emissions • Polishing powder in electronic components (hard disk drives- HDDs), silicon wafers, display screens, mirrors and optical glass • As a desulfuriser in steel industry and to strengthen deterioration resistance, to stimulate the precipitation of graphite nodules. Act in aluminum alloys for corrosion resistance and strength • Mischmental alloy as lighter flint • Oxidant to decolorize any intense discolouration • Stabilizer for glasses against UV effects • Green phosphors for lighting and display panels • Engineering ceramics, including ceramic capacitors and refractories • Purification of water • Substitute of other rare earth in magnet alloys
Praseodymium	• Didyminum to produce neodymium iron boron (NdFeB) • Ceramic and glass industries for yellow colour pigment • Pigments for glass in welding goggles • Dopant in ceramic capacitors
Neodymium	• NdFeB magnets used in electric motors for portable consumer electronics. Automotive industry use in small electric motors- brake systems, seat adjusters and car stereo speakers. Medical magnetic imaging (MRI). • Wind turbine generators and HEVs • Glass and tile colouring and tinting. It can be used as decolouriser in potassium silicate and lead glasses

	• Welding googles for lenses protection • Neodymium-doped yttrium-aluminum-garnets • To boost ceramic capacitors • To dope gadolinium-gallium-garnet (GGG) crystals • In precious metal capacitors
Samarium	• Samarium cobalt (SmCO) magnets - higher stability at high temperatures • Neutron absorber in nuclear reactors.
Europium	• Energy efficiency lighting – red and blue for display screens • Used in the phosphors in anti-forgery marks on Euro bank notes • Neutron absorber in nuclear reactors and control rods
Gadolinium	• It is alternative to neodymium in NdFeB magnets • Contrast agent for MRI patients • Nuclear magnetic resonance (NMR) relaxation agent • Neutron poison, control rods and neutron absorbing coatings in nuclear reactors • Gadolinium salt- green phosphors production to be used in Plasma display panels (PDPs) • Superconductor technology • Magnetic refrigeration • Alternative to diamonds, substrate for magneto-optical and lasers
Terbium	• Energy efficient fluorescent lamps and display screens. • The magnetostrictive alloy Terfenol-D, which contains terbium, has the highest magnetostriction of any alloy and has uses in sonar sensors and actuators • It´s alloy is used for magneto-optic recording films, such as TbFeCo
Dysprosium	• The manufacture of NdFeB permanent magnets • Doping lasers
Holmiun	• Glass production • Doping lasers • Nuclear control rod
Erbium	• It´s salt provide pink coloring to optical and decorative glassware. Physical decolouriser to neutralize colour impurities • the most common dopant in optical fibre amplifiers to transmit longdistance signals • Surgical applications
Thulium	• Glass colouring • Phosphors • Fibre optics medical irradiation • Ceramic magnets

	• Lasers
Ytterbium	• Thermal barrier coatings for nickel, iron and other transition metal alloy substrates • Fiber amplifier and fiber optic technologies • Laser applications • <u>useful in silicon photocells to directly convert radiant energy to electricity</u> • Increases his electrical resistance in high stresses. This stress gauges for monitoring ground deformations from earthquakes and nuclear explosions.
Lutetium	• <u>Base material in phosphor products for newly developed, warm-colour, white LEDs.</u> • Base material in X-Ray phosphors • Positron emission tomography (PET) detectors • Doping crystals • High refractive lenses
Yttrium	• <u>Phosphor production for display screens and energy efficient lighting</u> • Yttria-stabilised zirconia • Ceramic pots • Sintering agent to produce silicon nitride • Added to stainless steels. Performance improvement of some alloys • Yttrium-aluminium-garnet (YAG) crystals for lasers

* items related to environmental applications and increase in energy efficiency are underlined.

2.2 Occurrence, Reserves and Projects under Development

Rare earths are widely distributed in the earth's crust in low concentrations. The combined crustal abundance of rare earth elements is of the order of 0.02% (200mg.kg^{-1}). The REE are more abundant in granitic rocks than in basic igneous varieties, although the highest concentrations are found in alkaline igneous rocks and carbonatites. The REE are found in more than 160 discrete minerals, but 95% of all the world's rare earth resources occur in just four minerals (Papangelakis and Moldoveanu, 2014): bastnasite (Ce, La, Y) (CO_3) F, monazite (Ce, La, Pr, Nd, Th, Y) PO_4, xenotime YPO_4 and ion-adsorption clays. Bastnasite and monazite are minerals rich in LREE whereas xenomite and ion-adsorption clays are richer in HREE. The rare earth content in the deposits are usually low, seldom higher than 5% and the elements are usually extracted as by-products or co-products (Gupta and Krishnamurthy, 2005). An estimation of the rare earth reserves around the world (US Geological Survey, 2016) is shown in Figure 2.7. The data on the partition between monazite and bastnasite ores are not so recent (Gupta and Krishnamurthy, 2005) but demonstrate the relevance of both main rare earth carriers.

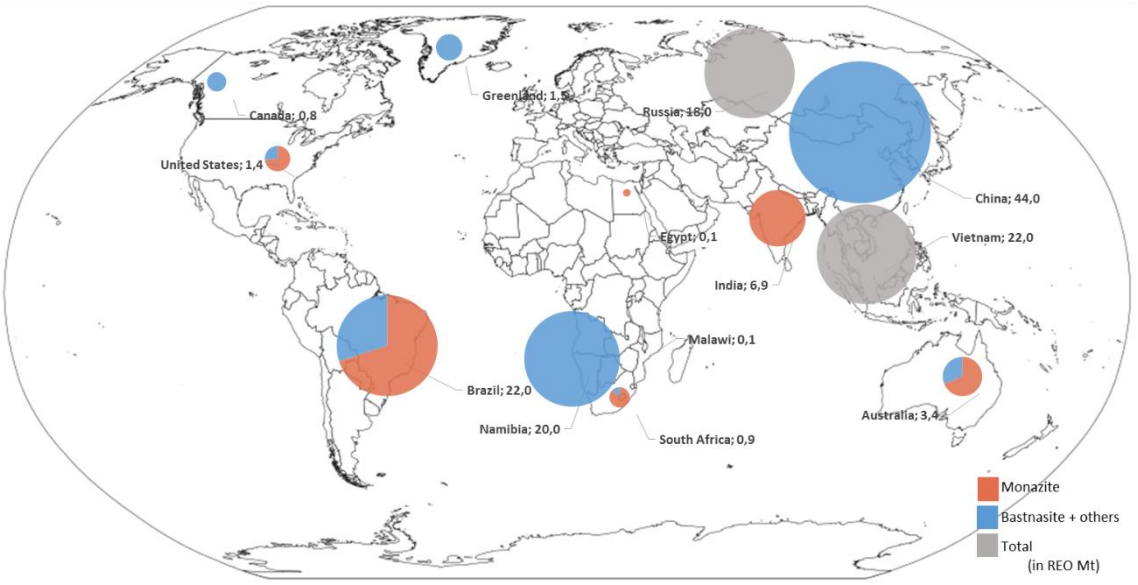

Figure 2.7 - Estimated global rare earth resources and its distribution between monazite and bastnasite. The gray circles belong to unidentified resources. Based on data combined from USGS (2016) and Gupta and Krishnamurthy (2005)

The visual aspect, chemical formula and crystal structure of the main REE-bearing minerals are displayed on Figure 2.8. Bastnaesite is a fluorocarbonate, which is pale yellow to brown in color, with a hardness of 4 to 4.5 and a specific gravity of 5. In a mineral body, bastnaesite concentration is generally 7% to 10% REO. Flotation concentrates of bastnaesite average about 60% REO but can be upgraded to 70% REO by acid leaching and to 85% REO by a combination of calcination and leaching (Gupta and Krishnamurthy, 2005). The largest known bastnaesite deposit occurs at Bayan Obo in Inner Mongolia (China), where it occurs in association with monazite as a complex series of Pre-Cambrian metamorphic rocks. Baiyun mine is a bastnaesite deposit, and Obo mine is a monazite deposit. Rare earths are separated as a by-product of the iron ore mining operations.

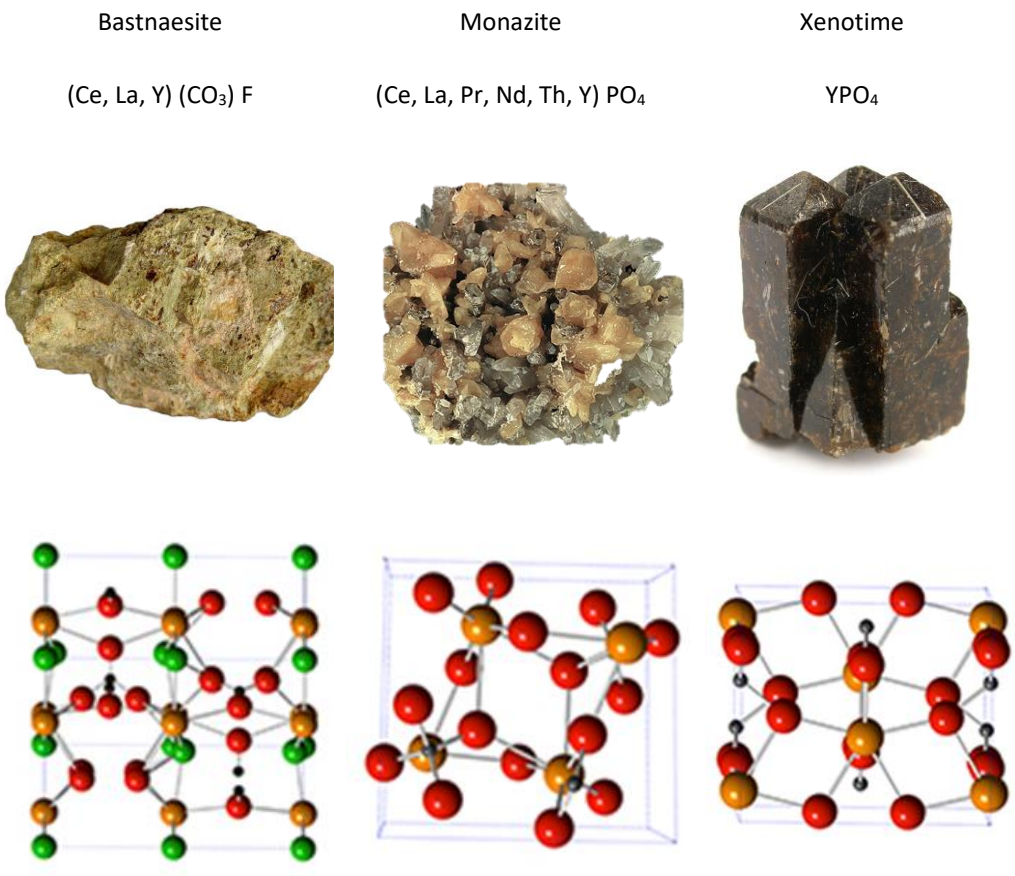

Figure 2.8 - Main REE bearing minerals, its chemical formula and crystal structure (www.irocks.com)

Monazite is a rare earth phosphate that contains up to 70% rare earth oxides in its chemical formula. It is yellow to reddish brown in color, has a hardness and specific gravity of 5 and is resistant to weathering. When amendable to physical concentration, its concentrate may reach between 55% and 65% REO in the concentrated ore. A limited amount of monazite is processed to produce rare earths, partly because of the cost of disposal or storage of the contained thorium oxide. Mt. Weld is a weathered monazite source associated with carbonatite being developed in Australia. Weathered or 'supergene' monazite ores have much lower thorium content than primary monazite ores. In the Mt. Weld ore approximately 350 $mg.kg^{-1}$ (0.035%) ThO_2, compared with concentrations of 6-7% ThO_2 in the by-product monazite from mineral sand operations. Levels of thorium are low because it is leached out of the monazite during weathering of the host carbonatite. This mechanism that also enhances the rare earth concentration (Roskill, 2015).

Xenotime is an yttrium phosphate that shows isomorphism with monazite. The crystal structure between them are different, xenotime having a tetragonal structure and monazite having a monoclinic-prismatic structure. It occurs in igneous and metamorphic rocks and in pegmatites, which usually contain uranium and thorium. Xenotime used to be recovered as a by-product of alluvial tin mining in Malaysia, Indonesia and Thailand. Mining of xenotime is limited due to associated environmental and occupational issues. However, some deposits are exploited, in particular to retrieve HREEs and yttrium. A potential project has been studied at a producing tin mine in Pitinga, Brazil (Neto et al, 2013).

Ion-adsorption clays (also known as ion-adsorption ores) occur in Southern China in several provinces; large resources are located in Jiangxi and Guangdong, but are also found in Fujian, Hunan and Guangxi. The deposits are formed as a result of intense weathering of phosphatic minerals such as apatite and xenotime. Rare earths and yttrium are contained within the clays through adsorption on the surface of alumino-silicate minerals like kaolin. The clays tend to be enriched in heavy rare earths and are depleted in cerium. The composition of the ionic clays can vary significantly from source to source. The 2011 spike in prices (Figure 2.5) has drove junior mining companies to start several REE projects spread around the word. Table 2.2 show a list with some of the more

advanced projects. It is easy to notice that the clear majority are monazite/bastenaesite projects.

Table 2.2. Main rare earth mineral projects under development (Verban, 2015)

Property	Owner	Country	Development Stage	Host Rock	REE Carrying Minerals	% TREO Ore	% HREO relative	Reference
Bokan Mountain	Ucore Rare Metals Inc.	USA	PEA	Alkaline rock-associated	Thalenite, bastnasite, xenotime, monazite	0.65	40	Bentzen et al., 2013
Browns Range	Northern Minerals Ltd.	Australia	FS	Alkaline rock-associated	Xenotime	0.66	87	Northern Minerals, 2015
Dubbo	Alkane Resources	Australia	FS	Alkaline rock-associated	Eudialyte, bastnasite, zircon, natroniobite, columbite	0.9	25	Alkane Resources, 2012
Kvanefjeld	Greenland Minerals	Greenland	FS	Alkaline rock-associated	Steenstrupine (complex sodic phospho-silicate)	1.2	11.8	Greenland Minerals, 2015a
Nechalacho	Avalon Rare Metals Inc.	Canada	FS	Alkaline rock-associated	LREE in bastnasite, synchisite, monazite and allanite. HREE in zircon, fergusonite and xenotime	1.72	27.3	Ciulescu et al., 2013
Norra Karr	Tasman Metals Ltd.	Sweden	PFS	Alkaline rock-associated	Eudialyte	0.59	52	Short et al., 2015
Port Hope Simpson	Search Minerals Inc.	Canada	PEA	Alkaline rock-associated	Allanite, fergusonite, chevkinite	1.07	19.6	Dreisinger et al., 2014
Round Top	Texas Rare Earth Resources Corp.	USA	PEA	Alkaline rock-associated	Yttrofluorite	0.06	72	Hulse et al., 2014
Strange Lake	Quest Rare Minerals Ltd.	Canada	PEA	Alkaline rock-associated	Complex silicates, phosphates and zircon	0.93	39	Gowans et al., 2014
Zeus	Matamec Explorations Inc.	Canada	FS	Alkaline rock-associated	Eudialyte	0.41	37	Saucier et al., 2013
Ashram	Commerce Resources Corp.	Canada	PEA	Carbonatite	Monazite, trace bastnasite, xenotime	1.81	4.7	Gagnon et al., 2015
Bayan Obo	CN Northern Rare Earth (Grp)	China	Operating	Carbonatite	Bastnasite / monazite	6		Zhi Li and Yang, 2014

Property	Owner	Country	Development Stage	Host Rock	REE Carrying Minerals	% TREO Ore	% HREO relative	Reference
Bear Lodge	Rare Element Resources Ltd.	USA	PFS	Carbonatite	Bastnasite, synchysite, monazite, cerianite, ancylite	4.7	4.4	Dahlberg, 2014
Gakara	Rainbow Rare Earths Limited	Burundi	Reserves Development	Carbonatite	Monazite, bastnasite	54.3	1.1	Rainbow Rare Earths, 2015
Lofdal	Namibia Rare Earths Inc.	Namibia	PEA	Carbonatite	Xenotime	0.1	76	Dodd et al., 2014
Montviel	GeoMega Resources Inc.	Canada	PEA under development	Carbonatite	Ba-Ce carbonates and monazite	1.5	1.8	Belzille et al., 2015
Mountain Pass	Molycorp Inc.	USA	Care and Maintenance	Carbonatite	Bastnasite	8	1	Molycorp 2014 a, b, 2015
Mt Weld	Lynas Corp. Ltd.	Australia	Operating	Carbonatite	Monazite, apatite	15.4	3	Lynas, 2005
Ngualla	Peak Resources Ltd.	Tanzania	PFS	Carbonatite	Bastnasite, monazite	4.54	1.9	Peak Resources, 2014
Songwe Hill	Mkango Resources Ltd.	Malawi	PFS	Carbonatite	Synchysite, apatite	1.6	6.8	Croll et al., 2014
St-Honoré	Magris Resources Inc.	Canada	unknown	Carbonatite	Bastnasite / monazite	1.65		
Zandkopsdrift	Frontier Rare Earths Ltd.	South Africa	PFS	Carbonatite	Monazite	1.9	7.8	Harper et al., 2015
Serra Verde	Mineracao Serra Verde	Brasil	PFS (not published)	Ionic clay	N/A	0.16	25 (37 if no Ce)	Rocha et al., 2013 and 2014
Tantalus	Tantalus Rare Earths AG	Madagascar	Reserves Development	Ionic clay	N/A	0.09	19 (30 if no Ce)	Desharnais et al., 2014
Eco Ridge	Pele Mountain Resources Inc.	Canada	PEA	Vein / sedimentary	Monazite + U minerals	0.15	11.4	Cox et al., 2012
Nolans Bore	Arafura Resources Ltd.	Australia	FS	Vein / sedimentary	Apatite, allanite	2.6	4	Arafura Resources, 2014
Steenkampskraal	Great Western Minerals Grp Ltd.	South Africa	FS	Vein / sedimentary	Monazite	14.4	3.8	Clay et al., 2014

2.3 Rare Earth Processing

Rare Earth processing can be divided in five main stages, as follows: physical beneficiation, chemical conversion (usually called cracking), leaching, purification and separation. Each stage will be discussed briefly in the next paragraphs, with focus in the chemical conversion. The chemical conversion followed by leaching and purification will produce a mixed concentrate that is usually fed in large solvent extraction facilities to separate the rare earth elements. These compounds, usually oxide, carbonates, chlorides, and others, are sold to their final application or may be further processed to increase the purity level (Gupta and Krishnamurthy, 2005).

Rare earth processing, in general, have remained unchanged although advances in beneficiation techniques and equipment such as column flotation and flotation modelling/simulation software have improved mineral recovery. Flotation is the most widely used method of concentration for rare earth ores. In addition to flotation, gravity, magnetic and electrostatic separators are often used to produce a mineral concentrate. As the rare earth deposits have a relatively low REO content, its amenability to physical concentration will depend on how complex the REE carrier is. Monazite is usually present in regions that have undergone a strong weathering process. The occurrence of finely dispersed monazite particles in the host material due to the weathering process, results typically in poor mineral liberation and low recoveries in ore beneficiation. It is possible to go further on the discussion of physical separation, but the topic is outside the scope of the present work.

All rare earth ores, except for ion adsorption clays, need to be ‘cracked’ to make possible further aqueous dissolution of the rare earth elements contained in the original mineral. The cracking or chemical conversion usually involves a hydrometallurgical processing that can be preceded or not by a pyrometallurgical treatment. Figure 2.9 shows a simplified flowsheet with the general cracking processing routes applied for processing the different ores. There are several adaptations to each process route to match the specifics of each ore. The most common commercial routes are discussed in chapter 4.

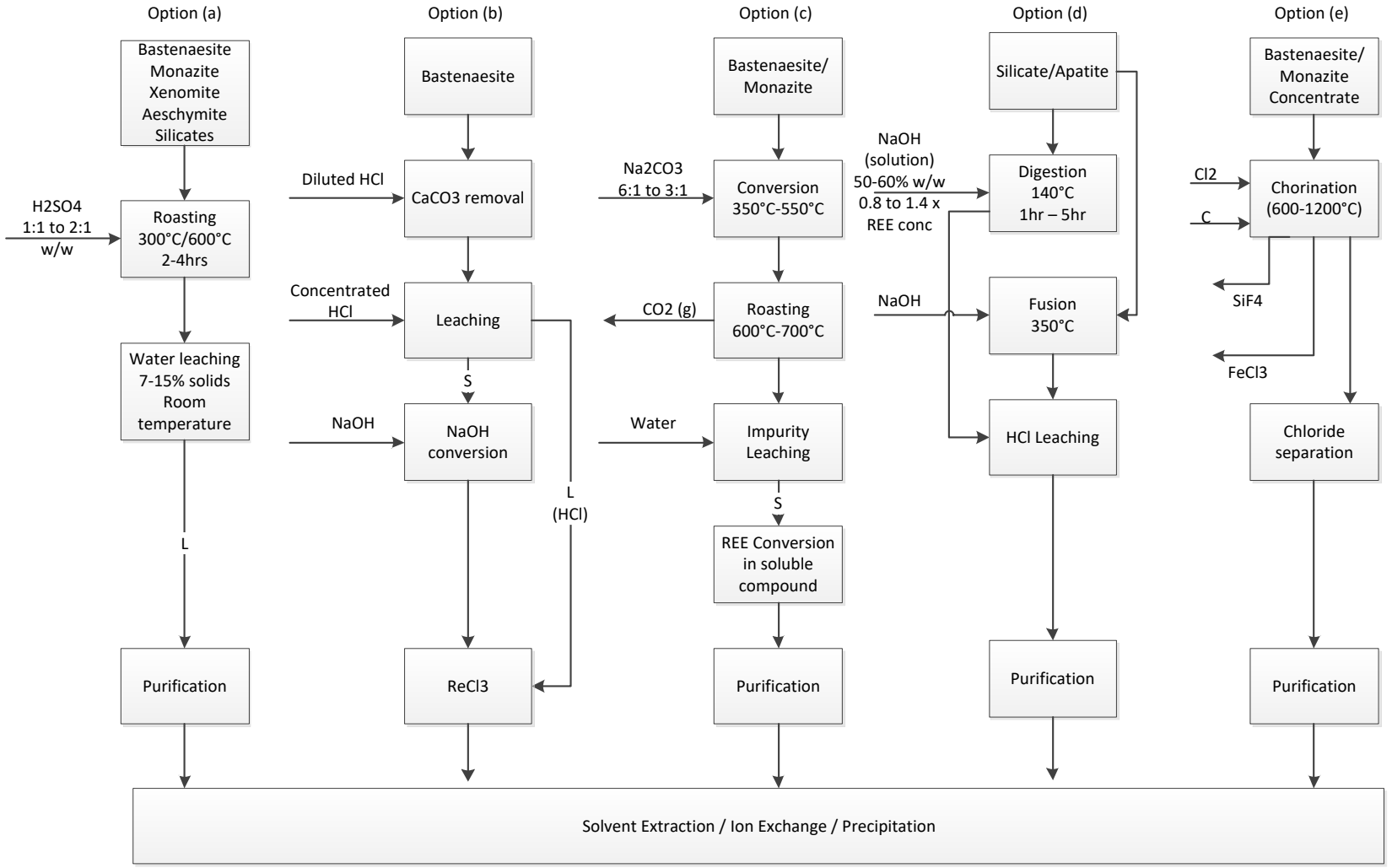

Figure 2.9 - Simplified flowsheets for the most relevant REE carrying minerals (Zhang et al, 2015)

The standard sulfuric acid process applied to monazite ores and others (option “a”, first flowsheet from left to right) consists in acid addition to the ore (the ratio acid/ore may vary widely), followed by baking, dissolution in water (Lucas et al, 2015) and purification to obtain a rare earth compound. The low temperature roasting enhances the sulfation reaction kinetics but promotes undesired increase in conversion of impurities into sulfates. The high temperature roasting promotes the decrease in thorium solubility during leaching stage. In China, Bayan Obo process a mixed of bastenaesite and monazite using this process. The sulfuric processing of monazite will be further detailed in chapter 3.

The hydrochloric acid route (option “b” in Figure 2.9) is frequently applied to bastenaesite processing. Diluted HCl is used to remove carbonates from the ore, increasing the REE content. The bastenaesite in the remaining solid is converted into chloride by concentrate HCl. Rare earth fluorides are not leached in this process and remain in the solid. Sodium hydroxide is added to convert the remaining REE into hydroxide that are then mixed with the concentrate chloride solution, converting the hydroxide into chloride. Molycorp’s Mountain Pass plant (USA) used an alternated flowsheet, in which a roasting stage removed CO_2 from the concentrate and oxidized Ce (III) to Ce (IV). The material leaving the furnace was leached in 30% HCl solution, bringing the rare earth elements to solution but leaving the Ce (IV) as solid.

The option “c”, in Figure 2.9, can be applied to low grade (20–30 % REO) bastnaesite and monazite concentrate that is decomposed through 350–550°C roasting with sodium carbonate at a mass ratio of concentrate to sodium carbonate from 6:1 to 3:1. After roasting, the soluble salts are leached out using water or dilute acid. The rare earth oxide will stay in the solids and the grade can be increased from 20–30 % to 50–60 %. After that, REE must be converted into a soluble form and goes to further purification followed by separation.

Monazite can also be processed by using hydroxide, particularly when associated with apatite, as shown in Figure 2.9, option “d”. In the standard hydroxide method, represented by equation (2.1) sodium hydroxide is added to the ore under low heat (around 140°C) to generate solid rare earth hydroxides. The rare earth hydroxide mud generated in this process may be water leached under controlled pH conditions, or reacted directly with an acid, like hydrochloric

acid. The liquid phase obtained from the filtration of the mud can be used to recover phosphor as trisodium phosphate (Gupta C. K. and Krishnamurthy N., 2005; Lucas J. et al, 2015). The dissolution and downstream processes should be chosen taking in consideration the impurities presented in the ore, final compound to be produced and its purity. The rare earth concentrate can also be decomposed with fused NaOH at higher temperatures of approximately 350°C or higher. However, the REE products of fused NaOH decomposition are difficult to dissolve. For this reason, this process has been abandoned by the rare earth industry (Zhang et al, 2015).

$$(\mathrm{RE})\mathrm{P}O_4(s) + 3NaOH(aq) \rightarrow Na_3PO_4(aq) + (RE)(OH)_3(s) \quad (2.1)$$

There is also a process that is claimed to be able to treat all types of ore, the chlorination process, shown in Figure 2.9 option “e”, in which chlorine gas is added in a furnace together with carbon and $SiCl_4$. The temperature is adjusted between 600-1200°C, allowing the formation of gaseous SiF_4 and iron chloride. (REE, Ba, Ca) Cl_3 is formed and leaves the furnace in the solid state for subsequent dissolution and purification. This technique has never been used industrially.

Ionic clays are an exception, since there is no need for cracking, because it is already in an adsorbed state in the mineral and follows ion exchange laws for extraction. The first-generation process for the Ion clays deposits used heap and tank leaching with mild acid solution. The most recent operations employ in situ leaching (Zhang et al, 2015).

Leaching of soluble REE compounds are carried out in most relevant flowsheets. During the leaching stage, soluble rare earth compounds are transferred to the aqueous phase. This process is usually performed by using water or slightly acidified solutions. The percentage of solids during leaching usually varies from 5 to 20%. Leaching time may vary from 0.5 to 4 hrs. A purification stage usually follows the leaching stage and may include a simple neutralization step using alkaline reagents such as lime, limestone, magnesium oxide, magnesium or sodium carbonate. Care must be taken when using calcium-based reagents in sulphuric media because REE co-precipitation with gypsum can lead to significant REE losses. Elements such as Th, Fe, P and Al are usually

targeted to be removed in this stage. The REE solution may go straight to the separation stage or may be precipitated and re-leached in order to attain further purification prior to the separation stage.

Separation of the individual rare earth elements, however, is much more difficult as the lanthanides display similar chemical properties as a result of lanthanide contraction. Solvent extraction and ion exchange processes are normally used to separate the individual rare earth elements taking advantage of small variations in their basicity caused by the contraction. Other separation processes, such as free-flow electrophoresis, are being developed.

The presence of large amounts of iron and alkali in the ore leads to increased acid consumption and complexity of the liquors obtained after the extraction stage, thus increasing production costs. There are elements often associated with monazites, such as thorium and uranium, as well as their radioactive decays. These elements cannot follow rare earth in the final product and must be removed.

2.4 Relevance and Objectives of this Work

Brazil hosts significant reserves of REE in its territory, almost 75% of which are present as monazite. The main monazitic deposits are located in the southeast of the country, many of which are igneous deposits that have undergone intense weathering. Due to these characteristics, monazite is finely dispersed in the ore and often associated with iron minerals. Monazite also has co-occurrence with other phosphate minerals, such as apatite, and usually has thorium in its composition. Dissemination hinders physical concentration (such as flotation, magnetic and gravitational concentration), and the production of a high-grade concentrates. Additionally, the presence of large amounts of iron and alkali in the feed leads to increased acid consumption during leaching, and increased complexity of the solution to feed the purification stage. This scenario will result in high operational costs, which are a barrier to making the mineral deposit economically feasible.

The current work investigates a new selective process for iron-rich, monazite deposits, which decreases the extraction of iron and thorium as an approach to reduce the operating costs.

The increased offer of REE in the market is expected to lead to lower prices, which would, in turn, promote broader adoption of clean energy technologies dependent on REE, such as wind energy. It may also boost emerging markets such as electric cars. Both applications are of fundamental importance for decarbonization initiatives.

The objectives of the present work are to:

i. Identify a process condition to achieve selective REE extraction in iron-rich ores containing thorium, where REE are finely disseminated,
ii. Understand the thermodynamic behavior of sulfated monazite roasting;
iii. Understand the mechanism behind the high-temperature roasting of phosphate-rich minerals, such as monazite associated with apatite;
iv. Explore the effect of controlling atmosphere during roasting of phosphate minerals as an attempt to improve process performance;

v. Explore alternative cracking options, such as chlorination.

This work is divided into eight chapters. The first chapter corresponds to a brief introduction in Portuguese, contextualizing the work done. The second chapter refers to a more comprehensive introduction, describing the main applications for the rare earth elements, the market, natural occurrences, and a brief description of the extraction, purification, and separation processes of these elements. The main objectives of this study, as well as its relevance for the academy, industry, and society, can also be found in this chapter.

The third chapter investigates a new process for selective rare earth roasting, based on the supposed selective decomposition of rare earth sulfate relatively to the decomposition of iron and thorium sulfates. The assumptions, based on thermodynamic simulations of the system, were compared with the experimental data using lanthanum sulfate.

The fourth chapter goes further into the understanding of the mechanism behind the selectivity identified in the works carried out with the decomposition of sulfates. In this chapter, the effect of the presence of phosphorus is studied and its impact on the selective roasting process is elucidated. Thermodynamic simulations again served as a guide for understanding the system.

The fifth chapter investigates the effect of the gas atmosphere on selective roasting, specifically the effect of a reducing atmosphere on the decomposition temperature of the REE and the main impurities present in the system. The impact of this new process on the solubility of target elements in aqueous systems was also evaluated.

The sixth chapter assesses the possibility of performing selective roasting without the need for an earlier sulfation stage. Instead, the exchange reaction between phosphates and sulfates is studied. Along the same line, the possibility of carrying out a double exchange between phosphates and chlorides is also addressed, with the intention of producing soluble rare earth chlorides.

The seventh chapter houses the general conclusions, the most relevant points obtained from the study, the list of publications generated from this study, and other related ones. The eighth chapter is a Portuguese summary of the conclusions.

Appendix A brings the material generated during geometallurgy studies to make a quick diagnosis about the susceptibility of a given sample to the new roasting process based only on the TGA analysis of a sulfated sample. This approach helps saving time and resources that would be spent on bench tests for the sulfation and leaching steps.

2.5 References

Neto A., Pereira V., Pires A., Barbanson, L., Chauvet A., (2013). Fluorine-rich xenotime from the world-class madeira Nb-Ta-Sn deposit associated with the albite-enriched granite at Pitinga, Amazonia, Brazil. The Canadian Mineralogist. 50. 1453-1466. 10.3749/canmin.50.6.000.

Gupta, C. K.; Krishnamurthy, N. (2005) Extractive metallurgy of rare earths, CRC Press, Nova York.

Hosseinifar M. (2009), Physical Metallurgy and Thermodynamics of Aluminum Alloys Containing Cerium and Lanthanum, Doctor of Philosophe Thesis, McMaster University, Canada.

Liu H., Tan D. and Hu F., Rare Earth: Shades of Gray, China Water Risk, (2016)

Lucas J.; Lucas P.; Le Mercier T., Rollat A.; Davenport, W.G.I. (2015) Rare earth: science, technology, production and use, 1st ed., Elsevier.

Papangelakis V. G. and Moldoveanu G., Recovery of Rare Earth Elements from Clay Minerals, ERES2014: 1st European Rare Earth Resources conference, Milos (2014)

Roskill Information Service, Rare Earth: Market Outlook to 2029 (2019), Sample Page, 19th Edition, London.

Roskill Information Service, Rare Earth: Market Outlook to 2020 (2015), Fifteenth Edition, London.

SNL/S&P Global, historical prices (2017), (www.snl.com). Accessed 8 July 2018.

U.S Geological Survey (2016), Mineral commodity summary, Reston, Virginia, USA.

Verbaan N, Bradley K, Brown J, Mackie S (2015) A review of hydrometallurgical flowsheets considered in current REE projects, In: Simandl GJ and Neetz M (eds.) Symposium on Strategic and Critical Materials Proceedings. British Columbia Ministry of Energy and Mines, British Columbia Geological Survey Paper

Zhang J., Zhao B. and Schereiner B. (2016) Separation hydrometallurgy of rare earth elements, Springer, Switzerland.

3 SELECTIVE EXTRACTION OF RARE EARTH ELEMENTS FROM MONAZITE WITH HIGH IRON CONTENT[1]

3.1 Introduction

The existence and need for different processing routes, in particular for monazite, was presented in the previous chapter. This section focuses on the need for a processing route that can extract rare earth elements from complex ores. The term complex ores mean, in this context, ores that show poor performance under conventional mineral beneficiation (e.g. flotation and gravity concentration, among others) due to very fine, micro-level association between the main REE carrying mineral (monazite) and the gangue material. This type of ore does not allow relevant REE upgrades prior to the hydrometallurgical processing and, within its composition, may also carry acid consuming elements and impurities (e.g. Fe, Mg, Th, U, and F, among others) that will bring technical difficulties and negative economic impacts to the project. An efficient extraction process should minimize the impurities carried to downstream steps and keep acid consumption as low as possible. The selective roasting, as discussed here, allows for the separation of iron and thorium from the rare earth elements, significantly decreasing the impurity levels in the liquor obtained by water leaching. The experimental results will demonstrate the selective extraction of rare earth elements, particularly with respect to iron and thorium. The effect of the roasting temperature on the selective extraction will be presented, as well as the decomposition behavior of sulfates during roasting by means of mass loss. A thermodynamic evaluation of the proposed process, including both the sulfation and roasting stages, will also be reported.

3.2 REE Extraction from Monazite Ores

Rare earth extraction usually involves a physical beneficiation and a hydrometallurgical processing. A pyrometallurgical step may also be required to prepare the ore for the hydrometallurgical stage. The physical beneficiation produces the concentrate (almost no market outside China), whereas the pyro and hydrometallurgical processing of the concentrate produces a mixed rare

[1] This chapter is an extract of Teixeira et al. (2019) Mining, Metallurgy and Exploration 36:235-44

earth material (restricted market). This material must comply with market specifications in order to proceed to the separation stage. Several steps of liquor purification are added to the flowsheet to attain this specification. The mixed material is then fed in the separation plants (these plants usually operate large solvent extraction facilities) to produce the separated rare earth elements. The rare earth compounds, usually oxides, carbonates, chlorides, among others, are sold to their final application or may be even further processed to increase purity level or to be turned into a different compound (e.g. metallic form in alloy) (Gupta and Krishnamurthy, 2005).

The beneficiation and chemical extraction of rare earths depends strongly on the mineral carrier. The physical beneficiation of monazite ores is usually difficult due to high weathering profiles of the deposits. Beneficiation may involve gravity concentration or magnetic/electrostatic separation. Flotation may be applied in a few cases, as it is better established for bastnaesite and is present in most industrial circuits that treat this type of ore (Gupta and Krishnamurthy, 2005; Pradip and Fuerstenau, 1991).

Due to its wide variation in chemical composition and weathering profile, monazite has a wider range of processing options than does bastnaesite. The treatment of monazite ores is usually divided into two main groups - the hydroxide and sulfuric acid processes – the latter of which is of interest in the present investigation.

The standard sulfuric acid process of monazite consists of (i) acid addition to the ore (the ratio acid/ore may vary widely), followed by (ii) heating in order to increase the conversion of rare earth phosphates to rare earth sulfates, (iii) dissolution in water (Lucas et al., 2014), and (iv) purification to obtain a rare earth compound (such as hydroxide, oxalate, chloride, or carbonate). The selection of the acid/ore ratio (usually between 1/1 and 2/1w/w, according to Zhang et al., 2016) is very important, since it has a direct impact on the process's economic performance and amount and type of impurity that will be carried downstream. The acid-ore mixture is usually heated in a rotary kiln under temperatures ranging from 200°C to 600°C to enhance the sulfation reaction. The higher the acid to ore ratio, the higher the dissolution of impurities during leaching. The heating stage can be divided into low temperature (below 300°C) and high temperature (above

300°C) (Zhang et al., 2016). Sulfates generated during the sulfation and the heating stages (Eqs. (3.1) and (3.2)) will dissolve during water leaching, generating a rich liquor in rare earth but also containing several impurities. After leaching, the rare earths are then precipitated as double sulfates, which in turn are converted to hydroxides, dried, and leached with nitric acid to remove Th and Ce. Rare earths in the liquor are re-precipitated as mixed hydroxides and sent to the separation plants. The low temperature process is older and renders a complex solution after leaching, making it more difficult to remove impurities. The high temperature process decreases thorium extraction due to the formation of insoluble ThP_2O_7 (Zhang et al., 2016).

$$2(\mathrm{REE})PO_{4(s)} + 3H_2SO_{4(aq)} \rightarrow 2H_3PO_{4(aq)} + (REE)_2(SO_4)_{3(s)} \quad (3.1)$$

$$Th_3(PO_4)_{4(s)} + 6H_2SO_{4(aq)} \rightarrow 4H_3PO_{4(aq)} + 3Th(SO_4)_{2(s)} \quad (3.2)$$

The previously described process routes are the standard flowsheets for rare earth processing. Modifications are required to address specific characteristics of the ore, such as high iron content. There are several modifications of the standard processes as an attempt to reduce impurity dissolution and acid consumption, as well as to increase rare earth extraction. A summary of some modifications of the standard process for REE extraction is show on Table 3.1. Those modifications can be divided into two groups. One group [4,5] attempted to use another type of mineral acid to improve REE extraction. Another group [1-3,6-8] attempted to use different reagents or process conditions to promote a selective extraction of rare earths. These processes may have the aim of separating thorium as an insoluble compound [1,6,7] or minimizing extraction due to temperature related formation of insoluble compounds.

Berni (2013) presented a process route in which iron is separated from rare earth in monazite ores by using a sulfation stage followed by selective roasting. This process was modified by the author Teixeira and Silva (2014) by introducing intensive mixing, which allowed direct leaching in water, yielding a large rare earth extraction ratio even without roasting.

Table 3.1. Relevant process modifications for REE extraction of monazite ores using sulfation/leaching/roasting techniques

Author	Yeah	Ore	Extraction type	Acid	Heating
Merrit [8]	1990	Monazite	Leaching	HCl	977-1187°C
Reneau and Tognet [9]	2003	Monazite	Sulfation	H_2SO_4	780°C
Huang et al [10]	2009	Monazite	Leaching	H_2SO_4	231-600°C
Mackowski et al [11]	2009	Monazite Apatite	Sulfation Leaching	HCl/HNO_3/ H_2SO_4	230°C
Boudreault et al [12]	2012	Several	Leaching	HCl/HNO_3/ H_2SO_4	80-225°C
Berni et al [13]	2013	Monazite	Sulfation Leaching	H_2SO_4	400-800°C
Teixeira and Silva [14]	2014	Monazite Tailings Industrial residue	Sulfation Leaching	H_2SO_4	Optional (650-750°C)
Onal et al [15]	2015	Scrap	Sulfation Leaching	H_2SO_4	750-800°C

A roasting stage may take place at 700°C to decompose iron sulfate into iron oxide, the latter being insoluble at pH higher than 2, and the sulfur trioxide released can be recovered and reused in the process. In 2015, Onal (2015) presented a similar process for Nd recovery from FeBNd scrap, where selective roasting is applied between 650-750°C. Verbaan (2015) reviewed 18 concentrate leaching projects and noticed that 11 of these used sulfuric acid as a primary lixiviant. Among these projects, seven are using roasting as part of the flowsheet. The authors state that, although sulfuric acid roasting is considered a mature technology in China, it is not a common processing technology in the Western World.

As mentioned in the previous paragraphs, there are several process routes for monazite processing, but none of them are clear with regards to their mechanisms or industrial advantages. The process described by Berni (2013) and further developed by Teixeira and Silva (2015) shows the possibility of rare earth extraction with low acid consumption and low impurity loading into the leaching solution, but the mechanisms behind this process are still unclear. Thus, the objective of the present investigation is to provide a thermodynamic background for the selective roasting method and apply such a technique to complex, iron-rich, monazite ores. The behavior of rare earth, thorium, and iron during this process is also discussed.

3.3 Experimental Procedure

3.3.1 Materials

Reagent grade ferric sulfate ($Fe_2(SO_4)_3$. xH_2O, Fe 22.0%min), 97.5% w/w sulfuric acid (Anidrol), 99.9% Lanthanum sulfate (Fmaia, La_2O_3/REO > 99.99%), and natural fines (<74µm) of a monazite ore from a phosphate mine were used in the experiments.

3.3.2 Rare Earth extraction

The extraction experiments were comprised of the following steps: (i) separation of natural fines (<74 µm) by scrubbing a 50% w/w suspended solid ore pulp for 15 min and passing this material through a 74 µm sieve (Testa et al., 2016); (ii) sulfation by mixing the natural fines (200g minimum) with sulfuric acid 97.5% w/w for 30 minutes using a 1.5 L mechanical mixer (Marconi, model MA259); (iii) roasting in a muffle-type furnace (K-type thermocouple) under air for 2 hours. The temperature profile of the furnace was measured and the highest region was used to set the target temperature The crucible was placed in this spot to ensure accuracy on temperature reading (iv) cooling the charge to 20°C, and (v) leaching the solids in water at 10% w/w for 2 hours at room temperature, under mechanical mixing (200-300 rpm). The pH was controlled (when necessary) between 1.5 and 2.0 by adding sulfuric acid (Mettler Toledo pH meter type M400). The REE extraction was performed following the procedure described by Teixeira and Silva (2015) and Berni (2013). The amount of acid added to each sample changed based on its composition, ranging from 0.21 to 0.34 kg of acid per kg of sample. Roasting temperature ranged from 200°C to 800°C.

3.3.3 Analytical Methods

The TGA-DTA analyses were performed in a NETZSCH STA 449F3 equipment, under synthetic air atmosphere in an alumina crucible with a heating rate of 10K min-1 up to 1000°C (1400°C for $La_2(SO_4)_3$). Sample mass varying from 30 to 45mg. Protective gas flow (nitrogen) of 20ml/min and purge gas flow of 20ml/min for nitrogen and 10ml/min for oxygen. Total atmosphere composition of 20% oxygen and 80% nitrogen.

Solid and aqueous solutions were analyzed by Inductively Coupled Plasma Optical Emission Spectrometry-ICP-OES (Varian, VISTA PRO model) and Inductively Coupled Plasma Mass Spectrometry (PerkinElmer ICP-MS, model NexION 300D). Duplicates, blanks and standards (DBS) were used during ICP analysis. Samples were subjected to an acceptable duplicate maximum mean error (ME) that varied with the method, the element and concentration. Prior to chemical analyses solid samples were dried in an oven at 100°C for at least one hour and pulverized to a condition in which 95% of the particles (in mass) were below 74 µm. The solid samples containing rare earth elements, thorium and uranium (DBS every 24 samples, ME between 10% and 5%) were treated by fusion with $Li_2B_4O_7$ or with H_2O_2 followed by dissolution in 10% (v/v) nitric acid (65% v/v). For the analyses of the remaining elements (DBS every 20 samples, ME between 10% and 5%), the samples were treated by fusion with Na_2CO_3 and $Na_2B_4O_7$, followed by dissolution in 67% (v/v) hydrochloric acid. The concentrations of aluminum, iron, phosphorous, sulfur, and the rare earths (Pr, Nd, and Sm) in the solids (after fusion/dissolution) and in aqueous solution after leaching were analyzed by ICP-OES (DBS every 20 samples, ME between 10% and 5%). The concentration of the remaining rare earth elements and other impurities (both from solid samples and leach solutions) were analyzed by ICP-MS, after dilution in 2% v/v nitric acid (65% v/v). Rare earth analysis from leach solutions had DBS analyzed every 20 samples and ME between 10% and 5%. The ferrous iron concentration in the leach solution was measured by straight titration with $K_2Cr_2O_7$ in acid solution using barium diphenylamine sulfonate as an indicator.

Samples for X-ray diffraction analysis (XRD) were ground below 74 µm (200 Mesh Tyler) and analyzed on PANalytical Model X´PERT PRO MPD (PW 3419) equipped with a PW3050/60 (θ/θ) goniometer, X-ray ceramics tubes, Co anode (Kα1=1.78897Å), and a PW3373/00 model detector (2000W-60kV). The diffraction patterns were acquired from 4º to 78° (2θ) at 0.02 steps. The identification of all minerals was done with X´PertHighScore version 2.1b software from PANalytical by using ICDD (International Center for Diffraction Data) files as a reference (2003 database).

Mineralogical characterization, modal composition, and mineralogical association were performed by XRD analysis, SEM, and QEMSCAN (Quantitative Evaluation of Minerals by scanning electron microscopy) analysis for fraction below 74µm. Polished sections were made for QEMSCAN and SEM analysis. The chemical results obtained for the given particle sizes were used for data reconciliation.

3.3.4 *Thermodynamic evaluation*

HSC chemistry (Outotec) version 8 (2015) provided the thermodynamic data (values for standard enthalpy, entropy, and Gibbs Free energy) and software to generate the stability diagrams.

3.4 Results and Discussions

3.4.1 Samples characterization

The chemical composition of the samples and the respective mineralogy are shown in Table 3.2 and Figure 3.1. The REO content of the samples is similar and falls within the range of 4-5% wt. The ore is rich in iron, with an Fe_2O_3 content of above 30% w/w in all samples, making iron the most abundant element. In the present work, light rare earth oxides (LREO) include elements from La to Nd, and heavy rare earth oxide (HREO) elements ranging from Pm to Lu, including Y and Sc; Gd was not analyzed due to Pr (141) interference. This definition is broadly accepted and better describes the samples. The LREO/REO ratio is similar in all samples (app. 96%).

Brod et al., (2000) defined the bebedourites as being comprised of diopside, phlogopite, magnetite, apatite, and perovskite, interpreted as the partially preserved portion of the intense phlogopitization undergone by the rocks of the complex. Foscorite are rocks composed of magnetite, apatite ($Ca_5(PO_4)_3(F,Cl,OH)$, and olivine $(Mg,Fe)_2SiO_4$, which is present as independent magmatic events, like veins or plugs cracking through silicate and carbonatite rocks in several directions. Ribeiro (2008) classified flogopitite as carbon-hydrothermal products derived from the bebedourite series. The lithotype definition is related to the unaltered rock. The samples of this study underwent transformation by weathering, resulting in a different mineralogy when compared to the lithotype definition.

Table 3.2 - Chemical composition of the selected samples

	Bebedourite	**Flogopitite**	**Foscorite**
Al (%)	2.96	3.16	2.80
Ba (%)	0.36	1.21	1.28
Ti (%)	12.34	7.53	9.88
Ca (%)	< 0.681	3.84	1.58
Fe (%)	25.79	21.81	24.05
Mg (%)	0.27	2.91	0.96
Mn (%)	0.64	0.78	0.77
P (%)	1.75	3.26	2.72
Si (%)	8.88	9.11	8.15
U (mg kg^{-1})	46	45	50
Th (mg kg^{-1})	352	181	233
REO	4.26	4.70	4.86
LREO/REO	96%	97%	96%

The samples used in this work were collected at the isalterite / aloterite level, which is marked by the disappearance of the phyllosilicates on a macroscopic scale. From this stage, the predominance of iron oxides/ hydroxides, clays, phosphates (primary and secondary), and minerals of supergenic alteration (anatase for example) can be observed.

The main REE carrier is monazite, but near to 5% w/w of REE is present in candrallite. This partition was estimated by EDS analysis and should be further investigated by an EPMA (Electron Probe Micro-Analyzer). Iron is mainly present as iron oxide/hydroxide and ilmenite (Figure 3.1).

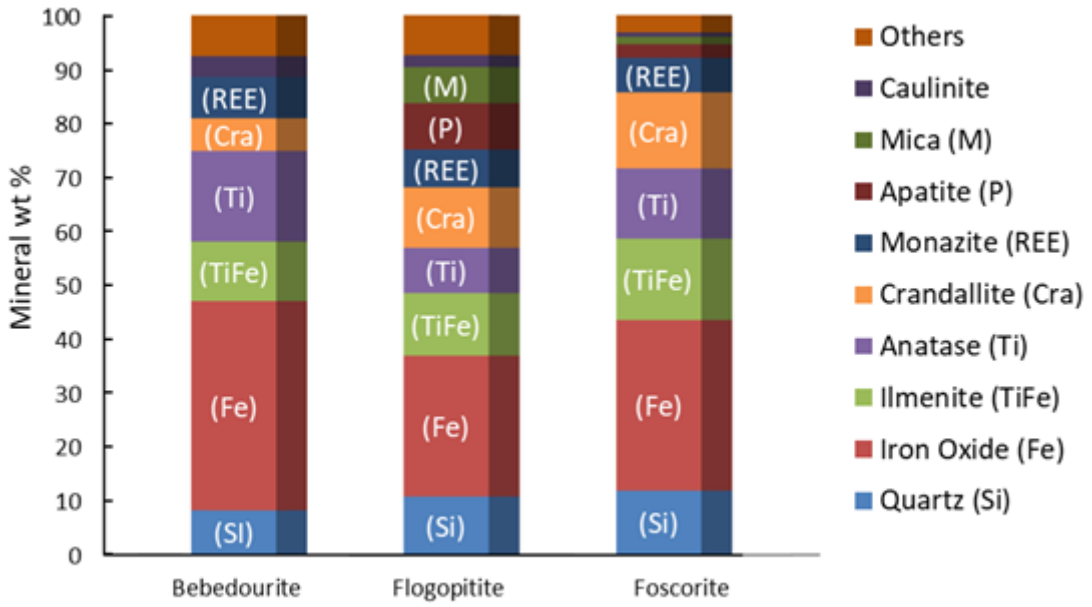

Figure 3.1 - Mineral composition diagram for Bebedourite, Flogopitite, and Foscorite samples (natural fines < 74 µm)

3.4.2 Thermodynamic analysis

In 1973, Bainbridge reported the possibility of achieving selective nickel extraction by gas sulfation, exploiting the difference in sulfate stability between iron and nickel. The same approach can be applied to iron-rich, rare earth ores. The stability of selected rare earth sulfates, iron sulfate, and other metal sulfates with respect to their oxides at the temperature range of 500-1000°C are shown in Figure 3.2. Sulfates formed by reactions at the top of this Fig. are less stable than those that appear at the bottom, with calcium being the most stable sulfate and aluminum the least stable. The results show a significant difference between the stability of iron and rare earth sulfates, particularly for cerium and lanthanum. The standard Gibbs free energy of formation of iron and aluminum sulfate becomes positive for temperatures over 800°C, while this property remains negative for the rare earth elements. This implies that the decomposition of iron and aluminum sulfate to their respective oxides (reverse reaction) may take place at higher temperatures, while the sulfates of rare earth elements will remain stable. Among the rare earth elements analyzed here, lanthanum sulfate is the most stable compound and neodymium the least stable.

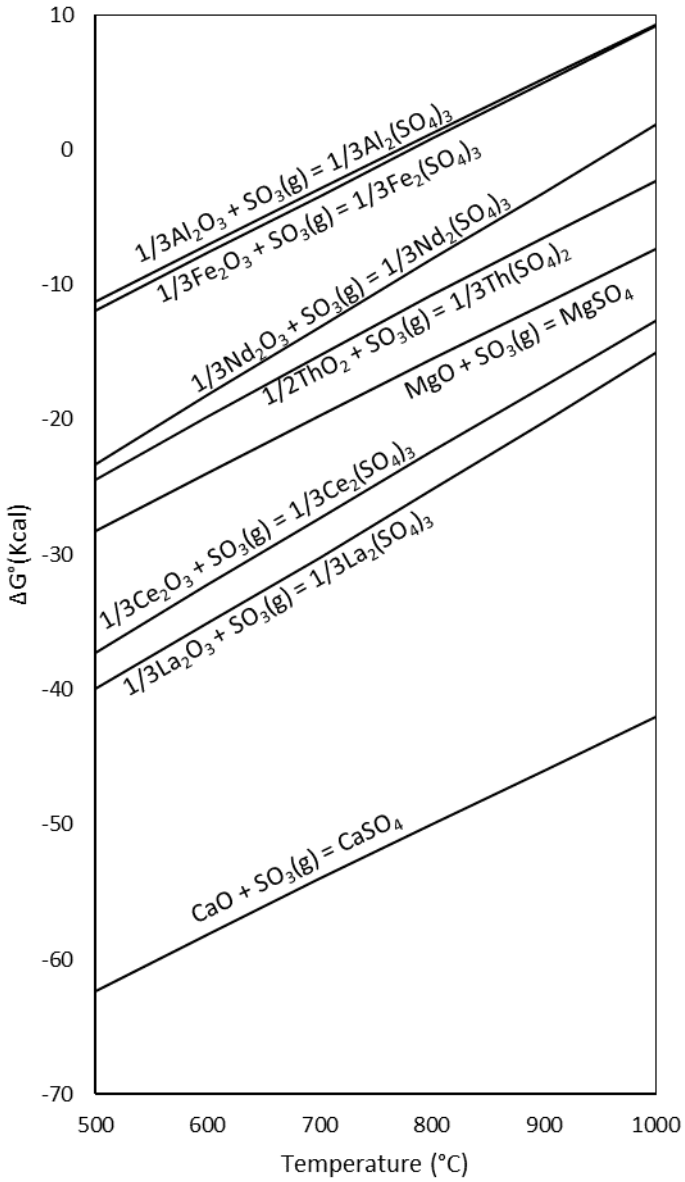

Figure 3.2 - Variation of the standard Gibbs free energy for the sulfation reaction for different oxides in the temperature range 500-1000°C (HSC v.8)

The thermal stability of different sulfates may also be discussed based on a thermal stability diagram, as shown in Figure 3.3. The diagram shows the stability of sulfates according to Eq. (3.3), where REE represent the rare earth elements and the Delta symbol indicates that heat is being added to the system.

$$REE_2(SO_4)_{3(s)} \xrightarrow{\Delta} REE_2O_{3(s)} + 3SO_{3\,(g)} \quad (3.3)$$

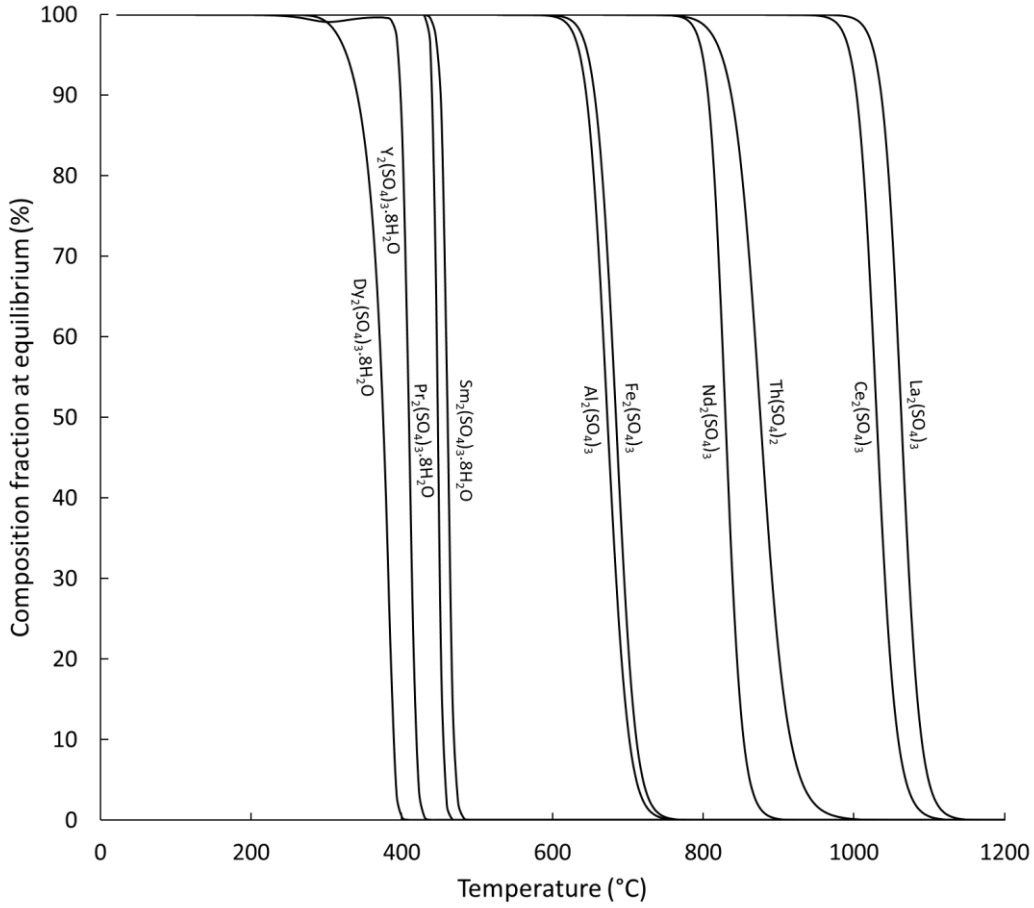

Figure 3.3 - Thermal stability for some rare earth sulfates and the main impurities present in the ore under simulated air atmosphere. The decrease in the fraction of the sulfate compound implies the proportional formation of the respective oxide.

The sulfation process proposed in this paper is expected to yield anhydrous sulfates, since no additional water is added during sulfation (the process occurs with only 2.5% wt. water contained in the concentrated sulfuric acid). The sulfation reaction itself is highly exothermic, thus driving off any water remaining in the ore. This is a favorable condition for the formation of anhydrous sulfates, and the presence of hydrated sulfates is unlikely. Nevertheless, the thermodynamic information for Dy, Y, Pr, and Sm were available only as hydrated sulfates and, therefore, these species were kept in the diagram for comparison purposes only. The diagram shows a significant temperature difference between the decomposition of iron sulfate and anhydrous rare earth sulfates: about 150°C for neodymium (750°C→900°C) and even higher for lanthanum (750°C→1100°C). These findings support the use of selective roasting at temperatures over 750°C and under 900°C (to avoid neodymium sulfate

decomposition). Temperatures between 750°C and 900°C would allow for the decomposition of iron sulfate and the formation of iron oxide while keeping most rare earth elements as soluble sulfates. Iron sulfate is soluble in water whereas ferric oxi-hydroxides are insoluble at pH higher than approximately 2. This approach would allow for a high extraction of rare earth elements and a low extraction of iron from a sulfated sample submitted to selective roasting. Following the diagram, hydrated sulfates of Dy, Y, Pr and Sm would also decompose into oxides, yielding low extraction values for these elements.

3.4.3 TGA analysis

To confirm the thermodynamic simulation, the decomposition of ferric sulfate and lanthanum sulfate was investigated by TGA analysis. The results are shown in Figure 3.4, including the result obtained for a sulfated (after mixing with sulfuric acid) foscorite sample. A very good agreement was observed between the simulated thermal behavior of the sulfates with the result obtained from the TGA analysis. Although not represented in Figure 3.4, the dehydration temperature for lanthanum sulfate took place at temperatures lower than 300°C, which is in agreement with other reports (Wendlandt and George, 1961). However, two points of disagreement may be pointed out: the temperature of dehydration of ferric sulfate and the decomposition pattern of lanthanum sulfate.

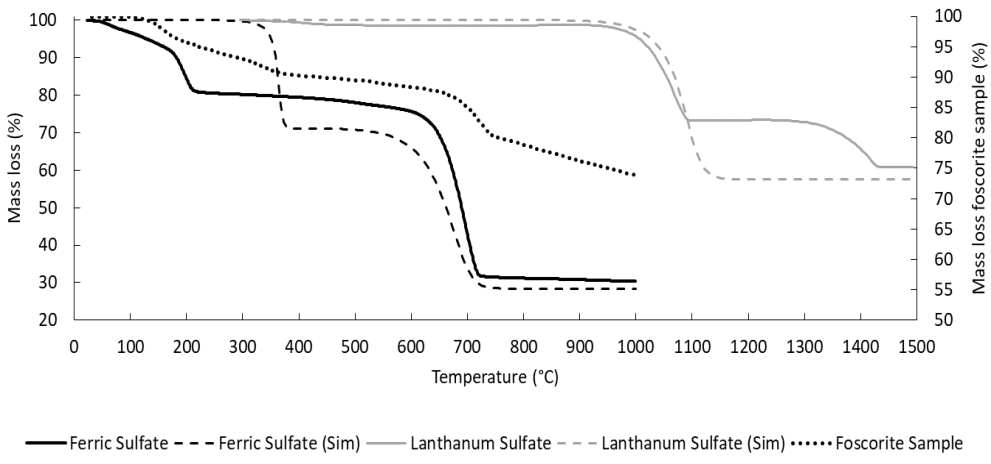

Figure 3.4 - TGA results for hydrated ferric sulfate ($Fe_2(SO_4)_3.9H_2O$) and anhydrous lanthanum sulfate under synthetic air atmosphere and 10K min^{-1}. The dotted lines are simulations based on HSC thermodynamic data.

The hydrated ferric sulfate loses its water molecules at temperatures below 250°C, but the simulated TGA shows temperatures of about 400°C. Although 150°C seems to be a considerable temperature difference, it is not relevant since the formation of hydrated sulfates in this system is unlikely to happen, as discussed before. The simulated system considered the dehydration of $Fe_2(SO_4)_3.9H_2O$ directly into an anhydrous ferric sulfate. The real process may take place following successive water loss, hence giving results like that obtained for the $Fe_2(SO_4)_3.7H_2O$ sample. The difference in the decomposition pattern of lanthanum sulfate is more relevant. The TGA result shows a two-step decomposition under a synthetic air atmosphere. The first step shows a mass loss of about 27%, while the expected total mass loss for complete sulfate decomposition is about 42%. This intermediary mass loss may indicate partial decomposition of lanthanum sulfate to oxysulfate, $La_2O_2SO_4$ (Nathans and Wendlandt, 1962; Lowell et al., 1970).

By using the same technique, Poston (2003) reported different decomposition temperatures, with lanthanum sulfate decomposition starting at 775°C. This difference was likely due to the different atmosphere applied during the TGA analysis. Oxidative atmospheres lead to higher decomposition temperature (1100°C), inert atmosphere to intermediate temperatures (775°C), and reducing atmosphere to low temperatures (610°C) (Hwdwgus and Fukker, 1956).

The foscorite sample is a complex assemblage of several compounds (Figure 3.1) and thus displays a mass loss during the entire temperature range of the experiment (Figure 3.4). However, it is possible to observe a sharp mass loss at 700°C, in good agreement with the simulated and the experimental decomposition temperature found from TGA for ferric sulfate decomposition to ferric oxide. The decomposition of trivalent rare earth elements and impurities like ferric sulfate can be described by Eqs. (3.4), (3.5), and (3.6). The existence and amount of SO_3 in the gas phase is defined by the equilibrium constant at a given temperature (Eq. (3.7)).

$$REE_2(SO_4)_{3(s)} \xrightarrow{\Delta} REE_2O_{2(s)}(SO_4)_{(s)} + 2SO_{2\,(g)} + O_{2\,(g)} \quad (3.4)$$

$$REE_2O_2(SO_4)_{(s)} \xrightarrow{\Delta} REE_2O_{3(s)} + SO_{2_{(s)}} + \frac{1}{2}O_{2\,(g)} \quad (3.5)$$

$$Fe_2(SO_4)_{3(s)} \xrightarrow{\Delta} Fe_2O_{3(s)} + 3SO_{2_{(g)}} + \frac{3}{2}O_{2\,(g)} \quad (3.6)$$

$$SO_{2(g)} + \frac{1}{2}O_{2\,(g)} \rightarrow SO_{3_{(g)}} \quad (3.7)$$

3.4.4 REO extraction

Sulfated samples of the three different lithotypes were submitted to temperatures ranging from 200°C to 800°C and leached in water under controlled pH. The REO extraction was calculated for each sample. It is defined as the ratio between the amount of remaining REO in the filter cake after water leaching and the initial amount contained in the sample. The results are shown in Figure 3.5. Maximum REO extraction was attained at about 700°C, which varied from 73% to 82%, depending on the sample (Figure 3.5 (a)). Acid addition ratios were 0.250, 0.210, and 0.340 kg of sulfuric acid per kg of ore, for foscorite, bebedourite, and flogopitite, respectively. The acid addition was a function of the sample composition in which elements from the alkaline and alkaline earth groups are the main acid consumers, followed by phosphor, iron, and aluminum. A sharp drop in REO extraction can be noticed for temperatures higher than 700°C, reaching extractions close to 0% at 800°C. This result is unexpected, since the decomposition of lanthanum sulfate (responsible for 24% of total rare earth oxides), is expected to take place at 1100°C, according to TGA results. The iron and thorium extraction (Figure 3.5 (b)) fell drastically at 700°C, reaching values of lower than 1%. This behavior agrees with TGA results and thermodynamic simulation. The low thorium extraction may be attributed to the atmosphere inside the sample, which may have affected its decomposition in the same way as it affected the rare earth decomposition at temperatures higher than 700°C. This drastic decrease in Th extraction takes place at temperatures 50°C lower than that for REE, creating a window for selective extraction for rare earth. If the ore is heated at 700°C, it is expected to attain a maximum REO extraction and a lower Th and Fe extraction. This scenario is favorable for downstream processing, because iron should be extracted before REE separation by solvent

extraction. Thorium, in particular, will follow REE in the downstream process, and even if it is further removed, it may cause disposal problems due to its radioactive nature.

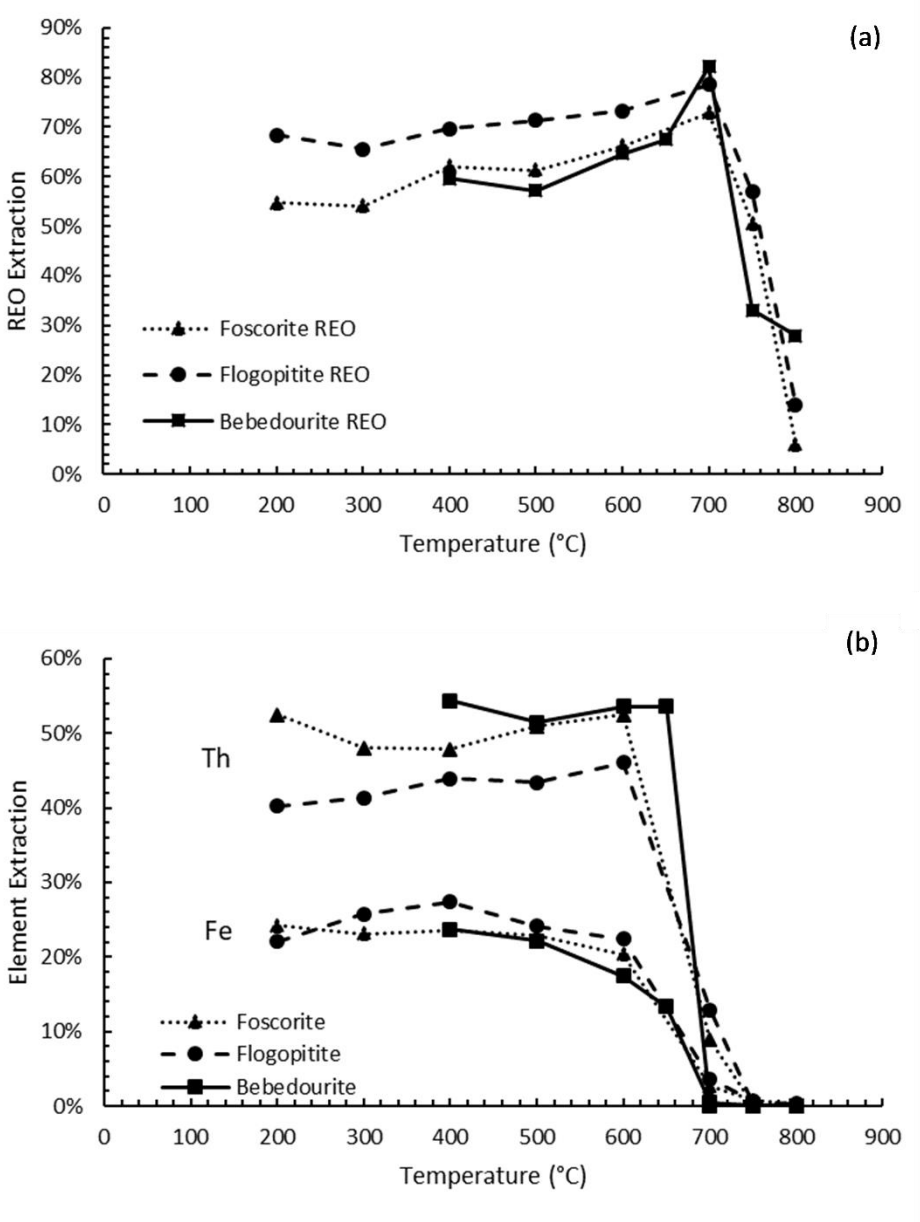

Figure 3.5 - (a) Rare earths, and (b) iron and thorium extraction obtained for three different lithotypes. Sulfuric acid addition of 0.25, 0.21, and 0.34 kg/kg of ore. Mixing time of 15 min.

The decomposition behavior for some hydrated heavy rare earth sulfates (Dy, Y, Pr and Sm) shown in Figure 3.3 (300-500°C) was not confirmed by the experimental data, since the ratio LREE/HREE was kept the same after roasting at 700°C and water leaching. This decomposition behavior agrees with that reported by Nathans and Wendlandt (1962).

Other reactions, apart from Eqs. (3.1) to (3.7), may be taking place during heating. Eq. (3.8) and Eq. (3.9) are examples of the reverse reaction for sulfation and may take place at temperatures higher than 400°C where sulfuric acid has already decomposed into gaseous SO_3 and H_2O. The formation of insoluble phosphates or the presence of a reducing atmosphere inside the ore charge may be responsible for the decrease in rare earth extraction at temperatures of higher than 750°C, and the decrease in thorium extraction at temperatures of higher than 700°C. These mechanisms are under investigation and the results will be discussed in future works.

$$REE_2(SO_4)_{3(s)} + 2H_3PO_{4(l)} \xrightarrow{\Delta} 2REEPO_{4(s)} + 3H_2O_{(g)} + 3SO_{3\,(g)} \quad (3.8)$$

$$REE_2(SO_4)_{3(s)} + P_2O_{5(g)} \rightarrow 2REEPO_{4(s)} + 3SO_{3\,(g)} \quad (3.9)$$

The increase in REO extraction at 700°C may be due to structural changes taking place in the crandallite structure (Francisco et al., 2007), a mineral which hosts some of the REE present in the ore.

3.5 Conclusions

The behavior of rare earth, thorium, and iron during selective extraction of rare earth ores were discussed. Our findings indicated that rare earth bearing monazite ores may be selectively treated to separate iron and thorium from rare earth elements if submitted to sulfation, roasting at 700°C, and water leaching under controlled pH. This process promotes high rare earth extraction (between 70-80%), low iron, and thorium extraction (below 1%) with low acid consumption (between 0.21 to 0.34 kg of acid for 1 kg of ore). There was very good agreement for sulfate decomposition between thermodynamic simulation and TGA results for iron and lanthanum sulfates. The results also show that lanthanum sulfate decomposes in a two-step process, likely forming $La_2O_2SO_4$ as an intermediate compound, which could not be predicted from thermodynamic evaluation. The key stage for selective extraction is roasting, in which iron sulfate decomposes into iron oxide and releases SO_3 gas. The iron sulfate decomposition is achieved at 700°C, a condition in which rare earths achieve maximum extraction. The amount of insoluble rare earth compounds increases sharply at temperatures of

higher than 750°C, decreasing the amount of recoverable rare earth elements during the leaching step and therefore rendering the processes ineffective for rare earth extraction. This temperature is lower than expected for sulfate decomposition into oxides and may be related to the formation of phosphate compounds.

3.6 References

Bainbridge DW (1973) Sulfation of a nickeferous laterite, Materials Transaction 4 (7):1655-1658.

Berni TV, Pereira AC, Mendes FD, Tude AL (2013) System and Method for Rare Earth Extraction. Patent US 2013/0336856 A1.

Boudreault R, Primeau D, Fournier J, Simoneau R, Garcia MC, Krivanec H, Dittrich C (2012) Process for recovering rare earth elements from various ores, EP 3141621A1.

Brod JA, Gibson SA, Thompson RN, Junqueira-Brod TC, Seer HJ, Moraes LC, Boaventura GR (2000) Kamafugite affinity of the Tapira alkaline-carbonatite complex (Minas Gerais, Brazil), Revista Brasileira de Geociências 30:404-408.

Francisco EAB, Prochnow LI, Toledo MCM, Ferrari VC, Jesus SL (2007) Thermal treatment of aluminous phosphates of the crandallite group and its effect on phosphorus solubility, Sci. Adric., (Piracicaba, Brazil), 64(3):269-274 DOI (http://dx.doi.org/10.1590/S0103-90162007000300009)

Gupta, C K, Krishnamurthy, N (2005) Extractive metallurgy of rare earths, CRC Press, Nova York

HSC Chemistry 6/8 (2015), Equilibrium calculations, Outotec, Pori, Finland.

Huang X, Li H, Long Z, Liu Y, Zhao N, Zhang G (2009) A process of smelting monazite rare earth ore Rich in Fe, WO2009/021389

Hwdwgus AJ, Fukker K (1956) Ver. Gluhlampen-u. Elektrizitats-werke, A.-G., Tungsram, Budapest, Z. Anorg. Allg. Chem. 284:20-30.

Lowell PS, Schwitzgebel K, Parsons TB, Sladek KJ (1970) Selection of metals oxides for removing SO2 from fuel gas, I&DC Research Results Service, ACS.

Lucas J, Lucas P, Le Mercier T, Rollat A, Davenport, WGI (2014) Rare earth: science, technology, production and use, 1st ed., Elsevier.

Mackowski SJ, Raiter R, Soldenhoff KH, Ho EM (2009) Recovery of rare earth elements, US2009/0272230 A1.

Merritt, R R (1990) High temperature methods for processing monazite: reaction with calcium chloride and calcium carbonate, Journal of Less-Common Metals 166:197-210.

Nathans MW, Wendlandt WW (1962) The thermal decomposition of the rare-earth sulphates, J. Inorg. Nucl. Chem. 24:869-879.

Onal MAR, Borra CR, Guo M, Blanpain B. (2015) Recycling of NdFeB Magnets Using Sulfation, Selective Roasting and Water Leaching. J. Sustain Metall. 1:199-215.

Poston JA Jr, Siriwardane RV, Fisher EP, Miltz AL (2003) Thermal decomposition of the rare earth sulfates of cerium (III), cerium (IV), lanthanum (III) and samarium (III), Applied Surface Science 214:83-102.

Pradip, Fuerstenau, DW (1991) The role of inorganic and organic reagents in the flotation separation of rare-earth ores, Internal. J. of Min. Processing 32:1-22.

Renou A, Tognet J (2003) Procede de traitement d`un minerai de terres rares a teneur elevee en fer, FR2 826 667 – A1, France.

Ribeiro CC (2008) Geology, Geometallurgy, Controls and genesis of phosphorus deposits, rare earths and titanium of the Catalão carbonate complex I, Goias. Dr. Thesis, Universidade de Brasília (in portuguese).

Teixeira LAV, Silva RG (2014) System and process for selective rare earth extraction with sulphur recovery. Patent US 2015/0329940 A1.

Testa, FG, Avelar, AN, Silva, RG, Souza, CC (2016) mineralogical characterization and alternative to concentrate the rare earth lithotypes from alcaline complex of Catalão – GO. Associação Brasileira de Metalurgia, Materiais e Mineração, São Paulo, DOI (http://dx.doi.org/10.4322/2176-1523.1064)

Verbaan N, Bradley K, Brown J, Mackie S (2015) A review of hydrometallurgical flowsheets considered in current REE projects, In: Simandl GJ and Neetz M (eds.) Symposium on Strategic and Critical Materials Proceedings. British Columbia Ministry of Energy and Mines, British Columbia Geological Survey Paper 2015-3, Victoria, British Columbia, pp. 147-162.

Wendlandt WW, George, TD (1961) A Differential thermal analysis study of the dehydration of the rare-earth (iii) sulphate hydrates. The Heats of Dehydration, J. Inorg. Nucl. Chem. 19:245-250.

Zhang J, Zhao B and Schereiner B (2016) Separation hydrometallurgy of rare earth elements, Springer, Switzerland.

4 STABILITY OF LANTHANUM IN SULFATE AND PHOSPHATE SYSTEMS AND IMPLICATIONS FOR SELECTIVE RARE EARTH EXTRACTION[2]

4.1 Introduction

Rare earth elements (REE) are essential to modern industry. The main drivers for its consumption are the catalyst, magnets, polishing powders, and rechargeable battery electrodes. Other relevant applications for these elements can be found in the metallurgical, ceramics, phosphor, pigment, and glass industries (Lucas et al., 2015).

Rare earth elements are extracted from four main sources, namely, bastenaesite (Ce,La,Y)(CO_3)F, monazite (Ce,La,Pr,Nd,Th,Y)PO_4, xenotime (YPO_4) and ion-adsorption clays (Gupta and Krishnamurthy, 2005). China is the major producer, with Bayan Obo being its main production site. Mountain Pass (USA) and Mount Weld (Australia) are also worth mentioning for their relevance and production capacities. Figure 4.1 shows a simplified flowsheet for these three most relevant operations in the world. Mountain Pass is a typical bastnaesite deposit, while Bayan Obo processes a mixture of bastnaesite and monazite. Mount Weld, by contrast, is a weathered monazite deposit. All of these processing routes require a heating stage prior to the application of hydrometallurgical processes. This flowsheet configuration is also present in the processing design for new deposits, as most use sulfuric acid and require a heating stage as a preparation before leaching (Verban et al., 2015).

Bastnaesite ores often undergo physical concentration (flotation, magnetic concentration, gravity concentration) to about 60% Rare Earth Oxides (REO) prior to further processing. In China, the mixed concentrates are roasted with sulfuric acid (H_2SO_4) at approximately 500°C in a rotary kiln. This condition promotes the release of CO_2 and HF from the concentrates and the formation of water-soluble, REE sulfates. Mountain Pass also used to calcine the concentrate at a slightly higher temperature (650°C). This process, when carried out under an oxidative atmosphere, promotes the release of CO_2 from the concentrate while Ce (III) oxidizes to Ce (IV). The material leaving the furnace was leached in 30% (v/v) HCl solution at room temperature, a condition in which the REEs are

[2] This chapter was published by Teixeira et al. (2020), Minerals Engineering 155, p1-11.

dissolved, except Ce (IV), which remains in a solid phase (Gupta and Krishnamurthy, 2005). Following leaching, different approaches may be applied to solution purification, depending on the liquor composition.

In Mountain Pass, the purification removed iron and thorium by precipitation, followed by solvent extraction (SX), thus producing a purified solution ready for the final separation of the REE. In Bayan Obo, the purification selectively separates the REE by precipitation as double sulfates, which are then converted into hydroxides and leached in an HCl solution, prior to SX separation.

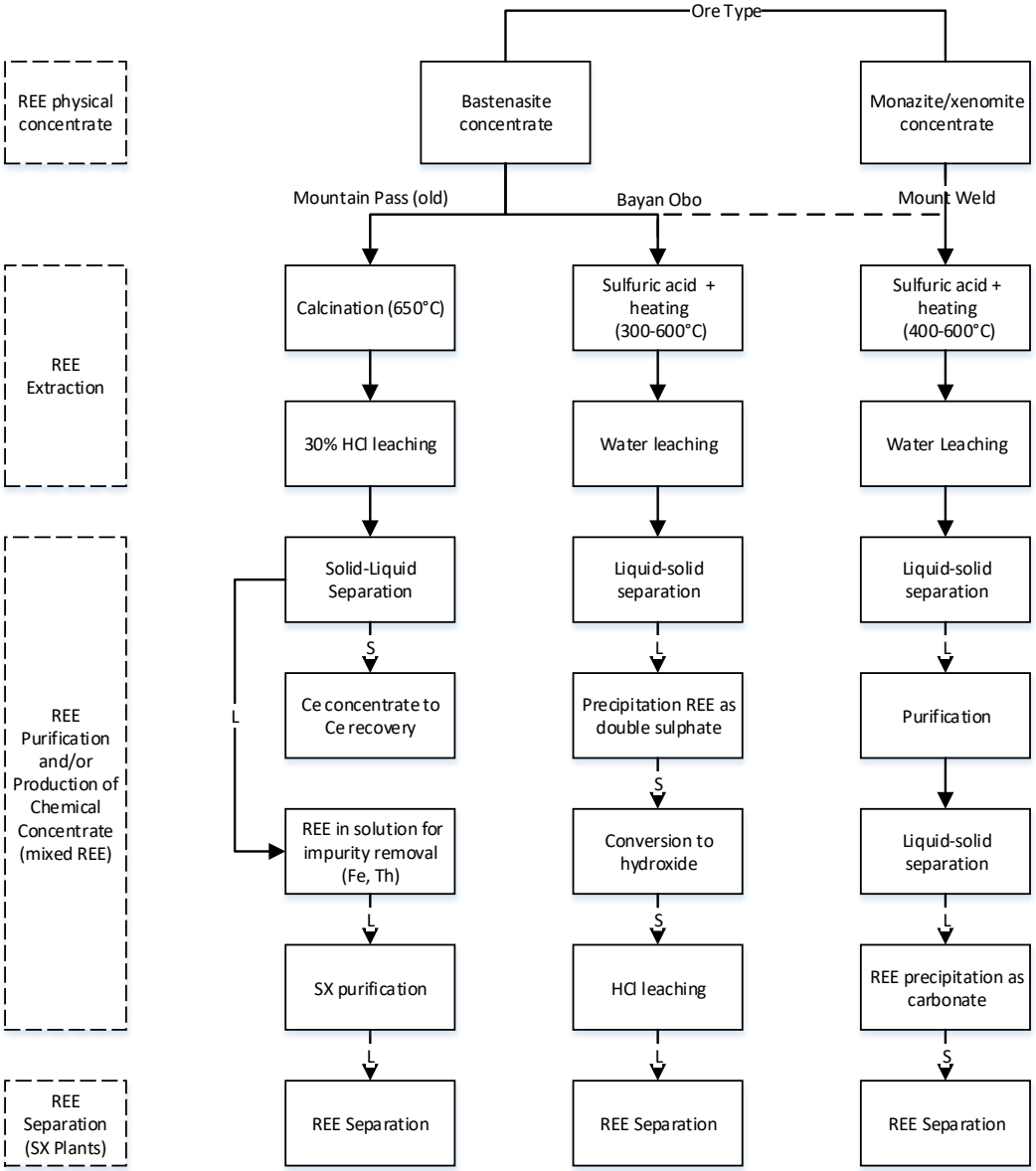

Figure 4.1 - The main rare earth processing routes (modified from Walters and Lusty (2011), after Lucas et al (2015) and Gupta and Krishnamurthy (2005))

Monazite is the second most important REE mineral and is usually found in complex ore bodies exposed to intensive weathering, thus resulting in refractoriness to conventional physical beneficiation due to very fine, micro-level association between the main REE-carrying mineral (monazite) and the gangue material (goethite and ilmenite, among others). This means that the solids fed to the leaching tanks often exhibit low REE content, but high content of acid-consuming contaminants, like iron. Mount Weld (Figure 4.1) is an exception to this general trend, as the ore is amenable to some degree of physical concentration. After sulfation, the concentrate is roasted within a range of 400-600°C and leached in water. Purification, REE precipitation, and final separation of the REEs are also reported.

As illustrated by Figure 4.1, the purification and precipitation stages following the REE dissolution consist of a number of unit operations, resulting in several possible process flowsheets (Silva et al., 2018). Therefore, approaches to minimize the dissolution of impurities during leaching would reduce the complexity and costs associated with the purification stages. Within this context, a selective process for REE extraction over iron and thorium was discussed by the authors (Teixeira et al., 2019). The process is based on a “temperature window” established by the differences in the decomposition conditions of sulfates, namely REE, iron, and thorium sulfates during roasting. A thermodynamic analysis of the system indicated a temperature gap of about 150°C: from 750°C (ferric sulfate decomposition) to 900°C (neodymium sulfate decomposition). However, experimental results obtained for a monazite ore from a phosphate mine demonstrated a much narrower gap, only 50°C, between 750°C and 800°C. Two possible phenomena may be taking place during the heating stage, according to the literature. The first would be the formation of an intermediary phase, such as the oxysulfate phase ($La_2O_2SO_4$) (Onal et al., 2015). These authors investigated the selective roasting of permanent magnet scrap, in an attempt to separate iron from neodymium and praseodymium. Thus, a maximum REE extraction at 750°C was observed. The extraction decreases as temperature increases, reaching 95% for Nd and Pr at 800°C and 85% at 850°C. Onal et al. (2015) attributed this decrease to the formation of an oxysulfate phase, as represented by equation (4.1).

$$(\mathrm{REE})_2(SO_4)_{3(s)} \xrightarrow{\Delta} REE_2O_2SO_{4(s)} + 2SO_{2(g)} + O_{2(g)} \quad (4.1)$$

As the oxysulfate phase is not water soluble, the REE extraction decreases. The formation of lanthanum oxysulfate was confirmed by Thermogravimetric Analysis (TGA), as described elsewhere (Teixeira et al., 2019). However, it took place only around 1000-1100°C, a temperature much higher than that of 850°C reported by Onal et al. (2015). The decrease in REE extraction between 750°C and 850°C described by these authors was significantly milder than the drop to extraction levels as low as 10% that it was observed in ore roasting.

A second hypothesis to explain the extraction drop would be the formation of insoluble REE phosphates due to the reaction between REE sulfate and excess phosphorus present in the monazite ore, extracted from a phosphate mine. Phosphoric acid (H_3PO_4) can be formed by the reaction between monazite and sulfuric acid:

$$2(\mathrm{REE})\mathrm{PO}_{4(s)} + 3\mathrm{H}_2\mathrm{SO}_{4(aq)} \rightarrow 2\mathrm{H}_3\mathrm{PO}_{4(l)} + (\mathrm{REE})_2(\mathrm{SO}_4)_{3(s)} \quad (4.2)$$

This hypothesis was suggested by Demol et al. (2018) during their investigation on the effect of a baking temperature of a rich (>90%) monazite sample. This high monazite content favored the release of phosphorus compounds, making the reagent available for back reaction. The occurrence of a similar phenomenon in the typical, complex mineralogical assembly of actual ore samples, has yet to be explored.

The present work is part of a broader investigation focusing on the application of roasting for improving the selective extraction of REE. More specifically, the hypothesis that soluble REE sulfates are back transformed to REE phosphate during roasting is analyzed in detail. The experimental approach encompassed the analysis of the leaching residue of an iron and phosphorus-rich monazite ore, thermodynamic simulation, and roasting experiments with pure reagents designed to clarify the phases involved and the mechanism behind phase transformation. The results are expected to contribute to a better understanding of the factors favoring selectivity in REE extraction over iron from monazite ores.

.

4.2 Experimental Procedure

4.2.1 Materials

Two distinct samples were used in this work: ore samples received from a Brazilian phosphate mine and a solid residue obtained from the production process of synthetic rutile (TiO_2). The ore sample was subjected to the REE extraction procedure, and the solid residue produced by step (v), as detailed below, was used in this investigation. The ore sample composition, described in detail elsewhere (Teixeira et al., 2019), showed REO, Fe, Th, and P ranging from 4.3-4.9%, 21.8-25.8%, 181-352 mg.kg-1, and 1.8-3.3%, respectively. The main mineral phases are iron oxides/hydroxides (25-35%), ilmenite (10-15%), anatase (5-20%), and quartz (5-10%). The REEs are present in the form of monazite (95%) and crandallite (5%).

The extraction experiments consisted of the following steps: (i) separation of natural fines (<74 µm) by scrubbing a 50% w/w suspended solid ore pulp for 15 min and passing this material through a 74 µm sieve (Testa et al., 2016); (ii) sulfation by mixing the natural fines (200 g minimum) with sulfuric acid (H_2SO_4) 97.5% w/w (Anidrol) for 30 min using a 1.5 L mechanical mixer (Marconi, model MA259); (iii) roasting in a muffle-type furnace (K-type thermocouple) under an air atmosphere for 2 h; (iv) cooling the charge to 20°C and (v) leaching the solids in deionized water at 10% w/w for 2 h at room temperature, under mechanical mixing (200-300 rpm). The pH was controlled using a pH meter (Mettler Toledo M400) and, when necessary, it was adjusted to between 1.5 and 2.0 by adding sulfuric acid. REE extraction was performed following the procedure described by Teixeira and Silva (2015) and Berni et al. (2013). The amount of acid added to each sample changed based on the amount of acid-consuming compounds in each sample, ranging from 0.21 kg to 0.34 kg of acid per kg of sample. Roasting temperature ranged from 200°C to 800°C.

REE phosphate from the secondary source (spray roaster residue) presented a very fine particle size, not requiring a screening step. This sample was submitted to the same procedure described above. The acid:residue mass ratio was fixed to 1.2:1.0.

Experiments were also performed using reagent grade lanthanum sulfate (Fmaia, 99.9% purity), phosphoric acid (Anidrol, 85% w/w purity), and phosphor

pentoxide (Sigma-Aldrich, >98% purity). The materials were mixed in an alumina crucible and submitted to 800°C for 2 h. The experimental setup allowed direct contact between the reagents, thereby promoting solid/liquid reactions (lanthanum sulfate + phosphoric acid) and solid/solid reactions (lanthanum sulfate + phosphorus pentoxide). Some additional experiments were carried out, using 2 concentric alumina crucibles, to investigate gas/solid reactions (Figure 4.2). While the gas releasing phases (phosphorus pentoxide or phosphoric acid) were added to the outer crucible, lanthanum sulfate was added to the inner crucible. The released gas flowed from the outer crucible into the inner crucible through sieve-like holes in the bottom of the inner crucible.

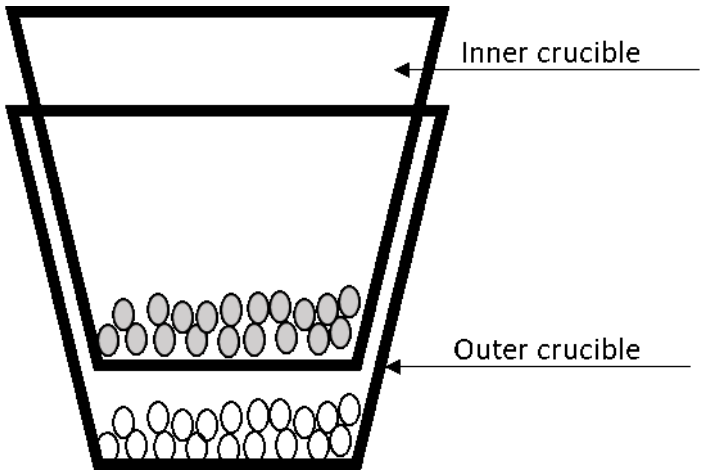

Figure 4.2 - Experimental apparatus used for gas/solid experiments. Lanthanum sulfate was added to the inner alumina crucible. This crucible had sieve-like holes in the bottom part. Phosphoric acid or phosphor pentoxide were added to the outer alumina crucible

4.2.2 Thermodynamic Simulation

HSC Chemistry (version 8, Outotec, 2015) provided the thermodynamic data (values for standard enthalpy, entropy, and Gibbs Free energy) and software to generate the stability diagrams. The thermodynamic data for the species considered in the simulations are listed in Appendix A.

4.2.3 Analytical Methods

The chemical composition of solids and aqueous solutions was determined by Inductively Coupled Plasma Optical Emission Spectrometry (ICP-

OES) (Varian, VISTA PRO model) and Inductively Coupled Plasma Mass Spectrometry (ICP-MS) (PerkinElmer, model NexION 300D). Duplicates, blanks and certified standards (DBS) were used during these analyses. All the samples were subjected to an acceptable (further defined) duplicate maximum mean error (ME) that varied with the method, the analyzed element and its concentration. Prior to the chemical analyses, the solid samples were dried in an oven at 100°C for at least one hour and pulverized to a condition in which 95% of the particles (in mass) were below 74 µm. The solid samples containing rare earth elements, thorium and uranium (DBS every 24 samples, ME between 10% and 5%) were digested by fusion with $Li_2B_4O_7$ or H_2O_2 addition followed by dissolution in 10% (v/v) nitric acid (HNO_3) 65% v/v (Anidrol). For analyses of the remaining elements (DBS every 20 samples, ME between 10% and 5%), the samples were digested by fusion with Na_2CO_3 and $Na_2B_4O_7$, followed by dissolution in 67% (v/v) hydrochloric acid (HCl) 35% (Anidrol). The concentrations of aluminum, iron, phosphorous, sulfur, and the rare earths (Pr, Nd, and Sm) in the solids (after fusion/dissolution) and in aqueous solution after leaching were analyzed by ICP-OES (DBS every 20 samples, ME between 10% and 5%). The concentration of the remaining rare earth elements and other impurities (both from solid samples and leach solutions) were analyzed by ICP-MS, after dilution in 2% v/v HNO_3 (65% v/v). Rare earth analysis from leaching solutions had DBS analyzed every 20 samples and ME between 10% and 5%. The ferrous iron concentration in the leach solution was measured by straight titration with $K_2Cr_2O_7$ in acid solution using barium diphenylamine sulfonate as an indicator.

The mineral composition, morphology and thermal behavior of solid samples were also evaluated in this work. Samples for X-ray diffraction analysis (XRD) were ground below 74 µm (200 Mesh Tyler) and analyzed on PANalytical Model X´PERT PRO MPD (PW 3419) equipped with a PW3050/60 (θ/θ) goniometer, X-ray ceramics tubes, Co anode (Kα1=1.78897Å), and a PW3373/00 model detector (2000W-60kV). The diffraction patterns were acquired from 4º to 78° (2θ) at 0.02 steps. The identification of all minerals was done with X´PertHighScore version 2.1b software from PANalytical by using ICDD (International Center for Diffraction Data) files as reference (2003 database).

The morphology of solid samples was characterized by SEM (Scanning Electron Microscope) using a Hitachi (SU3500) microscope equipped with EDS (energy-dispersive X-ray spectrometry) using a Bruker (XFlash 6/30) spectrometer and QEMSCAN 650. In order to avoid dissolution of sulfate compounds, polished sections for SEM images were prepared by using isopropyl alcohol during polishing.

The thermal behavior of solid samples was evaluated by thermogravimetric analysis (TGA) coupled to a quadrupole mass spectroscopy (QMS) using a Netzsch (STA 449 F3Jupiter) with alumina crucible with temperature ranging from 25°C to 1000°C at heating rate of 10°C/min under nitrogen atmosphere.

4.3 Results and Discussion

Figure 4.3 shows the REE extraction by leaching after sulfation and roasting at different temperatures. The results obtained from different lithotypes of a monazite ore are compared with those from a spray roaster residue obtained from anatase-rutile conversion. The composition of this residue is shown in Table 4.1. Compared to the ore, the residue contains lower iron (16%) and higher P (12%) and REE (10%) contents, being 96% of the REE comprised of La, Ce, Pr and Nd and 4% comprised of the remaining REE. The latter was tested to evaluate if the drastic extraction decreases at 800°C was a phenomenon related to the sample matrix. The REO extraction pattern was very similar to those obtained for the REE ore samples and displayed a sharp decrease in REO extraction for temperatures over 750°C. This result indicates that the selective roasting may be applied to a variety of raw materials, and that the phenomena behind the decrease in extraction at temperatures higher than 800°C is not related to the raw material genesis, but more likely to its composition or processing conditions. Other reactions, not considered in our original thermodynamic simulation, may have taken place during roasting, thus making the REE unamenable to further dissolution in an aqueous sulfate solution.

Table 4.1 - Chemical composition (mass %) of a REE-rich spray roaster sample from anatase-rutile conversion

Al	Ba	Ti	Ca	Fe	Mg	Mn
13.3	1.2	12.3	3.0	16.0	0.3	1.6

P	Si	K	S	U[1]	Th[1]	REE
11.7	<0.39	0.13	0.01	116	45.77	10.0

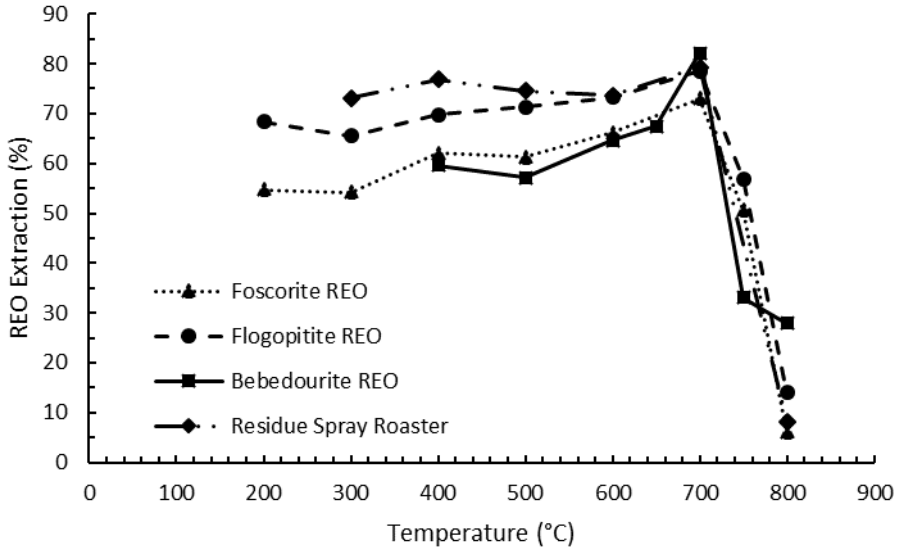

Figure 4.3 - Extraction of rare earth oxides from three lithotypes of a monazite ore and a REE-rich residue obtained from the production process of synthetic rutile. All samples were sulfated, roasted and leached as described in the text.

4.3.1 Microscopic evidence of neo-phosphate phases during roasting

Figure 4.4 shows typical images produced by Backscattered Electrons (BSE) obtained from particles containing REE after different stages of the sulfation-roasting-leaching process. The REE was associated with phosphorus in the initial monazite sample, as expected (Figure 4.4 (a)). After sulfation, the brightness of the REE-containing particles decreased, as shown in Figure 4.4 (b), most likely due to the presence of sulfur and oxygen. Small bright spots were noticed for sulfated samples roasted at 500°C, which increase with the increase in temperature. Samples roasted at 800°C showed a large number of bright spots (Figure 4.4 (c)), and the amount of sulfur proved to be lower when compared to any other condition (between 9-15 atomic percentage - at.%- for 700°C samples and about 2 at.% for 800°C samples). Phosphorus content associated with REE was higher in those samples (between 11-15 at.%) when compared to other temperatures (e.g., 4-5%, at 700°C). Different types of particle surfaces were revealed, like irregular small dots that may suggest the formation of a new compound at 800°C. The leaching residue from samples heated at 800°C is shown in Figure 4.4 (d) and resembles the initial ore sample, but the particles

show a porous texture and faded borders. In summary, analyses based on the Surface Electronic Microscope and Energy Dispersive Spectroscopy (SEM/EDS) analyses suggested the formation of neo-formed phosphate phases during the roasting of sulfated ore samples at 800°C. The same pattern can be found in the initial sample of the spray roaster residue (Figure 4.4 (e)) as well as in that after sulfation and roasting at 800°C (Figure 4.4 (f)). The initial sample is already a neo-formed material.

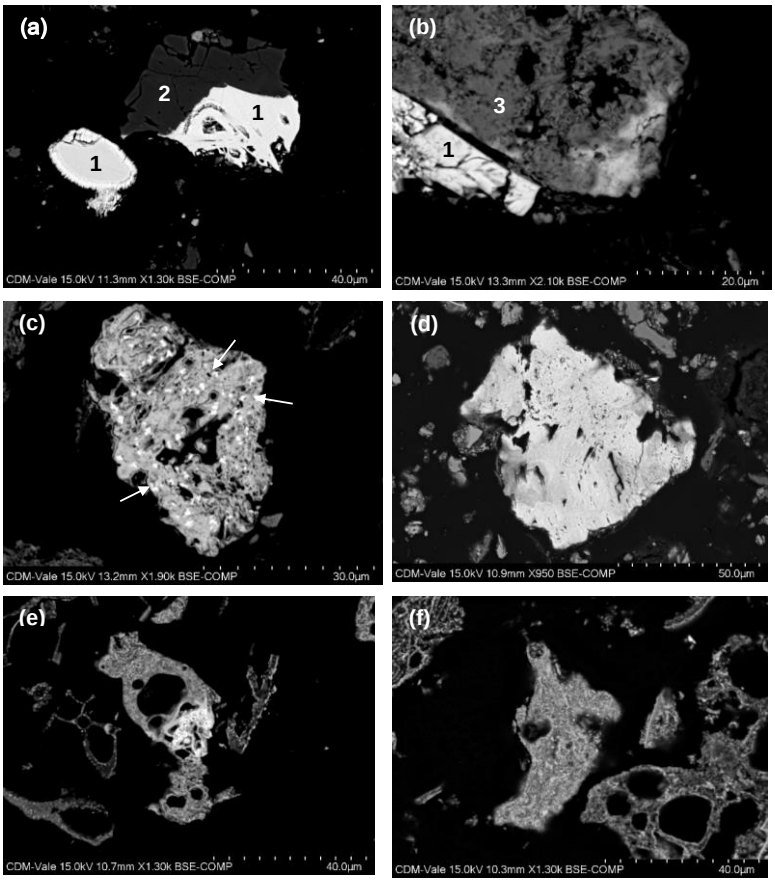

Figure 4.4 - SEM images showing REE bearing particles (bright particles) at different stages of the process. (a) Ore before processing: 1 – Monazite, 2 – Iron oxide, (b) After sulfation: 1 – unreacted REE, 3 – sulfated REE particle, (c) After sulfation and roasting at 800°C; arrows show P-enriched spots, (d) After sulfation, roasting (800°C) and leaching in water. (e) REE phosphate in the initial spray roaster residue sample. (f) REE Phosphate bearing particle in the spray roaster residue sample after sulfation and roasting at 800°C.

4.3.2 Thermodynamic simulation revisited

In a previous publication (Teixeira et al. (2019), Figure 4.5), thermodynamic simulations and thermogravimetric analysis were carried out in order to investigate the thermal stability of REE sulfates and impurities present in

REE ores with respect to their respective oxides. The aim of the simulation was to identify a window for a selective transformation of iron sulfates to oxides by roasting, which would avoid iron dissolution during water leaching. In this work, the reactions that could take place during sulfation-roasting were also considered. Figure 4.5 (a) simulates the stability of the initial mineral phases present in the monazite ore, here represented by lanthanum phosphate and ferric oxide, with respect to ferric sulfate and lanthanum sulfate. This system was simulated assuming equal amounts of $LaPO_4$ and Fe_2O_3, as well as stoichiometric amounts of sulfuric acid, for complete reaction with both components (equations ((4.3)) and (4.4)). These reactions are represented at room temperature by:

$$2LaPO_{4(s)} + 3H_2SO_{4(aq)} \rightarrow 2H_3PO_{4(l)} + (La)_2(SO_4)_{3(s)} \quad (4.3)$$

$$Fe_2O_{3(s)} + 3H_2SO_{4(aq)} \rightarrow Fe_2(SO_4)_{3(s)} + 3H_2O_{(l)} \quad (4.4)$$

The simulations indicated that when sulfuric acid is added to an REE ore, one may expect a complete conversion of REE and Fe into sulfates in temperatures below 450°C and 750°C, respectively (Figure 4.5 (a)). High temperatures will favor the reconversion of sulfates to phosphates. An additional source of P in the ore is fluorapatite ($Ca_5(PO_4)_3F$). Due to lack of thermodynamic data on fluorapatite, hydroxy-apatite – $Ca_5(PO_4)_3OH$ – was used in the simulations. The phosphoric acid produced by equation (4.3) may react with apatite to produce monocalcium phosphate – $Ca(H_2PO_4)_2$ – as described by equation (4.5) and shown in Figure 4.5 (b) for temperatures lower than 150°C:

$$Ca_5(PO_4)_3OH_{(s)} + 7H_3PO_{4(l)} \rightarrow 5Ca(H_2PO_4)_{2(s)} + H_2O_{(l)} \quad (4.5)$$

(a)

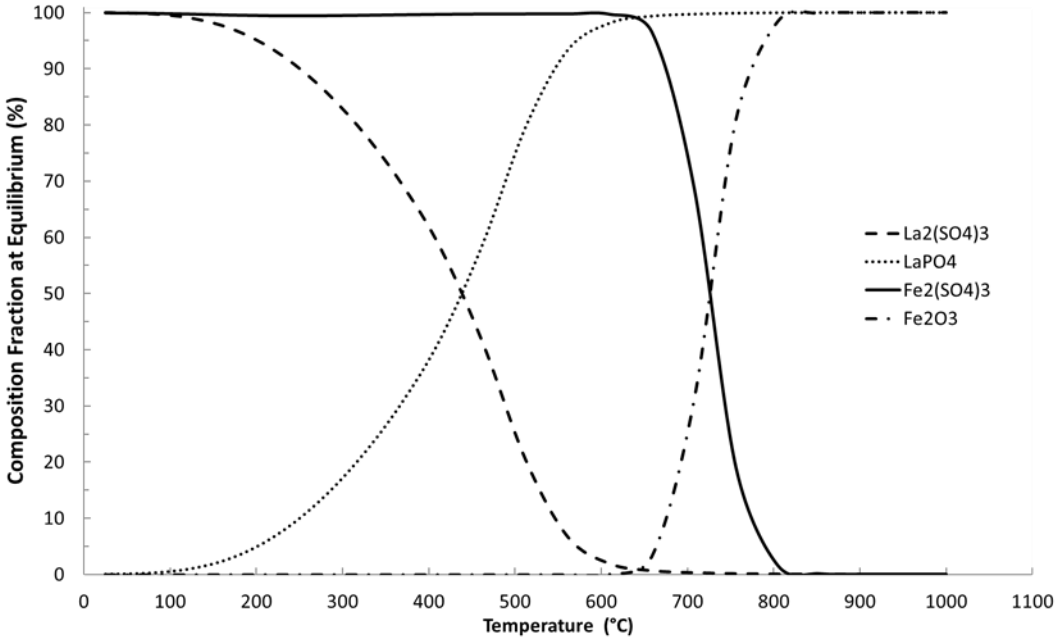

(b)

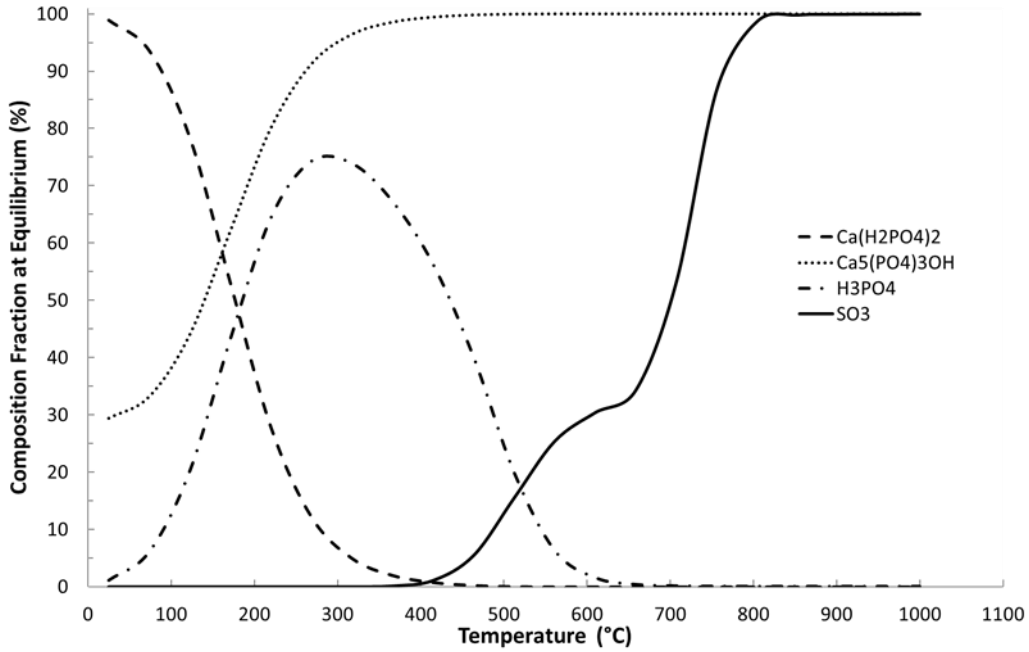

Figure 4.5 - System composition at equilibrium from room temperature to 1000°C. (a) illustrates the stability of metal sulfates with respect to lanthanum phosphate and iron oxide. (b) represents stability of phosphor compounds and sulfur trioxide. Initial system composition with equal amounts of Fe_2O_3, $LaPO_4$, stoichiometric amount of H_2SO_4, and excess $Ca_5(PO_4)_3OH$

Experimentally, the formation of monocalcium phosphate in the system is easy to observe, since it grants a plastic feature to the mixture, making the mixing

process very difficult to carry out. When heated, the monocalcium phosphate decomposes into a phosphoric acid and apatite-like phase. As described by equation (4.6) and shown in Figure 4.5 (b), under heating, phosphoric acid also decomposes into gas phases (water and P_2O_5 not shown in the Figure 4.5 (b)). This reaction becomes noticeable at temperatures higher than 300°C:

$$2H_3PO_{4(l)} \xrightarrow{\Delta} P_2O_{5(g)} + 3H_2O_{(g)} \quad (4.6)$$

Thus, the decomposition of phosphate compounds promotes an increase in the P_2O_5 partial pressure in the system atmosphere, which drives the conversion of REE sulfate into REE phosphate at roasting temperatures higher than 400°C (Figure 4.5 (a)).

$$La_2(SO_4)_{3(s)} + P_2O_{5(g)} \rightarrow 2LaPO_{4(s)} + 3SO_{3(g)} \quad (4.7)$$

This reaction is assumed to be responsible for the early, unexpected SO_3 release at about 400°C (Figure 4.5 (b)). For a system simulated in the absence of P_2O_5, SO_3 is released at about 1000°C (Figure 3.4). As P_2O_5 partial pressure equilibrium increases, it converts lanthanum sulfate into phosphate, releasing SO_3 in the process. It is important to note that the conversions represented in Figure 4.5 are under equilibrium conditions. An actual system would require higher partial pressures in order to allow appreciable reaction rates.

Figure 4.6 shows the partial pressure of P_2O_5 in equilibrium with phosphoric acid and monocalcium phosphate for temperatures ranging from room temperature to 1000°C. In both cases, at higher temperatures, the atmosphere will be made up of 3/4 water and 1/4 P_2O_5 (equation (4.6)), as indicated by the constant P_2O_5 partial pressure of 0.25 bar.

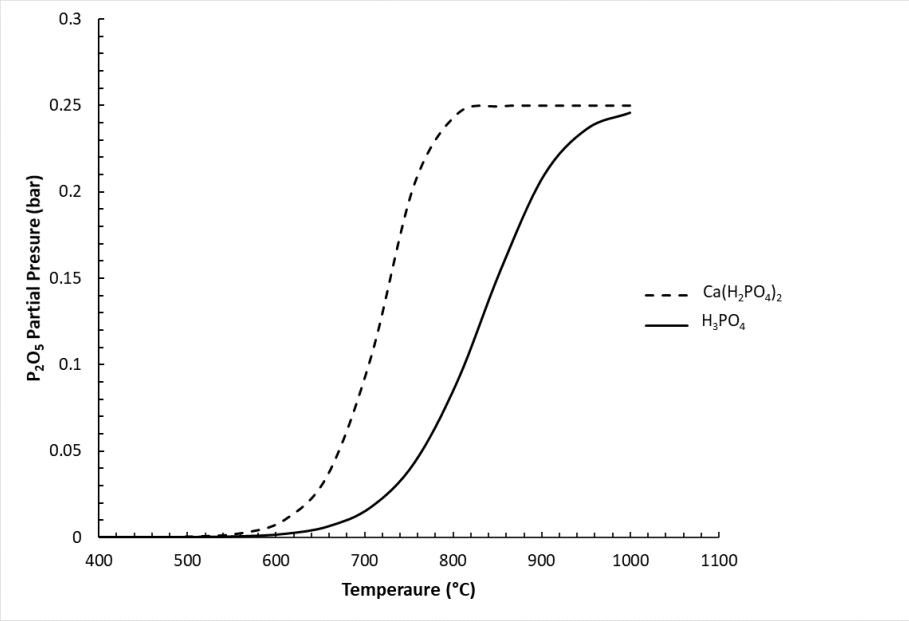

Figure 4.6 - Change in the equilibrium P_2O_5 partial pressure by the decomposition of $Ca(H_2PO_4)_2$ and H_3PO_4 with the increase of temperature according to equations 3.5 and 3.6

Thermodynamic calculations were also performed to evaluate the required P_2O_5 partial pressure to convert $La_2(SO_4)_3$ to $LaPO_4$ (equation (4.7)). The results indicated that a partial pressure of about 1.16 x 10^{-20} is required for such conversion at 800°C. This partial pressure is attained at approximately 80°C, according to the simulation. This is the minimum required partial pressure for conversion in equilibrium condition; kinetics was not considered. Figure 4.6 also shows that, depending on the phosphorus compound existing in the system, an appreciable amount of P_2O_5 (approximately 0.03 bar) gas may exist for temperatures at 650°C (monocalcium phosphate) and 750°C (phosphoric acid).

In fact, REE phosphates are very stable compounds. Figure 4.7 shows the equilibrium P_2O_5 partial pressure in the reaction involving phosphate compounds and their oxide form, as represented by equation (4.8). Lanthanum phosphate shows the lowest associated partial pressure, in comparison to ferric and aluminum phosphates, thus indicating its high stability; the SO_3 partial pressure associated with the formation of $La_2(SO_4)_3$ is higher. Another way of interpreting the data is that a very small P_2O_5 partial pressure is required to convert lanthanum oxide into phosphate.

$$La_3O_3 + P_2O_{5(g)} \rightarrow 2LaPO_{4(s)} \quad (4.8)$$

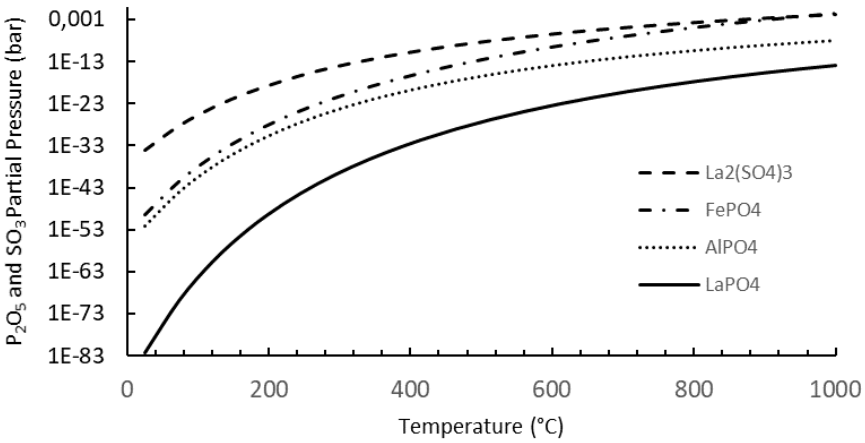

Figure 4.7 - The SO_3 and P_2O_5 partial pressures in equilibrium with $La_2(SO_4)_3$ and $FePO_4$, $AlPO_4$, $LaPO_4$, respectively, as a function of temperatures.

4.3.3 The mechanism of REE sulfate-phosphate reconversion

To assess the conversion of REE sulfates into phosphates at temperatures higher than 750°C, reagent grade lanthanum sulfate was contacted directly and indirectly (through a gas phase) to both phosphoric acid and solid phosphorus pentoxide as earlier described. The products of this series of experiments were analyzed by XRD (Figure 4.8) and chemical analysis. The results show that lanthanum sulfate was converted to lanthanum phosphate by reacting directly and indirectly with both phosphoric acid and phosphorus pentoxide.

In Figure 4.8 (a, b), the XRD patterns for the reagent are compared to the standard $La_2(SO_4)_3$. The XRD pattern measured for the product obtained after direct contact with this reagent with phosphoric acid was fitted to monoclinic $LaPO_4$ (Figure 4.8 (c, d)). The patterns measured for the products obtained after indirect contact with phosphoric acid and phosphorus pentoxide were better fitted to lanthanum polyphosphate $La(PO_3)_3$ (Figure 4.8 (e, f, g)). The anhydrous lanthanum sulfate pattern (Figure 4.8 (h)) was also included in the comparison to rule out the possibility that the new compound obtained could be the dehydration product of heated hydrated lanthanum sulfate. To eliminate this possibility, the product was analyzed for its phosphorus content. The results indicated 23.4% and 25.7% of phosphorus contained in the product obtained through the gas phase reaction with P_2O_5 and with H_3PO_4, respectively. These values match the amount expected for polyphosphates, such as $La(PO_3)_3$, which is 24.7% phosphorus.

The XRD findings were also compared to the diffraction pattern for lanthanum oxy-sulfate (Figure 4.8 (i)) in order to verify the hypothesis proposed by Onal et al. (2015). No agreement was found between the samples and the standard. Nevertheless, small amounts of sulfur, which may be related to the presence of minor amounts of oxy-sulfates or unreacted material, were detected together with REE phosphates by EDX analysis.

After roasting of REE sulfate concentrate, Demol et al. (2018) reported the formation of thorium and REE polyphosphates after roasting of REE sulfate concentrates by using XRD, EBS images, EDS analysis, and FTIR analysis. Amorphous REE polyphosphates formed at temperatures higher than 400°C, resulting in a mild decrease of REE extraction. However, the dramatic decrease in rare earth dissolution when heating the sample at temperatures higher than 800°C was explained by the formation of a crystalline phase, named “reformed” monazite, identified by XRD.

Figure 4.9 shows the SEM images for the products obtained from the direct and indirect contact experiments. The direct contact between H_3PO_4 and $La_2(SO_4)_3$ produced a highly crystalline, needle-like structure (Figure 4.9 (a)), which is seldom seen in ore samples. The direct contact between P_2O_5 and $La_2(SO_4)_3$ formed a glass-like structure, transparent to XRD (Figure 4.9 (b)). This may well be the result of the presence of polymeric chains from excess P_2O_5, being the reason for the formation of the glass-like phase also observed by Demol et al. (2018). The indirect contact between H_3PO_4 (Figure 4.9 (c)) and P_2O_5 (Figure 4.9 (d)) with $La_2(SO_4)_3$ formed a proper polyphosphate crystalline phase, $La(PO_3)_3$.

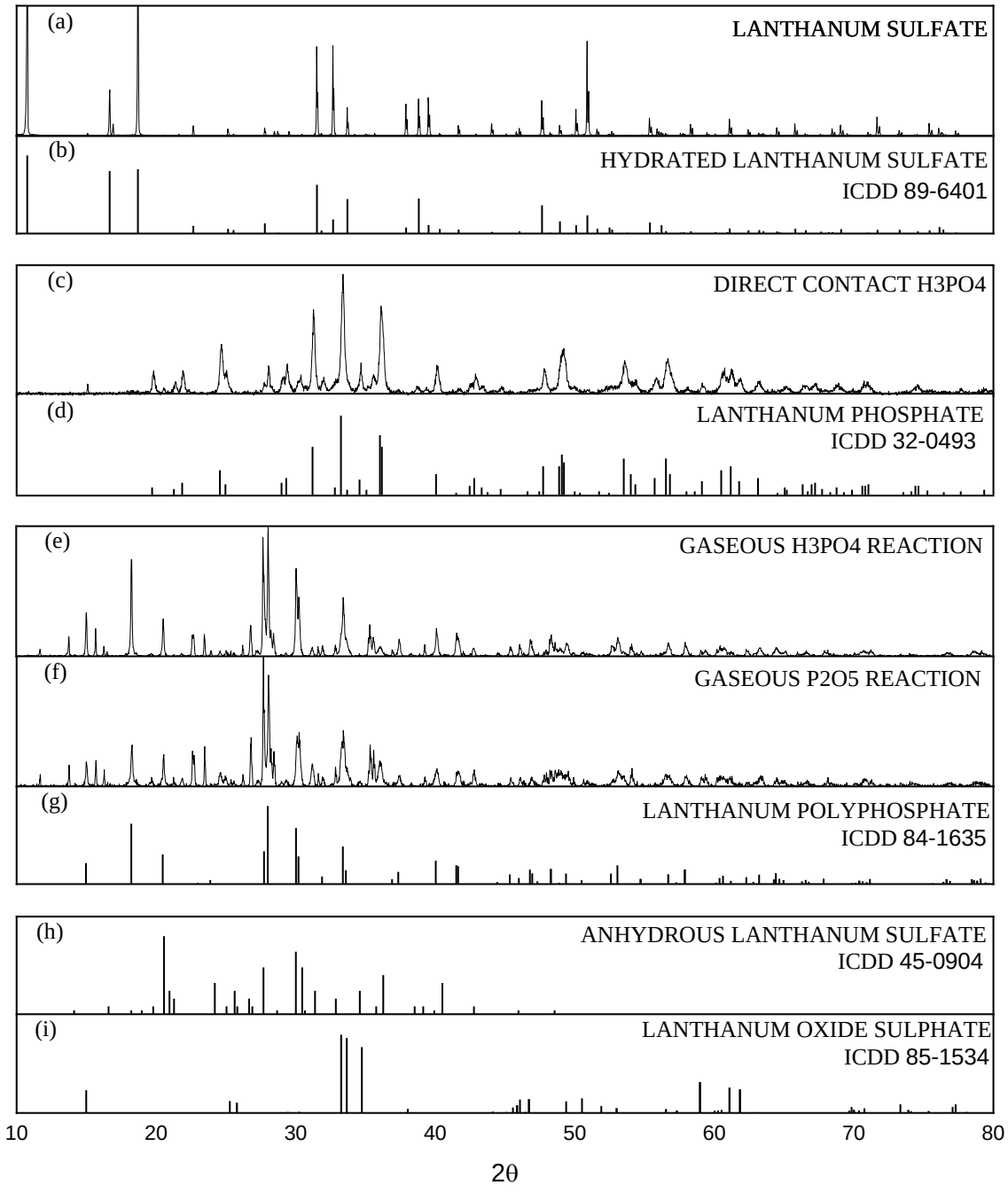

Figure 4.8 - X-ray diffraction patterns for hydrated $La_2(SO_4)_3$ and the products from its direct and indirect (gas phase) conversion into phosphates ($LaPO_4$ and $La(PO_3)_3$). The anhydrous lanthanum sulfate and lanthanum oxide sulphate patterns are also shown.

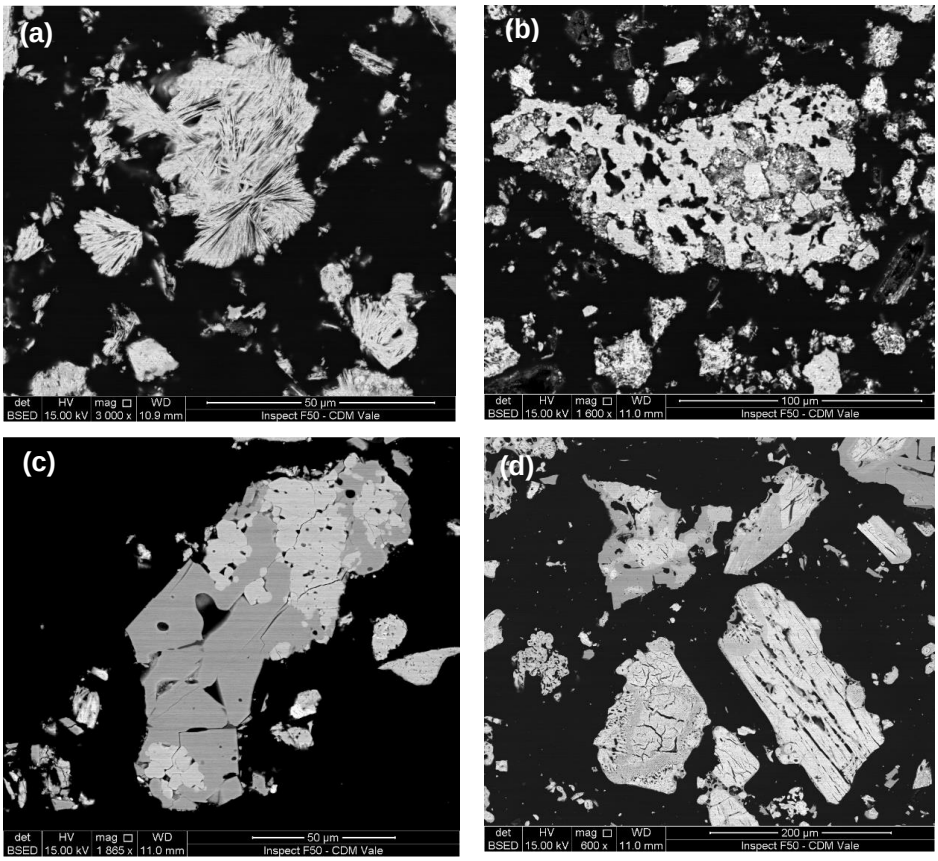

Figure 4.9 - SEM images from the reagent grade experiments results. (a) $LaPO_4$ formed from direct contact between $La_2(SO_4)_3$ and H_3PO_4. (b) Lanthanum phosphate phase formed from the direct contact between $La_2(SO_4)_3$ and solid P_2O_5. This phase did not yield a typical XRD of a crystalline structure. (c) $La(PO_3)_3$ formed from the indirect contact between $La_2(SO_4)_3$ and H_3PO_4. (d) $La(PO_3)_3$ formed from the indirect contact between $La_2(SO_4)_3$ and P_2O_5.

The formation of polyphosphates, a polymeric phosphorus structure, during experiments conducted by Demol et al. (2018), may be attributed to the large amount of phosphorus in the sample (93% monazite), with no other possible phosphorus sequestrant. It is well-known that phosphorus forms glass-like polymeric chains (Richardson 1974). This is probably the reason for the formation of an amorphous phase at temperatures between 400°C and 650°C. As presented in Figure 4.6, there is a significant increase in the P_2O_5 partial pressure in equilibrium with different phosphorus compounds at temperatures higher than 600°C. When phosphorus leaves the system, new material may be formed as a result of insufficient network formers, giving rise to new crystalline structures, such as monazite or $REE(PO_3)_3$.

It seems to be clear that when newly formed monazite is detected in the leaching residue, this is due to the conversion of REE sulfate into phosphate by

the reaction with phosphorus (e.g., phosphoric acid). When polyphosphate is detected, it was generated under a P_2O_5-rich atmosphere, and the conversion of REE sulfates into phosphates takes place by a solid-gas mechanism, as described by equation (4.7).

The gas-solid reaction mechanism should prevail over any possible solid-solid reaction due to a better access of the gas phase to the reacting interface. The gas-phase mechanism should also prevail over the solid-liquid mechanism (phosphoric acid) for two reasons. In typical low-grade ores, the possible amount of phosphoric acid generated by the addition of sulfuric acid is relatively low when compared to the total volume of ore. This hinders the contact between the liquid acid and the REE sulfate. To attain a significant reduction in REE, such as that observed in Figure 4.3, effective contact between the phosphorus source and the REE sulfate is required, with the solid-gas mechanism being the most favorable.

To confirm the mechanism of SO_3 displacement at lower temperatures, the off gas from a TGA analysis of a mixture of reagent grade lanthanum sulfate and reagent grade phosphorus pentoxide was analyzed by mass spectroscopy, the results of which are shown in Figure 4.10. The earlier release of SO_3 is indicated by a concentration peak at 483°C (atomic mass 48 for SO^+ and 64 for SO_2). There is also a significant mass 16 (O) and 32 (O_2) gas release at 444°C. These results confirm the behavior predicted by equation (4.7) and Figure 4.5, which is the reconversion of sulfated REE to the insoluble phosphate compounds.

4.3.4 Implications to the processing of REE

The selective roasting of iron-rich, REE ores would not be recommended when processing high- grade REE concentrates containing low amounts of impurities, as compared to ROM (Run of Mine) ore. High grade concentrates can undergo sulfation and direct leaching, avoiding expensive high-temperature roasting. The low amount of impurities can be removed by hydrometallurgical downstream processes, such as pH-controlled impurity precipitation (Silva et al., 2018) and REE precipitation (Silva et al., 2019).

(a)

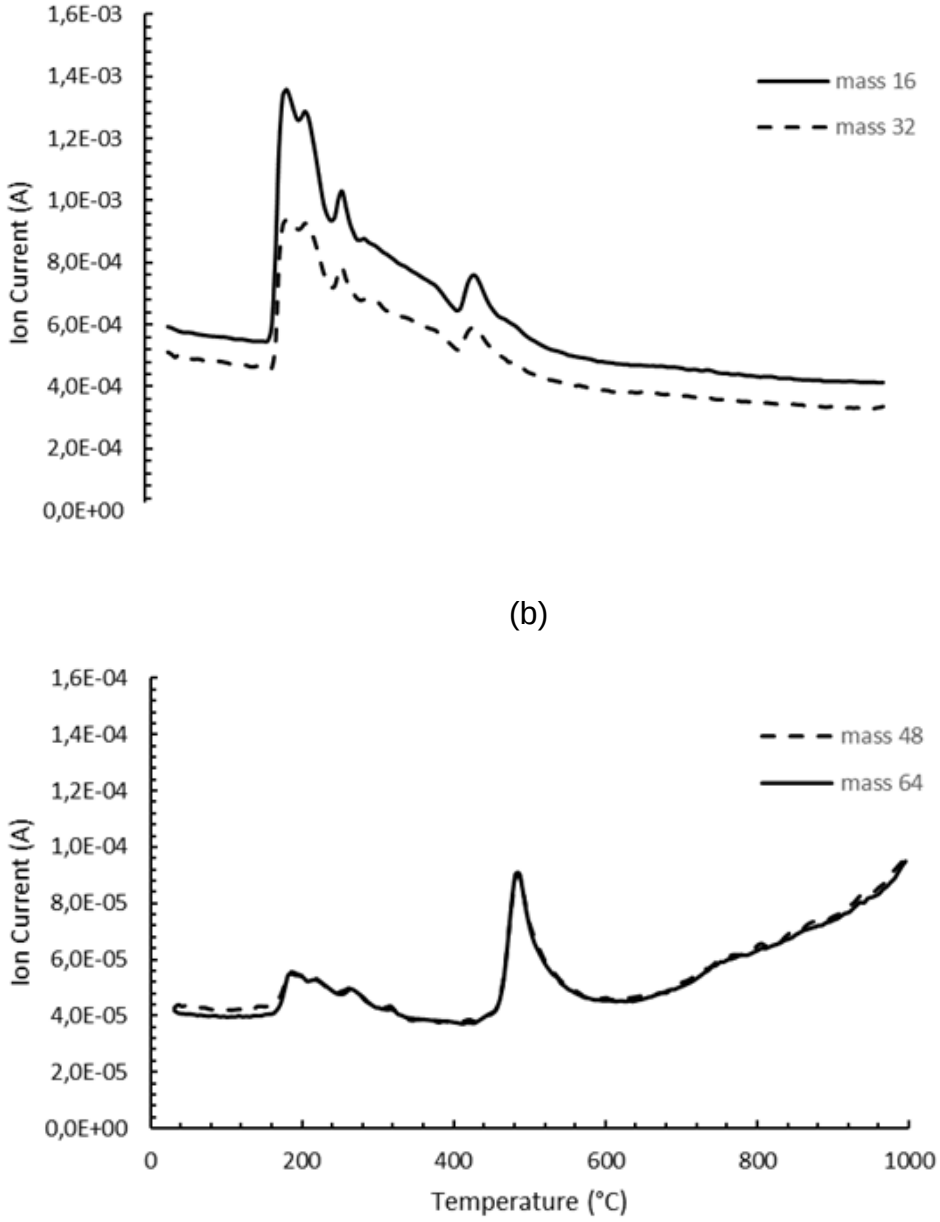

Figure 4.10 – Mass spectroscopy of the off gas from the TGA analysis of a mixture of reagent grade lanthanum sulfate and phosphor pentoxide. Relevant O (m.w. 16) / O_2 (m.w. 32) emission at 444°C, and SO^+(m.w. 48) / SO_2 (m.w. 64) emission at 483°C.

Sulfation followed by roasting may be used for thorium removal, but at lower temperatures (above 300°C and below 600°C), as described by Zhang (2016).

Unless phosphate is converted into a very stable compound (displaying low P_2O_5 partial pressure at high temperatures), there will be the conversion of REE sulfate into REE phosphate at temperatures between 700-800°C, generating a small operational window for the furnace temperature (of about 50°C, between 700°C for ferric sulfate decomposition and 750°C for REE sulfate conversion into phosphate). This would require a careful selection for the roasting stage as the furnace must operate under a narrow temperature window.

4.4 Conclusions

In this work, the mechanism behind the selective REE extraction over iron by the roasting of sulfated monazite was clarified. The unexpected decrease in REE extraction from ores roasted at 800°C was explained by analyzing the phosphorus behavior in the system during sulfation and roasting stages. It was demonstrated that excess phosphorus remaining in the sulfated material may cause the reconversion of REE sulfates to REE phosphates, as well as the presence of phosphoric acid will lead to the formation of monazite-like compounds. High partial pressures of P_2O_5 will convert REE sulfates into insoluble REE polyphosphates – $REE(PO_3)_3$. This high partial pressure may be attained by the decomposition of phosphoric acid formed during the sulfation of the ore or by newly formed phosphorus compounds, such as monocalcium phosphates. The solid-gas mechanism is the most favorable, as the gas phase can promote better contact with all REE sulfate particles present in the system, making it possible to achieve the drastic decrease (conversion into phosphate compounds) observed at 800°C.

4.5 References

Bard A. J., Parsons R., Jordan J., Standard potentials in aqueous solution, Marcel Dekker Inc., New York, 1985.

Barin I., Knacke O., Kubaschewski O., Thermochemical properties of inorganic substances, Supplement, Springer-Verlag, Berlin, 861, 1977.

Barin I: Thermochemical Data of Pure Substances, Part I, VCH Verlags Gesellschaft, Weinheim, 1993.

Barin I: Thermochemical Data of Pure Substances, Part II,VCH Verlags Gesellschaft, Weinheim, 1993.

Barin I: Thermochemical Data of Pure Substances, VCH Verlags Gesellschaft, Weinheim, 1989.

Belov, G., Iorish, V., Yungman, V., IVTANTHERMO - database on thermodynamic properties and related software,Calphad 23(2) (1999) 173-180.

Berni T.V., Pereira, A. C., Mendes, F.D., Tude, A.L. (2013), System and Method for Rare Earth Extraction. Patent US 2013/0336856 A1.

Chase M. W., Jr., Davies C. A., Downey J. R., Jr., Frurip D. Journal, McDonald R. A., Syverud A. N., JANAF thermochemical tables third edition part II, Cr-Zr, J. of Phys. and Chem. Ref. Data, Vol.14, No.1, pp.927-1856, 1985.

Chase Malcolm, NIST-JANAF, Thermochemical Tables - Fourth Edition, J. of Phys. and Chem. Ref. Data, Mononograph No. 9, 1998.

Dean J.A., Lange's Handbook of Chemistry, Thermodynamic Properties, McGraw-Hill, New York, 1985.

Demol J., Ho E., Senanayake G. (2018), Sulfuric Acid Baking and Leaching of Rare Earth Elements, Thorium and Phosphate from a Monazite Concentrate: Effect of Baking Temperature from 200 to 800 °C, Hydrometallurgy 179: 254-267.

Fabricius G., Liukkonen S., Sundholm G.: Fysikaalisen kemian taulukoita. Otatieto, Espoo, 1994.

Frenkel, M., Kabo, G. J., Marsh, K. N., Roganov, G. N., Wilhoit, R. C., Thermodynamics of organic compounds in the gas state, Vol. 1, 1994.

Giauque, W. F., Hornung, E. W., Kunzler, J. E., Rubin, T. R., The Thermodynamic Properties of Aqueous Sulfuric Acid Solutions and Hydrates from 15 to 300°K, J. Amer. Chem. Soc. 82(62) (1960) 62-70.

Glushko Thermocenter of the Russian Academy of Sciences, IVTAN Association, Izhorskaya 13/19, 127412 Moscow, Russia, 1994.

Glushko Thermocenter of the Russian Academy of Sciences, IVTAN Association, Izhorskaya 13/19, 127412 Moscow, Russia, 1996.

Gupta, C. K. and Krishnamurthy, N. (2005) Extractive Metallurgy of Rare Earths, CRC Press, Nova York.

Karapet'yants, M. Kh., Maier, A.I., Soldatova, T.A. Enthalpies of Formation of Certain Praseodymium Selenites. Inorganic Materials, Vol. 6, No. 6, pp. 976-979, 1970.

Landolt-Börnstein: Thermodynamic Properties of Inorganic Material, Scientific Group Thermodata Europe (SGTE), Springer-Verlag, Berlin-Heidelberg, 1999.

Lidin, R. A., Andreeva, L. L., Molochko, V. A., Constants of Inorganic Substances, A Handbook, Revised and Augmented Edition, Begell House inc., New York, 1995.

Lucas J, Lucas P, Le Mercier T, Rollat A, Davenport, WGI (2014) Rare earth: science, technology, production and use, 1st ed., Elsevier.Mackowski S. J., Raiter R., Soldenhoff K. H., Ho E. M. (2009), Recovery of Rare Earth Elements, US2009/0272230 A1.

Majzlan, J., Navrotsky, A., Stevens, R., Donaldson, M., Woodfield, B.F., Boerio-Goates, J., Thermodynamics of monoclinic Fe2(SO4)3, J. Chem. Thermodynamics, Vol. 37, pp. 802-809, 2005.

Onal, M. A. R., Borra, C. R., Guo, M., Blanpain, B. (2015), Recyclcing of NdFeB Magnets Using Sulfation, Selective Roasting and Water Leaching. J. Sustain Metall. 1:199-215.

Pankratz L.B.: Thermodynamic Properties of Carbides, Nitrides, and other Selected Substances. U.S. Dept. of the Interior, Washington, DC, pp. 957, 1995.

Popa, K., Konings, R. J. M., High-temperature heat capacities of EuPO4 and SmPO4 synthetic monazites, Thermochimica Acta 445 (2006) 49-52.

Richardson F. D., Physical Chemistry of Melts in Metallurgy, Volume 1, Academic Press London - New York, 1974

Robie R. A., Hemingway B. S., Fischer J., Thermodynamic properties of minerals and related substances at 298.15K and 1bar pressure and at higher temperatures, US Geological Survey Bulletin 1452, US Government Printing Office, Washington, 456, 1979.

Robie, R. A., Hemingway, B. S., Thermodynamic Properties of Minerals and Related Substances at 298.15 K and 1 Bar (105 Pascals) Pressure and at Higher Temperatures, U.S. Geological Survey Bulletin 2131, 1995, 461 p.

Ruzinov L. P. and Guljanickij B. S.: Ravnovesnye prevrasoenija metallugiceskin reaktseij, Moskva, 416, 1975.

Silva R. G., Morais C. A., Teixeira L.V., Oliveira E. D. (2018). Selective Removal of Impurities from Rare Earth Sulphuric Liquor Using Different Reagents, Miner. Eng., 127:238-246. https://doi.org/10.1016/j.mineng.2018.08.007

Silva R. G., Morais C. A., Teixeira L.V., Oliveira E. D. (2019). Selective Precipitation of High-Quality Rare Earth Oxalates or Carbonates from a Purified Sulfuric Liquor Containing Soluble Impurities, Mining, Metallurgy and Exploration. https://doi.org/10.1007/s42461-019-0090-6

Teixeira L. A. V., Silva R.G., Avelar A., Majuste D., Ciminelli V. S. T. (2019). Selective Extraction of Rare Earth Elements from Monazite Ores with High Iron Content. Mining, Metallurgy and Exploration, 36:235-244.

https://doi.org/10.1007/s42461-018-0035-5

Teixeira L. A. V., Silva R.G. (2015) System and process for selective rare earth extraction with sulphur recovery. Patent US 2015/0329940 A1.

Testa, F. G., Avelar, A. N., Silva, R. G., Souza, C. C. (2016), Mineralogical Characterization and Alternative to Concentrate the Rare Earth Lithotypes From Alcaline Complex of Catalão – GO. Associação Brasileira de Metalurgia, Materiais e Mineração, São Paulo.

http://dx.doi.org/10.4322/2176-1523.1064

Thermodynamic Data for Fifty Reference Elements, NASA-TP-3287, N93-19977, 1993, 240 pages.

Thermodynamic Tables for Nuclear Waste Isolation. Prepared by S. L. Philips, F. V. Hale, L. F. Silvester, Lawrence Berkely Laboratory M. D. Siegel, Sandia National Laboratories, 182, 1988.

Thiriet, C., Konings, R. J. M., Javorský, P., Magnani, N., Wastin, F., The low-temperture heat capacity of LaPO4 and GdPO4, the thermodynamic functions of the monazite-type LnPO4 series, J. Chem. Thermodynamics 37 (2005) 131-139.

Verbaan N, Bradley K, Brown J, Mackie S (2015) A review of hydrometallurgical flowsheets considered in current REE projects, In: Simandl GJ and Neetz M (eds.) Symposium on Strategic and Critical Materials Proceedings. British Columbia Ministry of Energy and Mines, British Columbia Geological Survey Paper 2015-3, Victoria, British Columbia, pp. 147-162.

Walters A. and Lusty P., British Geological Survey (2011), Rare Earth Elements, Keyworth, Nottingham, United Kingdom.

Zhang J, Zhao B and Schereiner B, (2016), Separation Hydrometallurgy of Rare Earth Elements, Springer, Switzerland.

4.6 Appendix A

Table 4.2 - Thermodynamic data for the main compounds used in thermodynamic evaluation and mechanism proposal.

Species	$\Delta_f H^o$	S^o	$\Delta_f G^o$	References
	kJ/mol	J/(mol*K)	kJ/mol	
$La_2(SO_4)_3$	-3932	319	-3597,504	(a), (b), (c)
Fe_2O3	-824,781	87,4	-744,449	(d), (e), (f), (g), (h)
$Fe_2(SO_4)_3$	-2585,199	305,6	-2263,387	(j), (k), (m)
$LaPO_4$	-1969,599	108,239	-1850,323	(n), (o), (p)
H_3PO_4	-1278,999	110,499	-1118,918	(k)
$Ca_5(PO_4)_3OH$	-6738,5	390,371	-6339,078	(f), (q), (c), (r)
$Ca(H_2PO_4)_2$	-3115	189,535	-2812,02	(s), (t), (a)
$SO_3(g)$	-395,764	256,772	-371,011	(k), (u), (v)
$SO_2(g)$	-296,812	248,22	-300,092	(e), (u)
P_2O_5 (g)	-1124,369	366,572	-1056,245	(l)
$FePO_4$	-1296,998	93,721	-1184,656	(w), (s)
$AlPO_4$	-1733,431	90,792	-1617,487	(x)
O_2 (g)	0	205,149	0	(e), (u), (y), (i)
H_2O	-285,83	69,949	-237,141	(m), (l)
H_2SO_4	-813,988	156,904	-689,915	(e), (z), (aa)

(a) Lidin et al (1995), (b) Philips et al (1988), (c) Dean (1985), (d) Fabrichnaya et al (2010), (e) Barin (1993), (f) Robie and Hemingway (1995), (g) Barin et al (1977), (h) Glushko Thermocenter of the Russian Academy of Sciences (1996), (i) Landolt-Bornstein (1999), (j) Majzlan et al. (2005), (k) Barin (1989), (l) Glushko Thermocenter of the Russian Academy of Sciences (1994), (m) JANAF (1985), (n) Thiriet et al. (2005), (o) Popa and Konings (2006), (p) Pankratz (1995), (q) Robie et al. (1979), (r) Ruzinov and Guljanickij (1975), (s) Bard et al. (1985), (t) Karapet'yants et al. (1970), (u) Frenkel et al. (1994), (v) Belov et al. (1999), (w) Fabricius et al. (1994), (x) Barin et al. (1977), (y) Nasa (1993), (z) JANAF (1998), (aa) Giauque et al (1960). All data as reported by HSC Chemistry (2015)

5 ATMOSPHERE EFFECT ON SELECTIVE ROASTING OF RARE EARTH SULFATES

5.1 Introduction

Rare earth elements (REE) are widely distributed in low concentrations throughout the earth's crust. The combined crustal abundance of rare earth elements is of the order of 200 $mg.kg^{-1}$. The REE are more abundant in granitic rocks than in basic igneous varieties, although the highest concentrations are found in alkaline igneous rocks and carbonatites. Rare earths are found in more than 160 discrete minerals, but 95% of all the world's resources occur in just four minerals (Papangelakis and Moldoveanu, 2014): bastnaesite $(Ce,La,Y)(CO_3)F$, monazite $(Ce,La,Pr,Nd,Th,Y)PO_4$, xenotime YPO_4 and ion-adsorption clays. Bastnasite and monazite are minerals rich in LREE, whereas xenomite and ion-adsorption clays are richer in HREE. The rare earth content in the deposits is usually low, seldom higher than 5%, and the elements are usually extracted as a by-product or a co-product (Gupta and Krishnamurthy, 2005).

The challenge to increase REE availability in the market is often the problem of developing economically feasible process routes that can deal with low-grade ores and complex mineralogy. This scenario usually requires pretreatment, as sulfation and roasting, before ore leaching. (Verbaan et al., 2015). A selective roasting process was investigated by the authors (Teixeira et al., 2019) to treat iron-rich, monazite ores, and the reaction mechanism was detailed by further investigations (Teixeira et al., 2020). The results are discussed in chapters 3 and 4. However, these studies were limited to the roasting under air atmosphere.

The sulfate decomposition reactions taking place during roasting (Eq.(5.1), Eq. (5.2), and Eq. (5.3)) are all affected by the amount of oxygen available. The same is valid for iron sulfate decomposition (Eq. (5.4)). All sulfate decomposition depends on the SO_2 and SO_3 equilibrium partial pressures, as presented in Eq. (5.5). Hammerschmidt and Wrobel (2009) discussed the atmosphere effect on the decomposition reactions of Fe(II) and Fe(III) sulfates as a source of sulfur for sulfuric acid production. The authors showed that, at a given P_{SO2} and P_{O2}, the stability of sulfate or oxide phases would be defined by the temperature of the

system. The same analysis was shown to be extendable to other sulfates, namely, $CaSO_4$, $MgSO_4$, and $MnSO_4$.

$$REE_2(SO_4)_{3(s)} \xrightarrow{\Delta} REE_2O_{3(s)} + 3SO_{3(g)} \quad (5.1)$$

$$REE_2(SO_4)_{3(s)} \xrightarrow{\Delta} REE_2O_2(SO_4)_{(s)} + 2SO_{2(g)} + O_{2(g)} \quad (5.2)$$

$$REE_2O_2(SO_4)_{(s)} \xrightarrow{\Delta} REE_2O_{3(s)} + SO_{2(g)} + \frac{1}{2}O_{2(g)} \quad (5.3)$$

$$Fe_2(SO_4)_{3(s)} \xrightarrow{\Delta} Fe_2O_{3(s)} + 3SO_{2(g)} + \frac{3}{2}O_{2(g)} \quad (5.4)$$

$$SO_{2(g)} + \frac{1}{2}O_{2(g)} \rightarrow SO_{3(g)} \quad (5.5)$$

Calcium sulfate decomposition under air or reducing atmosphere has been intensively studied. Smith et al. (1976) evaluated the use of fluidized bed reactors filled with lime to remove sulfur from the burning process of fossil fuels. The lime reacts with sulfur under temperatures between 800-950°C and generates calcium sulfate, removing sulfur from the flue gas. The authors provided detailed information on the system thermodynamics and kinetics, and also reviewed data supplied by different investigations. The reductive decomposition was an option to reform the $CaSO_4$ back in oxide form, so it could be reused as sulfur sequestrant. Four different reductive agents were proposed: carbon monoxide (Eq. (5.6)), hydrogen (Eq. (5.7)), methane (Eq. (5.8) and elemental carbon (Eq. (5.9).

$$CaSO_4 + CO \rightarrow CaO + SO_2 + CO_2 \quad (5.6)$$

$$CaSO_4 + H_2 \rightarrow CaO + SO_2 + H_2O \quad (5.7)$$

$$4CaSO_4 + CH_4 \rightarrow 4CaO + 4SO_2 + CO_2 + 2H_2O \quad (5.8)$$

$$2CaSO_4 + C \rightarrow 2CaO + 2SO_2 + CO_2 \quad (5.9)$$

The previous rationale can be applied to the roasting of sulfated monazite ores in order to broaden the temperature window between rare earth and iron

sulfates decomposition to oxides. Previous studies (Teixeira et al., 2019) have shown the decomposition of rare earth sulfates starting between 1000-1100°C under air atmosphere. Poston et al., (2003) reported lanthanum sulfate decomposition starting at 775°C under nitrogen. Hegedus and Fuker (1956) reported initial decomposition at 610°C under a reducing atmosphere (H_2).

Both the thermodynamic fundamentals and the literature support the hypothesis that sulfate decomposition will take place at lower temperatures under reducing conditions. This approach may represent an opportunity to further improve the selective roasting technology, and operate the furnace at lower temperatures. The objective of this work is to investigate the effect of reducing atmospheres on REE sulfate decomposition. The findings are expected to contribute to a better understand and control the decomposition reactions during roasting, and to create conditions for process optimization.

5.2 Experimental Procedure

5.2.1 Materials

Reagent grade lanthanum sulfate 99.9% (Fmaia, La_2O_3/REO > 99.99%), 97.5% w/w sulfuric acid (Anidrol), natural fines (<74µm) of a monazite ore rich in magnetite from a phosphate mine and a solid residue obtained from the production process of synthetic rutile (TiO_2). were used in the experiments.

5.2.2 Rare Earth Extraction

The extraction experiments were comprised of the following steps: (i) separation of natural fines (<74 µm) by scrubbing a 50% w/w suspended solid ore pulp for 15 min and passing this material through a 74 µm sieve (Testa et al., 2016);-(ii) sulfation by mixing the natural fines (200g minimum) with sulfuric acid 97.5% w/w for 30 minutes using a 1.5 L mechanical mixer (Marconi, model MA259); (iii) roasting in a muffle-type furnace (K-type thermocouple) under air for 2 hours; (iv) cooling the charge to 20°C, and (v) leaching the solids in water at 10% w/w for 2 hours at room temperature, under mechanical mixing (200-300 rpm). The pH was controlled (when necessary) between 1.5 and 2.0 by adding sulfuric acid (Mettler Toledo pH meter type M400. The REE extraction was performed following the procedure described by Teixeira and Silva (2014) and

Berni et al (2013). The amount of acid added was 0.45 kg of acid per kg of ore. Roasting temperature ranged from 200°C to 800°C.

REE phosphate from the secondary source (spray roaster residue) presented a very fine particle size, not requiring a screening step. This sample was submitted to the same procedure described above. The acid:residue mass ratio was fixed to 1.2:1.0

Natural fines, rich in magnetite, were subjected to the procedure described above twice. In the second time, it was submitted to a pre-oxidizing roasting stage (before sulfation), in which the ore was fed to a stainless-steel rotary kiln and heated up to 1000°C and held for 4 hours under pure O_2 atmosphere (2 L/min) and rotation of 20 rpm.

The spray roaster oxide was also submitted to the procedure described above twice. In the second time, it was submitted to a reducing roasting stage (after sulfation), in which the ore was fed to a stainless-steel rotary kiln and heated up to 1000°C and held for 2 hours under pure CO atmosphere (2 L/min) and rotation of 20rpm.

5.2.3 Analytical Methods

The TGA-DTA analyses were performed in a NETZSCH STA 449F3 equipment, under 100% CO gas atmosphere in an alumina crucible with a heating rate of 10K min-1 up to 1500°C.

Solid and aqueous solutions were analyzed by Inductively Coupled Plasma Optical Emission Spectrometry-ICP-OES (Varian, VISTA PRO model) and Inductively Coupled Plasma Mass Spectrometry (PerkinElmer ICP-MS, model NexION 300D). Duplicates, blanks and standards (DBS) were used during ICP analysis. Samples were subjected to an acceptable duplicate maximum mean error (ME) that varied with the method, the element and concentration. Prior to chemical analyses solid samples were dried in an oven at 100°C for at least one hour and pulverized to a condition in which 95% of the particles (in mass) were below 74 µm. The solid samples containing rare earth elements, thorium and uranium (DBS every 24 samples, ME between 10% and 5%) were treated by fusion with $Li_2B_4O_7$ or with H_2O_2 followed by dissolution in 10% (v/v) nitric acid (65% v/v). For the analyses of the remaining elements (DBS every 20 samples, ME between 10% and 5%), the samples were treated by fusion with

Na_2CO_3 and $Na_2B_4O_7$, followed by dissolution in 67% (v/v) hydrochloric acid. The concentrations of aluminum, iron, phosphorous, sulfur, and the rare earths (Pr, Nd, and Sm) in the solids (after fusion/dissolution) and in aqueous solution after leaching were analyzed by ICP-OES (DBS every 20 samples, ME between 10% and 5%). The concentration of the remaining rare earth elements and other impurities (both from solid samples and leach solutions) were analyzed by ICP-MS, after dilution in 2% v/v nitric acid (65% v/v). Rare earth analysis from leach solutions had DBS analyzed every 20 samples and ME between 10% and 5%. The ferrous iron concentration in the leach solution was measured by straight titration with $K_2Cr_2O_7$ in acid solution using barium diphenylamine sulfonate as an indicator.

5.2.4 Thermodynamic evaluation

HSC chemistry version 8 (HSC Chemistry 2015) provided the thermodynamic data (values for standard enthalpy, entropy, and Gibbs Free energy) and software to generate the stability diagrams.

5.2.5 Sulfation and Pyrolysis

An ore received from a Brazilian phosphate mine was screened and the product below 74 µm was used for laboratory tests according to the procedure described by Testa et al (2016). The material was dried at 80°C and the sulfation stage was performed by mixing the ore with 0,45 kg of concentrate sulfuric acid (97.5% w/w, Química Moderna) per kg of ore using a 1.5 L mechanical mixer (Marconi, model MA259). Sulfuric acid was slowly added to the samples (of at least 200 g) for 10 minutes at 300 rpm. Roasting temperature ranged from 200°C to 800°C.

The same ore was subjected to a pre-treatment stage by roasting it at 1000°C for 4 hours under pure oxygen atmosphere in a rotary kiln, with gas flow of 2 L/min. This material was subjected to the same sulfation procedure described above.

The sulfated material was transferred to a mullite crucible. The crucible was inserted in a muffle-type furnace (Analógica, model AN1222) that was previously heated to the desired temperature. The temperature profile of the muffle furnace was previously acquired by means of a K-type thermocouple

attached to a data logger. The sample was left at a defined temperature (between 200-800°C) for 2 hours, then removed from the muffle and cooled down in a desiccator. The roasted sample was transferred to a beaker and water leached at 10% w/w at room temperature for 3 hours and 300rpm. The pH was controlled (by sulfuric acid addition) between 1.5 and 2.0 (Mettler Toledo pH meter type M400).

HSC chemistry (Outotec) version 8 provided the thermodynamic data (values for standard enthalpy, entropy and Gibbs Free energy) and software to generate the stability diagrams.

5.3 Results and Discussions

5.3.1 Lanthanum sulfate decomposition simulation and TGA results

The oxygen gas activity in the atmosphere (P_{O2}) will define the decomposition behaviour of the metal sulfate at a given temperature. Carbon monoxide was selected as the reducing agent, and the P_{O2} in the system will be given by the equilibrium between CO_2 and CO, as illustrated by equation (5.10).

$$CO_{(g)} + \frac{1}{2} O_{2(g)} \rightarrow CO_{2(g)} \quad (5.10)$$

Lanthanum sulfate decomposition was simulated (HSC 8.0) under different atmosphere conditions, with CO/CO_2 ratios varying from 10^{-7} and 10^{-1}. The result is shown in Figure 5.1. Any ratio higher than 0.1 did not affect the decomposition temperature and was therefore not displayed.

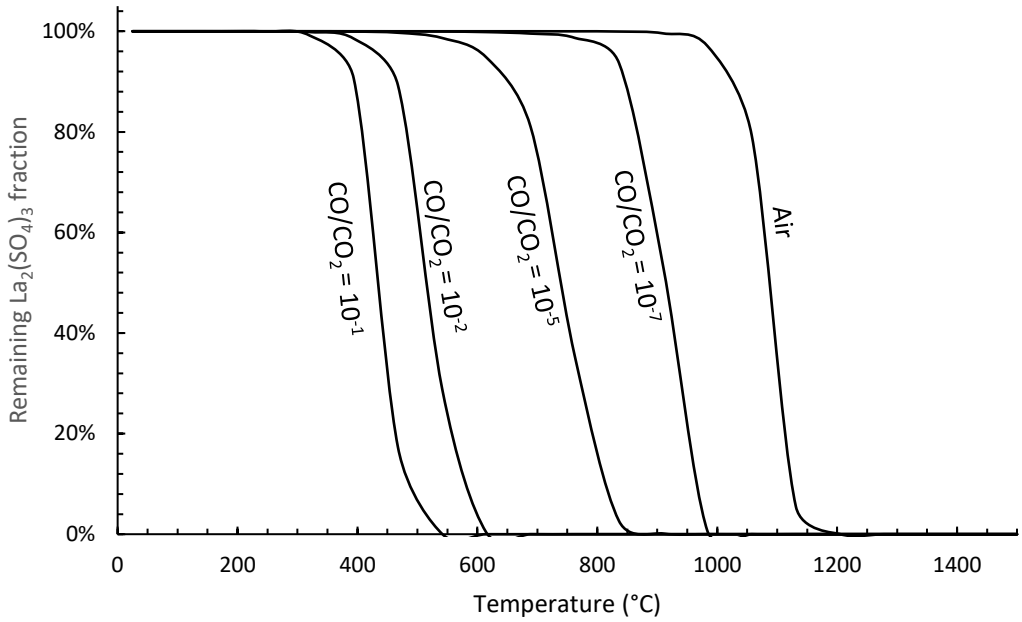

Figure 5.1 – Simulation of lanthanum sulfate decomposition under varying CO/CO_2 ratios (HSC 8.0, 2015)

The simulation (Figure 5.1.) suggests that the decomposition temperature may drop by about 500°C when applying reducing atmospheres, thus indicating an option for the roasting stage improvement. Reagent grade lanthanum sulfate was then submitted to TGA under 100% CO atmosphere, and the result is shown in Figure 5.2. A comparison with the data generated in previous work (Teixeira et al., 2019) is also included, to illustrate the good agreement between the simulation and the TGA data under synthetic air condition.

The results showed in Figure 5.2, suggest an equilibrium oxygen partial pressure corresponding to CO/CO_2 concentrations between 10^{-5} and 10^{-2}. As the TGA was performed using a standard equipment, a perfect control of the atmosphere may not be attained due to protective gas use and crucible materials. This may imply in higher oxygen pressure in the system than that expected for 100% CO atmosphere. It is also important to notice that, under reducing atmosphere, the lanthanum sulfate decomposition took place in one step, not passing through the formation of lanthanum oxysulfate, as identified for the decomposition under air conditions (Teixeira et al 2019).

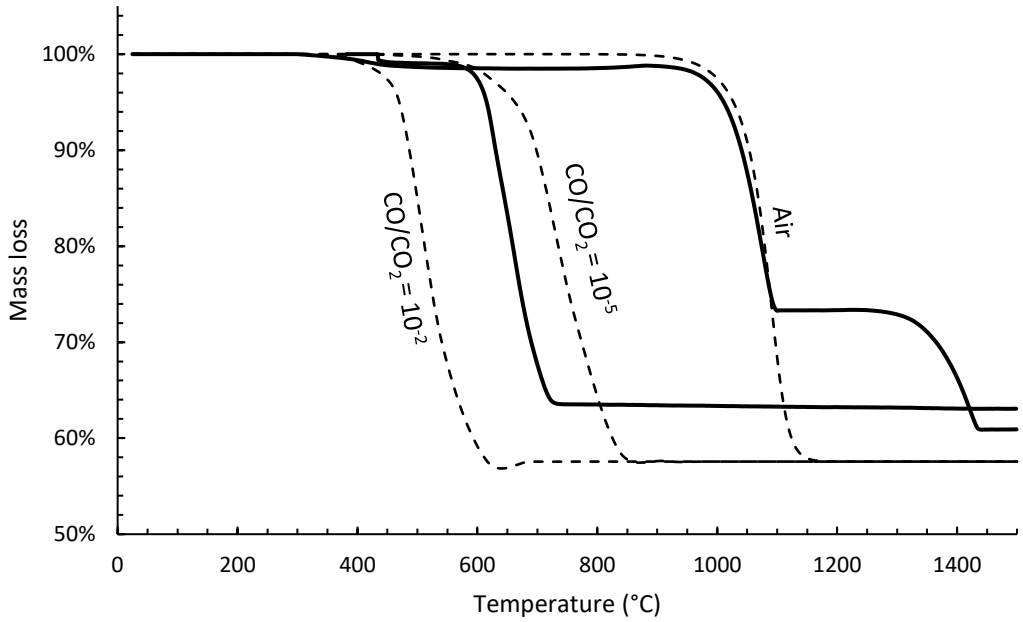

Figure 5.2 – Comparison between the mass loss attained from TGA under reducing atmosphere and synthetic air atmosphere (continuous lines) with the simulated data for the varying oxygen partial pressures (dotted lines)

The difference between the remaining mass fraction for the simulated and actual TGA results may be attributed to the correction of the base number, that is performed to remove the hydration water existent in the reagent grade used in the TGA (heptahydrated, see Appendix A for detailed results). For the sake of calculation, the first plateau is assumed to be the mass loss for hydration water. That value is then considered to be 100% mass for anhydrous sulfate.

5.3.2 Roasting under reducing atmosphere

The same condition (100%CO atmosphere) was applied to a residue containing REE obtained from a process for the production of synthetic rutile (TiO_2). The REE extraction by leaching after roasting under different atmospheres (CO and air) are shown in Figure 5.3. The temperature for maximum REE extraction dropped from 750°C to 400°C, as the experimental condition was changed from air to a reducing condition. Also, the maximum extraction increased from 79% to 92%. The use of a rotary kiln for the experiments under reducing conditions may have contributed to the increase in the maximum extraction, since the ore movement inside the furnace may favors gas percolation and may decrease local gas pressure.

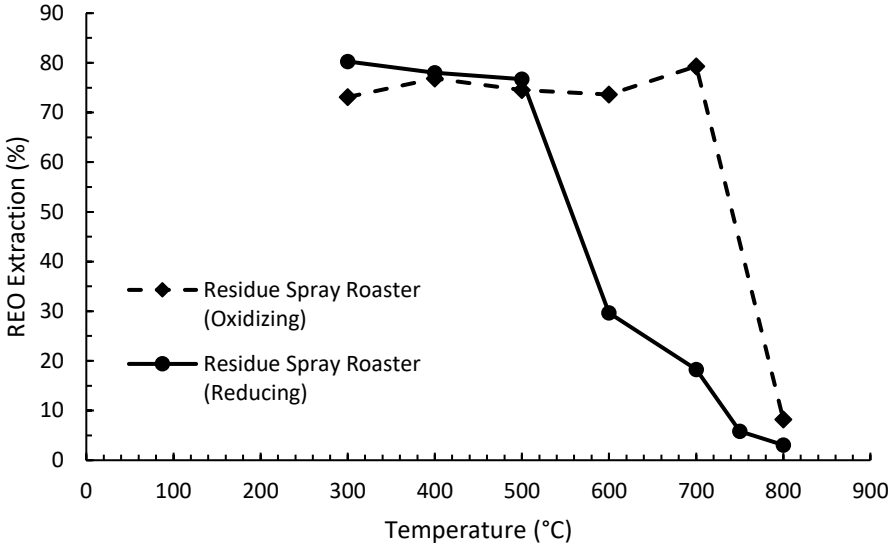

Figure 5.3 – Rare earths extraction by leaching, after roasting the samples under (i) an oxidizing atmosphere in a muffle furnace (dashed line), and (ii) under a reducing atmosphere using a rotary kiln (continuous line).

The impact of the applying oxidizing/reducing atmospheres on selectivity against iron and thorium was investigated. The extraction values for these target impurities are shown in Figure 5.4. The selectivity against thorium was improved. The extraction for the best temperature using oxidizing atmosphere (750°C) was about 10% and the extraction using reducing atmosphere (400°C) was about 4%. The behavior at 500°C is being reevaluated. On the contrary, selectivity against iron was worse under reducing conditions. The selectivity for oxidizing atmosphere, was attained for 80% REE extraction against 9% iron extraction. Under reducing atmosphere, those numbers were 80% and 7%, respectively. This result means that there is no significant change in the REE and iron extraction. However, thorium extraction was improved, reducing from 10% at 700°C under oxidizing atmosphere to 1% at 400°C under reducing atmosphere.

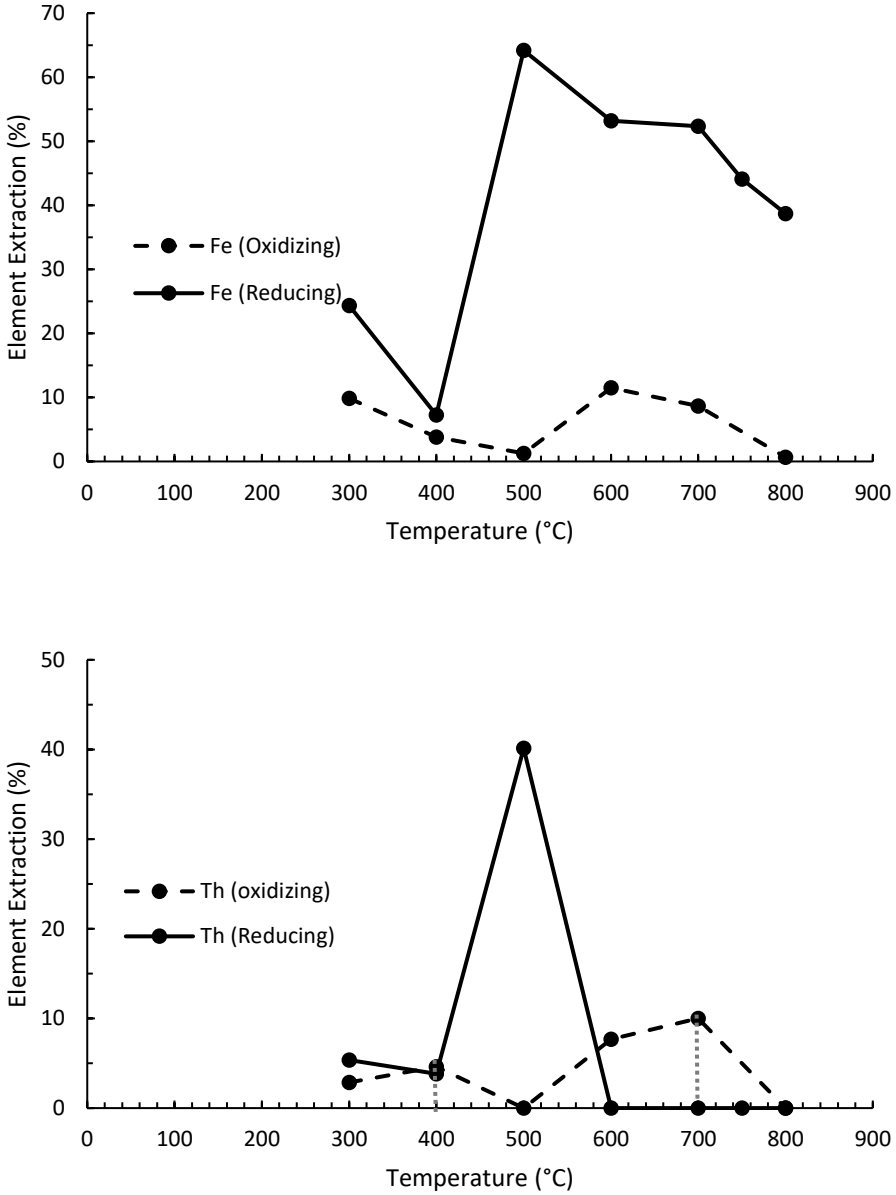

Figure 5.4 – Impurities (Fe and Th) extraction by leaching, after roasting the samples under (i) an oxidizing atmosphere in a muffle furnace (dashed line), and (ii) under a reducing atmosphere using a rotary kiln (continuous line). The vertical dotted lines highlight the maximum impurity extraction under maximum REE extraction, for oxidizing and reducing conditions.

The significant increase in iron extraction observed in Figure 5.3 was expected due to the conversion of iron (III) in iron (II), which has a much larger solubility under pH 1.5. The ratio Fe(II)/Fe(III) in the liquor is shown in Figure 5.5.

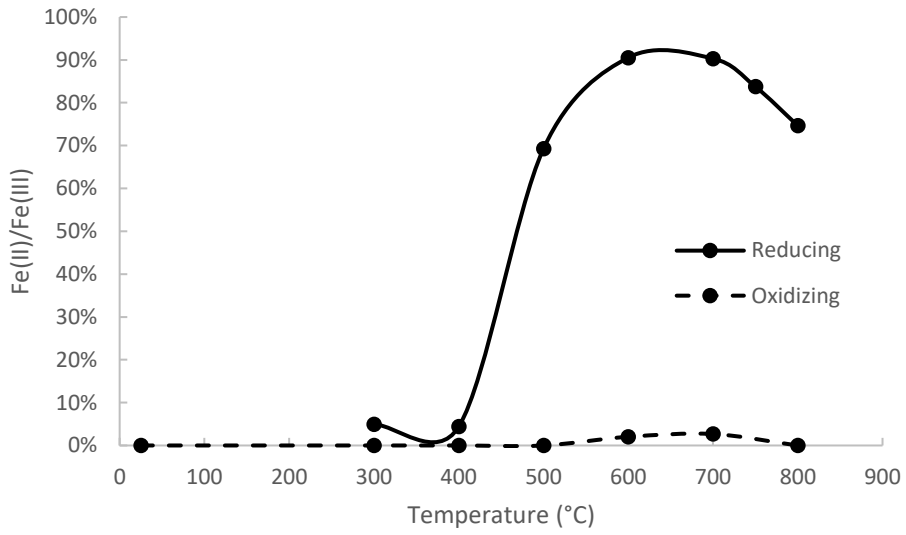

Figure 5.5 – Ratio Fe(II)/Fe(III) in the liquor after leaching the samples submitted to roasting (2h). Oxidizing conditions were attained by roasting under air atmosphere. Reducing atmosphere was attained by CO gas injection at a rate of 2l min^{-1}.

The results attained so far is preliminary, and further investigation is underway. The leaching residue is having its mineralogy being analyzed in order to verify if the insoluble REE compound attained when heating at 400°C under CO atmosphere is oxide formed from the sulfate decomposition or reconverted phosphate.

The atmosphere of the furnace may also be affected by the charge inside the furnace. A mineral sample containing high amount of magnetite was selected in order to evaluate the effect of reducing agent in the charge during heating under ar atmosphere. The preliminary results (not included) show that the optimal processing temperature have shift from 750°C to 600°C. The same sample was subjected to an oxidizing pretreatment, as detailed in section 5.2.2. The objective was to oxidize the magnetite before sulfation and clarify if the temperature shift would not take place. The results are not yet available.

5.4 Conclusions

Both thermodynamic simulation and experiments in a furnace, showed that the atmosphere of the kiln during roasting is a very important factor both in defining the temperature for optimal REE extraction during leaching, with the minimum solubilization of impurities. Experiments showed that when a reducing atmosphere (100% CO) was applied, the optimal extraction temperature was shifted from 700°C to 400°C. After 400°C there was a great reduction in the REE extraction. Thorium extraction was decreased from 10% to 1%. Iron extraction varied from 10% under an air atmosphere to 7% under a reducing atmosphere. Iron solubilization increases even more with increasing temperature, reaching values higher than 50%. This phenomenon is explained by the conversion from F(III) to Fe(III), which is much more soluble under the conditions adopted for leaching. Chemical analysis indicated that the percentage of Fe(II) in leached iron reached more than 90%.

5.5 References

Berni TV, Pereira AC, Mendes FD, Tude AL (2013) System and Method for Rare Earth Extraction. Patent US 2013/0336856 A1.

Gupta, C. K. and Krishnamurthy, N. (2005) Extractive Metallurgy of Rare Earths, CRC Press, Nova York.

Hamemerschmidt J. and Wrobel M. (2009), Decomposition of Metal Sulfates – A SO_2 Source for Sulfuric Acid Production, The Southern African Institute of Mining and Metallurgy, Sulphur and Sulphuric Acid Conference 87-100

Hegedus AJ, Fukker K (1956) Ver. Gluhlampen-u. Elektrizitats-werke, A.-G., Tungsram, Budapest, Z. Anorg. Allg. Chem. 284:20-30.

HSC Chemistry 8 (2015), Equilibrium calculations, Outotec, Pori, Finland.

Papangelakis V. G. and Moldoveanu G., Recovery of Rare Earth Elements from Clay Minerals, ERES2014: 1st European Rare Earth Resources conference, Milos (2014)

Poston JA Jr, Siriwardane RV, Fisher EP, Miltz AL (2003) Thermal decomposition of the rare earth sulfates of cerium (III), cerium (IV), lanthanum (III) and samarium (III), Applied Surface Science 214:83-102.

Swift W. M., Panek A. F., Smith G. W., Vogel G. J. and Jonke A. A. (1976), Decomposition of Calcium Sulfate – A Review of the Literature, National Technical Information Service, U. S. Department of Commerce

Teixeira LAV, Silva RG (2014) System and process for selective rare earth extraction with sulphur recovery. Patent US 2015/0329940 A1.

Teixeira L. A. V., Silva R.G., Avelar A., Majuste D., Ciminelli V. S. T. (2019). Selective Extraction of Rare Earth Elements from Monazite Ores with High Iron Content. Mining, Metallurgy and Exploration, 36:235-244.

Teixeira, L.A.V., Silva, R.G., Majuste, D., Ciminelli, V.S.T. (2020), Stability of Lanthanum in Sulfate and Phosphate Systems and Implications for Selective Rare Earth Extraction, Minerals Engineering, 155, Elsevier, p.1-11. https://doi.org/10.1016/j.mineng.2020.106440.

Testa, FG, Avelar, AN, Silva, RG, Souza, CC (2016) mineralogical characterization and alternative to concentrate the rare earth lithotypes from alcaline complex of Catalão – GO. Associação Brasileira de Metalurgia, Materiais e Mineração, São Paulo, DOI (http://dx.doi.org/10.4322/2176-1523.1064)

Verbaan N, Bradley K, Brown J, Mackie S (2015) A review of hydrometallurgical flowsheets considered in current REE projects, In: Simandl GJ and Neetz M (eds.) Symposium on Strategic and Critical Materials Proceedings. British Columbia Ministry of Energy and Mines, British Columbia Geological Survey Paper 2015-3, Victoria, British Columbia, pp. 147-162.

6 CERIUM AND NEODYMIUM PHOSPHATE-CONVERSION INTO SULFATE AND CHLORIDE BY HIGH TEMPERATURE EXCHANGING REACTION

6.1 Introduction

Rare earth elements (REEs) have been used in various advanced materials, such as magnets, catalysts, batteries and phosphor among others (Roskill 2019). In particular, the use of neodymium (Nd) with dysprosium (Dy) in heat resistance powerful magnetic materials are important with regard to the amount used in the production. Jones et al., (1996) have listed 245 minerals, including silicates. The more important REE minerals, representing 95% of the world's resource, are xenotime, Bastnasite (64%), monazite (9%), xenomite and ion-adsorption clay (25%), with unique occurrence in China (Aplan 1988, Ferron et al., 1991, Jackson and Christian, 1993). Monazite, a phosphate mineral containing light REE such as cerium and Nd [REE-PO_4], is used only in small amount for REE production, despite the high REE content existent in the pure mineral (about 70%) as same as bastnaesite. There is considerable incentive to establish green technologies to produce REE from monazite which may contribute to a more increasing and stabilization of REE supply.

In the monazite ores, REE constitute phosphate compounds which are thermodynamically stable and highly insoluble in weak acid. To achieve their selective dissolution from other mineral phases during leaching process, the conversion into a more reactive phase is beneficial for the following refining process. Sulfation and chlorination methods are widely known as extraction processes of REE from ores (Gupta and Krishnamurthy,2005, Zhang et al., 2016). The sulfation is performed by mixing concentrated sulphuric acid (96-98%) with REE ores and heated between 200-250 °C where REE sulfates are form and subsequently dissolved by adding water at room temperature. Chlorination is achieved by applying chlorine gas to REE ores in the presence of a reducing agent such as carbon (Hartley, 1952) at 900°C, reaching conversions of 85%. Both processes use a large amount of high concentration acid or toxic gas and include high risks for health and environment. Therefore the mild process for REE extraction is required. Recently, a selective roasting process using sulfuric acid

for low REE grade ores was developed (Teixeira et al., 2019). However, alternative processes that can further improve extraction costs are still required.

The decomposition of REE-phosphates by exchanging reaction with solid sulfate or chloride reactants to suppress the usage and emission of excess amount of sulfuric acid and chlorine is being considered in this work. The decomposition of $CePO_4$ and $NdPO_4$ were studied by exchange reactions with the alkaline and earth alkaline sulfates and chlorides. At first, the thermodynamics on exchange reactions was reviewed and selected reactions were examined by thermal analysis combined with the XRD analysis and possible exchange reaction to decompose REE-phosphate was clarified.

6.2 Thermodynamics of Decomposition of $CePO_4$ and $NdPO_4$ by Exchanging Sulfation and Chlorination

To discuss the sulfation or chlorination of REE-phosphates, the exchanging reactions of phosphates with sulfate and chloride are described in this session. Cerium is assumed to be trivalent for simplicity in this discussion. Here, thermodynamic data were mostly obtained from FactSage oxide database (Bale et al., 2009), and reaction entropies for Ce and Nd phosphates were assumed to be same with other phosphates.

Exchanging sulfation reactions of phosphates are described as the following equations, combining formation reactions of their phosphates and sulfates.

$$2M_3PO_4 + 3SO_3 = 3M_2(SO_4) + P_2O_5\ (M; Na) \quad (6.1)$$

$$M_3(PO_4)_2 + 3SO_3 = 3M(SO_4) + P_2O_5\ (M; Mg, Ca) \quad (6.2)$$

$$2MPO_4 + 3SO_3 = M_2(SO_4)_3 + P_2O_5\ (M; Fe, Ce, Nd) \quad (6.3)$$

The Gibbs energy changes of the exchanging sulfations are described in Table 6.1 and summarized in Figure 6.1 (a). Nd, Ce and Na phosphates are rather reactive with sulfur trioxide to form sulfates whereas Al, Fe and Mg phosphates are less reactive. Hence, it was predicted that the exchanging sulfation of Nd or Ce phosphate with Al, Fe or Mg sulfate would occur thermodynamically.

Exchanging chlorination reactions of phosphates are described as the following equations, combining formation reactions of their chlorides and phosphates.

$$2\,M_3\,PO_4 + 3\,Cl_2 = 6\,MCl + P_2O_5 + \frac{3}{2}O_2 \text{ (M; Na)} \quad (6.4)$$

$$M_3(PO_4)_2 + 3Cl_2 = 3MCl_2 + P_2O_5 + \frac{3}{2}O_2\ (M; Mg, Ca) \quad (6.5)$$

$$2M(PO_4) + 3Cl_2 = 2MCl_3 + P_2O_5 + \frac{3}{2}O_2\ (M; Fe, Ce, Nd) \quad (6.6)$$

The Gibbs energy changes of the exchanging chlorinations are described in Table 6.1Table 6.1 and summarized in Figure 6.1 (b). Na phosphate is rather reactive with chlorine to form chloride. Other phosphates are less reactive but the chlorination of $CePO_4$ is slightly more reactive than that of $MgPO_4$, indicating the possibility of the following reaction.

$$2CePO_4 + 3MgCl_2 = Mg_3(PO_4)_2 + 2CeCl_3 \quad (6.7)$$

Table 6.1 - Standard Gibbs energy of phosphation, sulfation and chlorination of components in monazite ore

Phosphation	
$Fe_2O_3 + P_2O_5 = 2Fe(PO_4)$	$\Delta G^o = - 639{,}000 + 247T$
$Al_2O_3 + P_2O_5 = 2Al(PO_4)$	$\Delta G^o = - 648{,}000 + 211T$
$3CaO + P_2O_5 = Ca_3(PO_4)_2$	$\Delta G^o = - 1096{,}000 + 254T$
$3MgO + P_2O_5 = Mg_3(PO_4)_2$	$\Delta G^o = - 846{,}000 + 253T$
$3Na_2O + P_2O_5 = 2Na_3(PO_4)$	$\Delta G^o = - 648{,}000 + 211T$
$Ce_2O_3 + P_2O_5 = 2Ce(PO_4)$	$\Delta G^o = - 634{,}000 + 250T$ *
$Nd_2O_3 + P_2O_5 = 2Nd(PO_4)$	$\Delta G^o = - 624{,}000 + 250T$ *
Sulfation	
$Fe_2O_3 + 3\ SO_3 = Fe_2(SO_4)_3$	$\Delta G^o = - 560{,}000 + 533T$
$Al_2O_3 + 3\ SO_3 = Al_2(SO_4)_3$	$\Delta G^o = - 546{,}000 + 179T$
$CaO + SO_3 = CaSO_4$	$\Delta G^o = - 396{,}000 + 177T$
$MgO + SO_3 = MgSO_4$	$\Delta G^o = - 257{,}000 + 179T$
$Na_2O + 3\ SO_3 = Na_2SO_4$	$\Delta G^o = - 546{,}000 + 179T$
$Ce_2O_3 + 3\ SO_3 = Ce_2(SO_4)_3$	$\Delta G^o = - 967{,}000 + 628T$
$Nd_2O_3 + 3\ SO_3 = Nd_2(SO_4)_3$	$\Delta G^o = - 901{,}000 + 636T$
Exchanging (sulfation)	
$2Fe(PO_4) + 3SO_3 = Fe_2(SO_4)_3 + P_2O_5$	$\Delta G^o = 79{,}000 + 286T$
$2Al(PO_4) + 3SO_3 = Al_2(SO_4)_3 + P_2O_5$	$\Delta G^o = 102{,}000 + 312T$
$Ca_3(PO_4)_2 + 3SO_3 = 3CaSO_4 + P_2O_5$	$\Delta G^o = - 92{,}000 + 277T$
$Mg_3(PO_4)_2 + 3SO_3 = 3MgSO_4 + P_2O_5$	$\Delta G^o = 75{,}000 + 284T$
$2Na_3(PO_4) + 3SO_3 = 3Na_2SO_4 + P_2O_5$	$\Delta G^o = - 227{,}000 + 220T$
$2Ce(PO_4) + 3SO_3 = Ce_2(SO_4)_3 + P_2O_5$	$\Delta G^o = - 333{,}000 + 378T$ *
$2Nd(PO_4) + 3SO_3 = Nd_2(SO_4)_3 + P_2O_5$	$\Delta G^o = - 277{,}000 + 386T$ *
Exchanging (chlorination)	
$2Fe(PO_4) + 3Cl_2 = 2FeCl_{3(l)} + P_2O_5 + 1.5O_2$	$\Delta G^o = 779{,}000 - 279T$
$2Al(PO_4) + 3Cl_2 = 2AlCl_{3(l)} + P_2O_5 + 1.5O_2$	$\Delta G^o = 1019{,}000 - 233T$
$Ca_3(PO_4)_2 + 3Cl_2 = 3CaCl_2 + P_2O_5 + 1.5O_2$	$\Delta G^o = 628{,}000 - 120T$
$Mg_3(PO_4)_2 + 3Cl_2 = 3MgCl_2 + P_2O_5 + 1.5O_2$	$\Delta G^o = 747{,}000 - 121T$
$2Na_3(PO_4) + 3Cl_2 = 6NaCl + P_2O_5 + 1.5O_2$	$\Delta G^o = 229{,}000 - 76.5T$
$2Ce(PO_4) + 3Cl_2 = 2CeCl_3 + P_2O_5 + 1.5O_2$	$\Delta G^o = 725{,}000 - 115T$ *
$2Nd(PO_4) + 3Cl_2 = 2NdCl_3 + P_2O_5 + 1.5O_2$	$\Delta G^o = 761{,}000 - 103T$ *

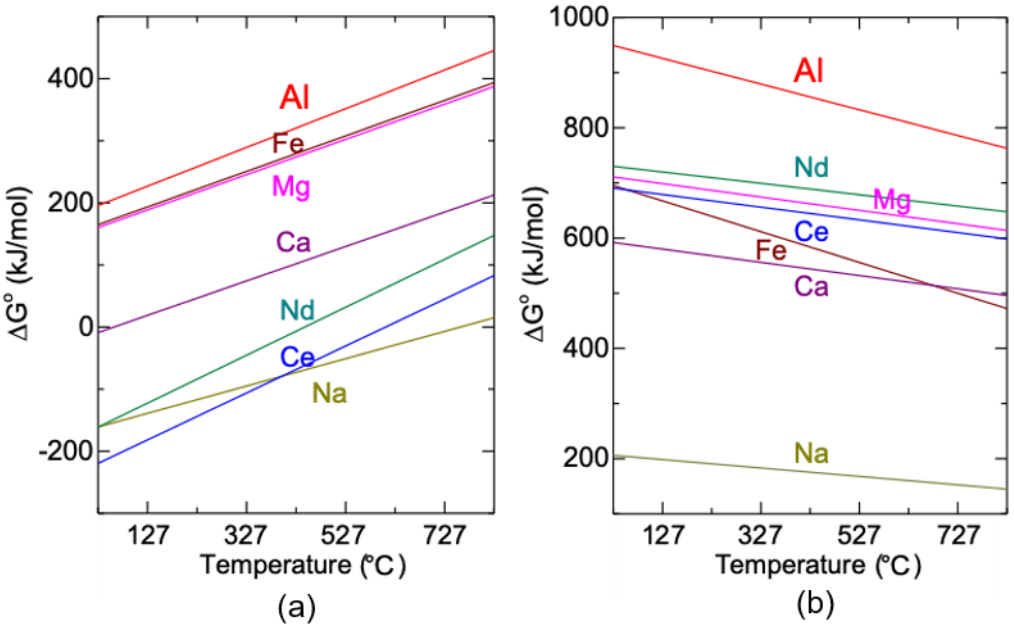

Figure 6.1 - Standard Gibbs energies for exchanging sulfation (a) and chlorination (b) reactions of phosphates.

6.3 Experimental

6.3.1 Materials

$NdPO_4$ and $CePO_4$ were prepared as follows; (1) after metallic Nd and Ce were dissolved in hydrochloric acid, $NdPO_4$ hydrate was precipitated by adding phosphoric acid and NaOH. (2) the precipitate were calcined at 540°C. Analytical reagent grade of $MgSO_4$ anhydrate, $CaSO_4$ anhydrate, $MgCl_2$ anhydrate, $Fe_2(SO_4)_3$, KCl were used after drying by heating at 400°C for more than 1 hr.

6.3.2 TG-DSC

Thermogravimetry - differential scanning calorimetry (TG-DSC, STA PT1600, Linseis Messgeraete GmbH, Bavaria, Germany) was used. Equimolar mixture of $CePO_4$ ($NdPO_4$) and sulfate or chloride was prepared from the dried powder. A 10-30 mg of mixture sample was pressed into tablet with 3 mm in diameter. The tablet was charged in an alumina crucible and set in the TG-DSC chamber. The chamber was evacuated by rotary pump for more than 20 mins, and subsequently refilled with dried air or pure Ar. At the gas flow rate of 20 ml/min, the sample heating profile was as follows: heating rate, 5°C/min; top temperature, 850°C for 10 min; cooling rate, 20°C/min; atmosphere, dried air or Ar gas; gas flow, 20 ml/min.

6.3.3 Characterization of the calcinated samples

Morphological observation of the surface structure of calcinated samples and analysis of chemical composition were performed with scanning electron microscopes (SEM) – energy dispersive x-ray spectroscopy (EDS) (JSM-6510LV, JEOL, Tokyo, Japan). Analysis of the crystal structure of the calcinated samples was performed with X-ray diffraction (XRD, SmartLab 3, Rigaku Corp., Tokyo, Japan). The analysis conditions were as follows: tube, Cu Kα or Mo Kα; power, 40kV/30mA.

6.4 Results and Discussion

6.4.1 Investigation of sulfation process

To examine the reactivity of $NdPO_4$ and $CePO_4$ with sulfate compounds, the phosphate –sulfate mixture was subjected to TG-DSC analysis. DSC curves obtained for couples of phosphate and sulfate are shown in Figure 6.2. For the mixture of $NdPO_4$-$MgSO_4$, the endothermic peak is seen around 750-820°C while the exothermic peak does not appear upon cooling. This suggests that some extent of chemical reaction, but not phase transition, occurs during heating of the mixture. The mixture of $NdPO_4$-$CaSO_4$, $CePO_4$-$MgSO_4$ and $CePO_4$-$CaSO_4$ did not show the apparent peaks, indicating insignificant reactions. The mixture of $NdPO_4$-$Fe_2(SO_4)_3$ and $CePO_4$-$Fe_2(SO_4)_3$ showed the broad endothermic peaks at 600–730°C and 600–750°C, respectively, and also showed the weight loss at corresponding temperatures, suggesting the decomposition of $Fe_2(SO_4)_3$ releasing SO_3. The other reaction was not clearly determined from DSC curves.

The mixture of $NdPO_4$-$MgSO_4$-KCl and $NdPO_4$-$CaSO_4$-KCl were examined for considering the KCl role of solvent after its melting. Endothermic peaks upon heating and exothermic peaks upon cooling were observed. Exothermic peaks starting from 816, 564 and 420°C were assumed to be liquidus for $KCl \cdot MgSO_4$, eutectic temperature for $KCl \cdot MgSO_4$ and KCl, and ternary eutectic temperature, referring the K-Mg-SO_4-Cl quaternary system in Figure 6.3 (a). Exothermic peaks starting from 757°C, 653°C were assumed to be liquidus for $CaSO_4$ and eutectic temperature for $CaSO_4$ and KCl, referring the K-Ca-SO_4-Cl quaternary system in Figure 6.3 (b). Both systems indicated the change from

initial equimolar composition with slight consumption of SO_4. Some reaction such as sulfate–phosphate exchange was hypothesized to occur by TG-DSC analysis.

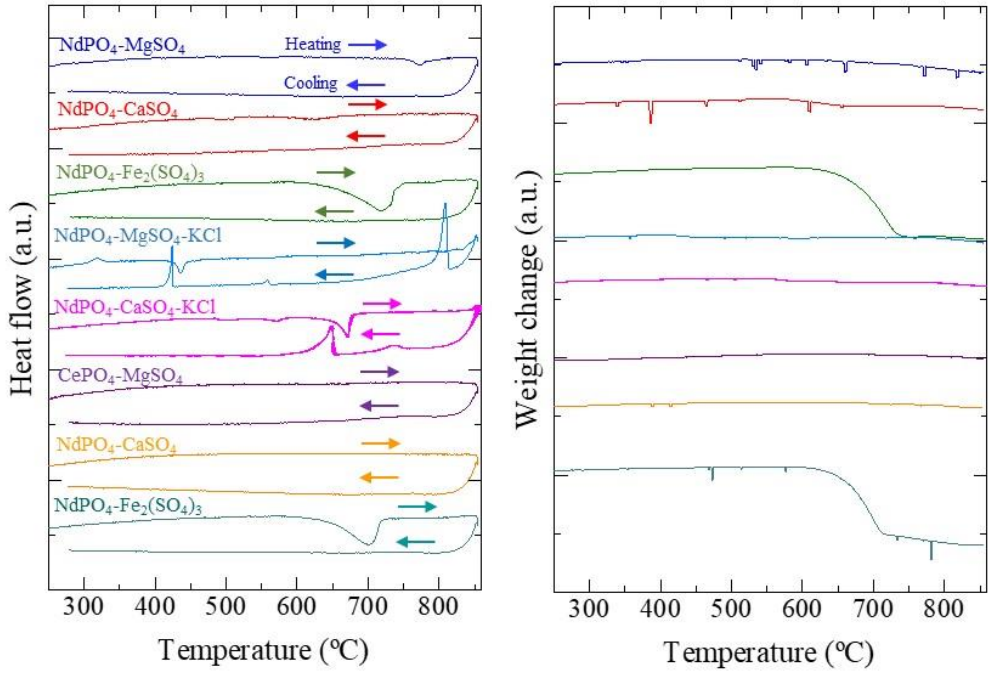

Figure 6.2 – DSC results (left) and TGA results (right) for phosphate-sulfate systems and phosphate-sulfate-chloride systems under argon atmosphere.

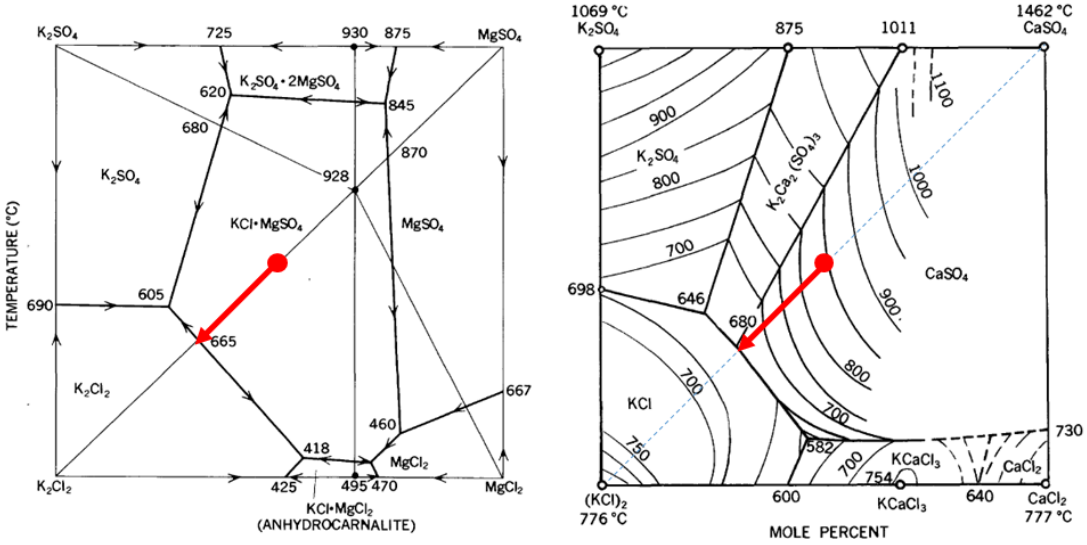

Figure 6.3 - Reported K-Mg-SO4-Cl (a) and K-Ca-SO_4-Cl (b) quaternary phase diagrams

Samples after DSC analysis were subjected to XRD analysis, and the results for binary mixtures are summarized in Figure 6.4. Basically, $NdPO_4$ and $CePO_4$ remain as major parts. The both $NdPO_4$-$MgSO_4$ and $CePO_4$-$MgSO_4$

mixtures show the diffraction peak at 15.0° as marked with arrows, which were not seen in the mixtures with $CaSO_4$ and $Fe_2(SO_4)_3$. It suggests the reaction phase formation according to $MgSO_4$. All the peaks for $NdPO_4$-$MgSO_4$ and $CePO_4$-$MgSO_4$ mixtures were assigned to $NdPO_4$ and $MgSO_4$, and $CePO_4$ and $MgSO_4$, respectively, although the significant broadening of peaks was seen for $CePO_4$-$MgSO_4$ mixture.

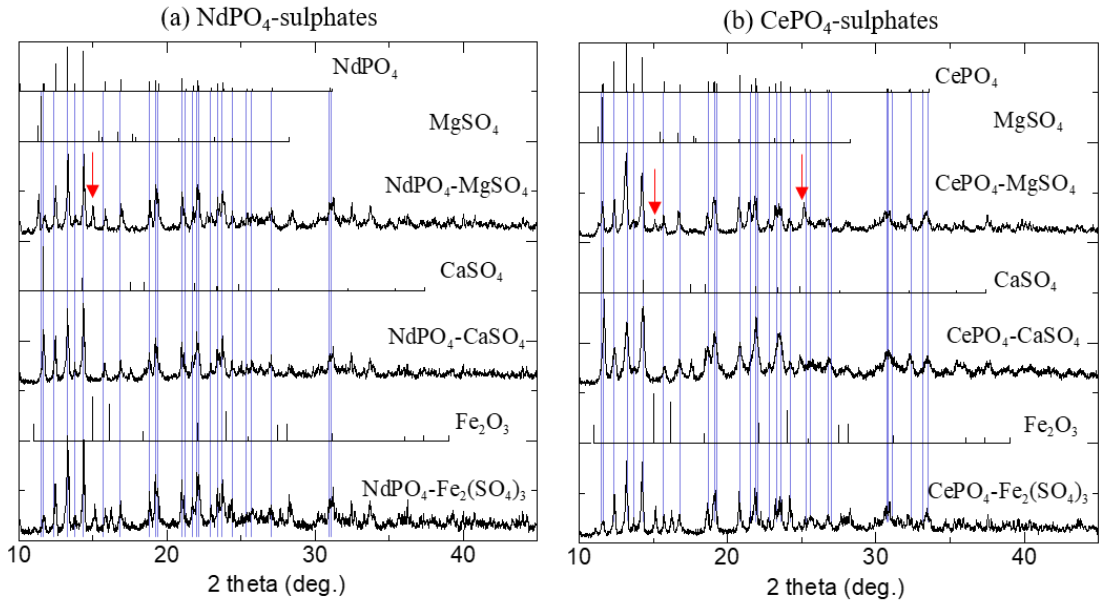

Figure 6.4 - XRD patterns for (a) NdPO4-sulphates and (b) CePO4-sulphates. (Mo-Kα)

Diffraction patterns for $NdPO_4$-$Fe_2(SO_4)_3$ and $CePO_4$-$Fe_2(SO_4)_3$ mixtures were assigned to $NdPO_4$ and corundum, and $CePO_4$ and corundum, respectively. $Fe_2(SO_4)_3$ decomposes to Fe_2O_3, which was also estimated from TG-DSC analysis. The peaks for corundum show deviation from the ones for Fe_2O_3, suggesting the solid solutions of Fe_2O_3.

The XRD patterns for the mixtures of $NdPO_4$-$MgSO_4$-KCl and $NdPO_4$-$CaSO_4$-KCl are summarized in Figure 6.5. The peaks for the $NdPO_4$-$MgSO_4$-KCl mixture were assigned to $NdPO_4$, $K_2Mg_2(SO_4)_3$ and KCl and those for $NdPO_4$-$CaSO_4$-KCl were assigned to $NdPO_4$, $CaSO_4$ and KCl. No significant reaction phase was thus identified.

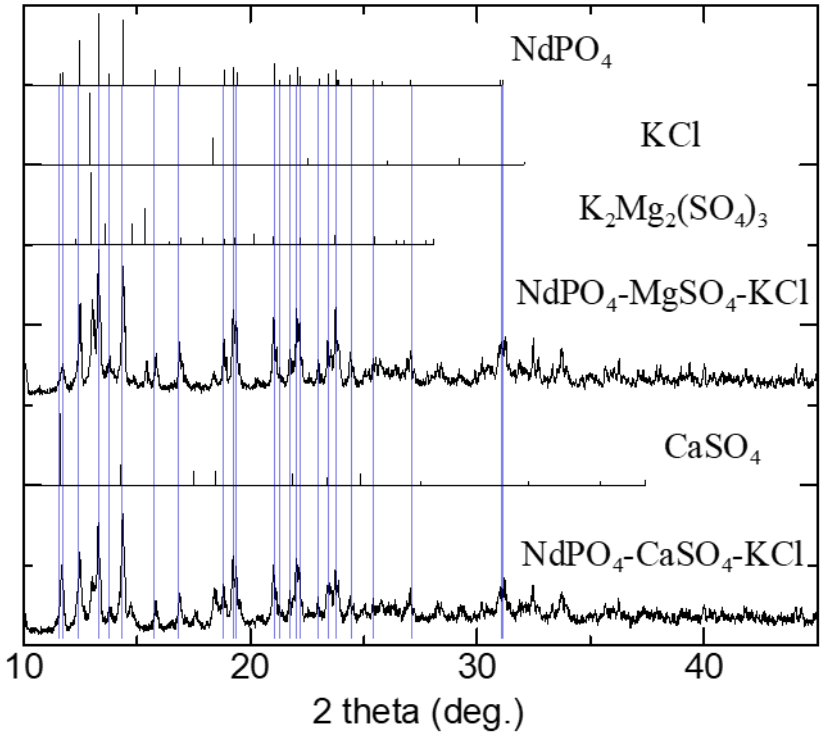

Figure 6.5 - XRD patterns for $NdPO_4$-sulphates-KCl. (Mo-Kα)

Accordingly, a slight reaction was found for $NdPO_4$-$MgSO_4$, $CePO_4$-$MgSO_4$, $NdPO_4$-$Fe_2(SO_4)_3$ and $CePO_4$-$Fe_2(SO_4)_3$, but seems not to clearly reflect the estimation from thermodynamic analysis. To correctly determine their reactivities, further study would be needed such as the effect of atmosphere (oxidizing, reducing) and the effect of particle size, among others.

6.4.2 Investigation of chlorination process

To examine the reaction of $NdPO_4$ and $CePO_4$ with $MgCl_2$, TG-DSC analysis were performed. The temperature and DSC pattern are shown in Figure 6.6**.**

For the reaction of $NdPO_4$ and $MgCl_2$ under Ar, the DSC signal showed endothermic broad peaks at 580-700℃ and 720-850℃, respectively. We assume the low temperature one to be eutectic melting and the high temperature one to be subsequent partial dissolution of $NdPO_4$ from the slight exothermic peak starting at 820℃ and the steep exothermic peak at 650℃ upon cooling. Similar behaviour of eutectic melting (620-700℃) and subsequent partial melting (720-850℃) is also seen for the reaction of $CePO_4$ and $MgCl_2$ under Ar.

On the other hand, the DSC signal showed the endothermic broad peaks at 580-700℃ and strong endothermic broad band 700-850℃ under dried air for the mixture between $NdPO_4$ and $MgCl_2$. The former one would be the eutectic melting from the similarity with the result under Ar although the latter is significantly different with it, suggesting the chemical reaction in the mixture. For the mixture of $CePO_4$ and $MgCl_2$ under dried air, the DSC signal showed broad endothermic band from 480℃ suggesting the endothermic chemical reaction in the mixture with comparing the tendency under Ar.

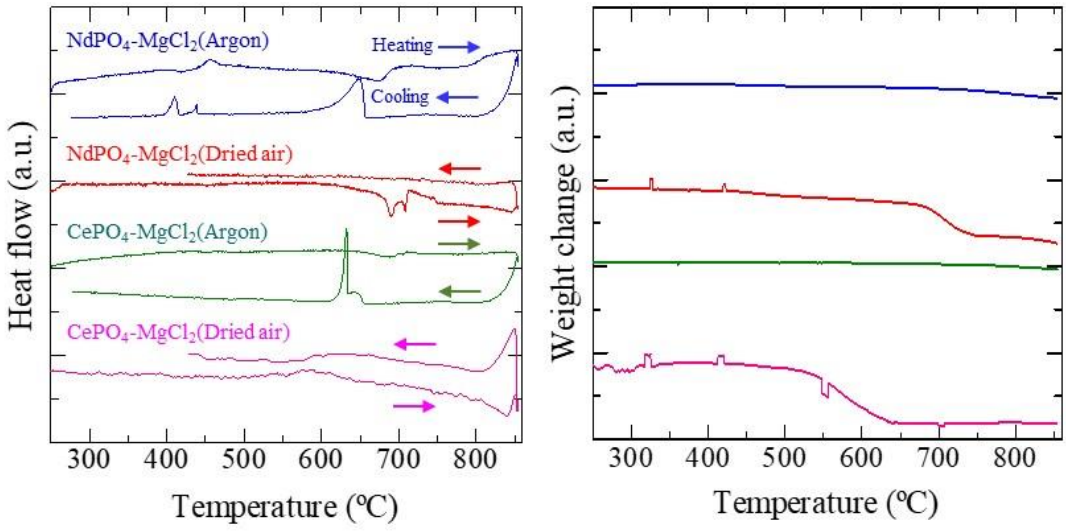

Figure 6.6 - Temperature profile and DSC signal of the mixture of REE-phosphate and $MgCl_2$. Left column is the reaction of $NdPO_4$ and $MgCl_2$, right is $CePO_4$ and $MgCl_2$. Top is the mixture heated under dried air, bottom is under Ar gas. Solid lines are temperature. Brake lines are DSC signals.

The samples after DSC analysis were subjected to XRD analysis, and the results are summarized in Figure 6.7((a) are the results for $NdPO_4$ and (b) the results for $CePO_4$)). For the mixture of $NdPO_4$ and $MgCl_2$, main product under dried air condition was NdOCl with $Mg_3(PO_4)_2$. On the other hand, under Ar condition, $NdPO_4$ remained unreacted. For the mixture of $CePO_4$ and $MgCl_2$, main product under dried air condition was CeO_2 with $Mg_3(PO_4)_2$. Also, under Ar condition, $CePO_4$ also remained unreacted. These results suggested that chlorination of REE phosphate using $MgCl_2$ was proceeded under air condition.

$$2NdPO_4 + 3MgCl_2 + O_2 \rightarrow 2NdOCl + Mg_3(PO_4)_2 + Cl_2 \uparrow \quad (6.8)$$

$$2CePO_4 + 3MgCl_2 + O_2 \rightarrow 2CeO_2 + Mg_3(PO_4)_2 + 3Cl_2 \uparrow \quad (6.9)$$

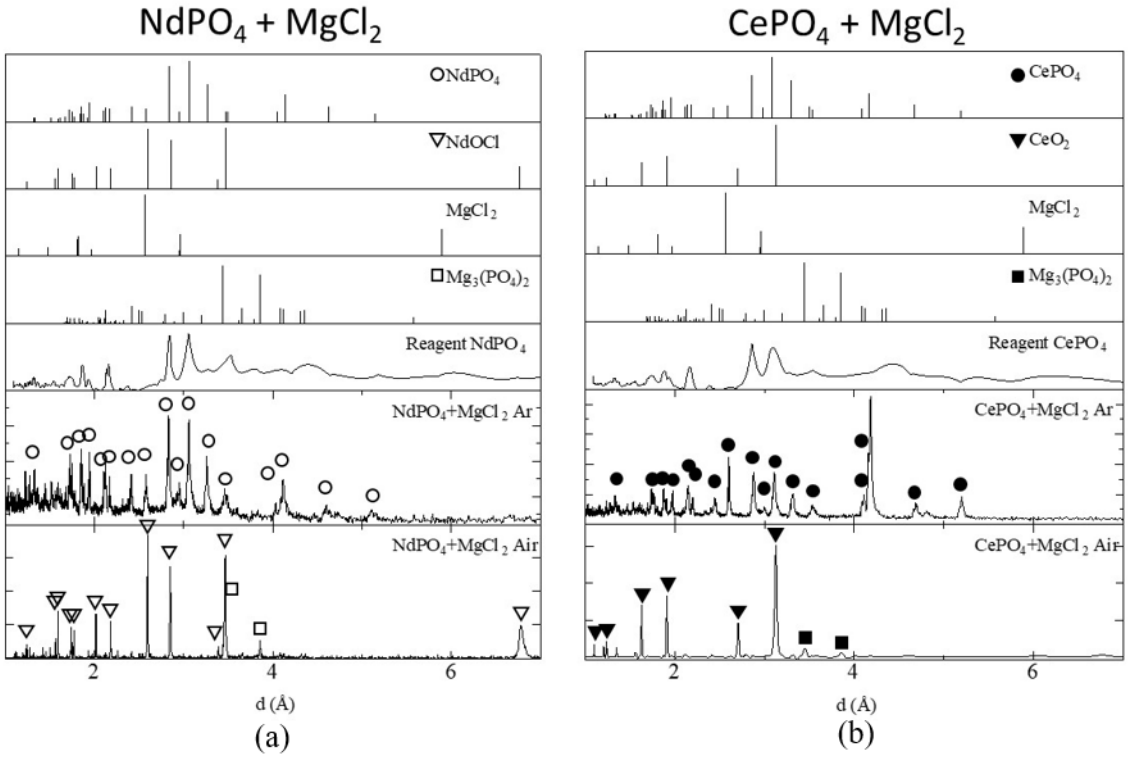

Figure 6.7 - XRD patterns for $NdPO_4$-chlorinates (a) and $CePO_4$-chlorinates (b)

This is a work in progress. New thermodynamic data will be generated, now considering the final products attained during the experiments.

6.5 Conclusion

Thermodynamic analysis has shown that exchanging reaction between Ce and Nd phosphate and Al, Fe or Mg sulfate may occur spontaneously. However, no reaction was detected for heating under inert atmosphere. Thermodynamic analysis has also shown that Ce and Nd phosphate chlorination may be possible by $MgCl_2$ exchanging reaction. Experiments have shown that chlorination of both Nd and Ce phosphates was possible under air atmosphere. Conversion reaction took place for temperature interval between 720-850°C for Nd and between 600-850°C for Ce. The main products were neodymium oxychloride (NdOCl) and CeO_2. Ce (IV) formation was related to the strong oxidizing atmosphere present by the combination of Cl_2 and O_2.

6.6 References

Aplan F.F. (1988) The processing of rare earth minerals. In Rare earths, extraction preparation and applications. TMS, Warrendale, P A., edited by R.O. Bautista, and M.M. Wong, (1988).pp.15-34.

Bale, CW, Bélisle, E, Chartrand, P, Decterov, SA, Eriksson, G, Hack, K, Jung, IH, Kang, YB, Melançon, J, Pelton, DA, Robelin, C, Petersen, S: (2009) FactSage thermochemical software and databases — recent developments. Calphad 33, 295 (2009).

Ferron C. J., Bulatovic S. M., Salter R.S., (1991) Beneficiation of rare earth oxide minerals International. Conference (Ed.), On Rare Earth Minerals and Minerals for Electronic Uses, Prince Songkla University, Hat Yai, TH (1991), pp. 251-269

Gupta, C. K.; Krishnamurthy, N. (2005) Extractive metallurgy of rare earths, CRC Press, Nova York.

Hartley, F. R. (1952) The preparation of anhydrous lanthanum chlorides by high temperature chlorination of monazite, J. Appl. Chem. 2: 24-31

Jackson W.D., and Christiansen G (1993), International strategic minerals inventory summary report-- Rare-earth oxides U.S. Geological Survey Circular 930-N, 1993, (68 p.)

Roskill Information Service, Rare Earth: Market Outlook to 2029 (2019), 19th Edition, London.

Teixeira L. A. V., Silva R.G., Avelar A., Majuste D., Ciminelli V. S. T. (2019). Selective Extraction of Rare Earth Elements from Monazite Ores with High Iron Content. Mining, Metallurgy and Exploration, 36:235-244.

Zhang J., Zhao B. and Schereiner B. (2016) Separation hydrometallurgy of rare earth elements, Springer, Switzerland.

7 FINAL CONSIDERATIONS

7.1 Overall Conclusions

Our findings indicated that rare earth bearing monazite ores may be selectively treated to separate iron and thorium from rare earth elements if submitted to sulfation, roasting at 700°C, and water leaching under controlled pH. This process promotes high rare earth extraction (between 70-80%), low iron, and thorium extraction (below 1%) with low acid consumption (between 0.21 to 0.34 kg of acid for 1 kg of ore), being adequate to be applied to highly weathered ores. Weathered monazite ores represent a large amount of the available resources in the world, in particular in Brazil.

There was very good agreement for sulfate decomposition between thermodynamic simulation and the experimental results. These results also show that lanthanum sulfate decomposes in a two-step process, likely forming $La_2O_2SO_4$ as an intermediate compound, which could not be predicted from thermodynamic evaluation. The key stage for selective extraction is roasting, in which iron sulfate decomposes into iron oxide and releases SO_3 gas. The iron sulfate decomposition is achieved at 700°C, a condition in which rare earths achieve maximum extraction. The amount of insoluble rare earth compounds increases sharply at temperatures higher than 750°C, decreasing the amount of recoverable rare earth elements during the leaching step and therefore rendering the processes ineffective for rare earth extraction. This temperature is lower than expected for sulfate decomposition into oxides and was shown to be related to the formation of phosphate compounds.

Excess phosphorus remaining in the sulfated material may cause the reconversion of REE sulfates to REE phosphates, and the presence of phosphoric acid will lead to the formation of monazite-like compounds. High partial pressures of P_2O_5 will convert REE sulfates into insoluble REE polyphosphates – $REE(PO_3)_3$. This high partial pressure may be attained by the decomposition of phosphoric acid formed during the sulfation of the ore or by newly formed phosphor compounds, such as monocalcium phosphates. The solid-gas mechanism is preferred, as the gas phase is able to promote better

contact with all REE sulfate particles present in the system, making it possible to achieve the drastic decrease (conversion into phosphate) observed at 800°C.

Thermodynamic simulations and laboratory experiments in a rotary kiln, showed that the furnace atmosphere during roasting is a very important factor both in defining the optimal temperature to maximize REE extraction and minimize the solubilization of impurities, such as iron and thorium, during leaching. Experiments showed that when a reducing atmosphere (100% CO) was applied, the optimal REE extraction temperature was shifted from 700°C to 400°C. Above 400°C there was a marked reduction in the REE extraction during leaching. REE extraction was unaffected and was kept at around 80%. Thorium extraction was reduced from about 10% at 700°C to 1% at 400°C. Iron extraction decreased from 9% under an air atmosphere to 7% under reducing atmosphere. Iron solubilization increases with increasing temperature, reaching values higher than 50%. This phenomenon is explained by the conversion from Fe(III) to Fe(II), which is much more soluble under the conditions adopted for leaching. Chemical analysis indicated that the percentage of Fe(II) in the leached iron reached more than 90%.

Thermodynamic analysis showed that the exchanging reaction involving Ce and Nd phosphate and Al, Fe or Mg sulfate may occur spontaneously. However, no transformation was detected by heating the reactants under inert atmosphere. Thermodynamic analysis has also shown that Ce and Nd phosphate chlorination may be possible by $MgCl_2$ exchanging reaction. Experiments corroborated the thermodynamic simulations by showing that chlorination of both Nd and Ce phosphates do occur under air atmosphere. The reactions took place within 720-850°C for Nd, and within 600-850°C for Ce. The main products were neodymium oxychloride (NdOCl) and CeO_2. Ce (IV) formation was related to the strong oxidizing atmosphere created by the combination of Cl_2 and O_2.

7.2 Original Contributions from this Thesis

The main scientific contributions of the present work are:

(i) Combination of thermodynamic and experimental evaluations to identify the optimum temperature for the selective roasting of monazite from iron-rich ores containing thorium.

(ii) The direct and indirect mechanisms of REE sulfate reconversion to phosphates – monazite-like and polyphosphates.

(iii) The effect of reducing/oxidizing conditions on the mechanism of REE sulfate roasting.

(iv)Experimental pieces of evidence for the formation $La_2O_2SO_4$ as an intermediate compound of lanthanum sulfate decomposition, under oxidizing but not under reducing conditions.

(v) Chlorination of both Nd and Ce phosphates under air atmosphere to produce neodymium oxychloride (NdOCl) and CeO_2.

In addition to the scientific contributions, the development of a selective REE extraction process route over iron and thorium is of fundamental importance to enable the development of several mineral projects around the world. Weathered monazite represents a significant part of the undeveloped projects. This type of deposit does not respond to ore beneficiation, which results in low-grade ore being fed in the extraction plant. This ore, due to intensive weathering, is also rich in iron oxide. This combination of low grade and high amount of iron results in high acid consumption, increasing the operation expenditure (OPEX) of the mining site. When large amount of acid is used, there will also be a high amount of impurities in the liquor after leaching. This increases the complexity of the purification processes, which will ultimately result in higher OPEX and lower metallurgical recovery.

The clarified operational conditions will also make possible the proper selection of engineering equipment, e.g. the correct furnace to operate in a narrow temperature window. By understanding the phenomenon behind the process, new adaptations can be made in order to avoid the early formation of insoluble phosphates, increasing the operational temperature window of the roasting stage, what could lead to less sophisticated equipment selection, reducing capital expenditure and enhancing metallurgical extraction. The

simplified roasting test using TGA enables a fast and cheaper geometallurgy analysis for new deposits, allowing several different lithotypes to be test and evaluated in a short time and with a minimum amount of sample.

7.3 Publications

i. TEIXEIRA, L.A.V., SILVA, R.G., MAJUSTE, D., CIMINELLI, V.S.T. (2017), Aplicação de Pirólise Seletiva para Minérios Ferruginosos Contendo Terras Raras, In: XXVII Encontro Nacional de Tratamento de Minérios e Metalurgia Extrativa, Belém, ENTMME 2017.

ii. TEIXEIRA, L.A.V., SILVA, R.G., MAJUSTE, D., CIMINELLI, V.S.T. (2018) Selective Extraction of Rare Earth Elements from Complex Monazite Ores, Extraction 2018: Proceedings of the First Global Conference on Extractive Metallurgy, 2381-2390, The Minerals, Metals & Materials Series, DOI: 10.1007/978-3-319-95022-8.

iii. TEIXEIRA L.A.V., SILVA R.G., AVELAR A., MAJUSTE D., CIMINELLI V.S.T. (2019) Selective Extraction of Rare Earths Elements from Monazite Ores with High Iron Content, Mining Metallurgy & Exploration (2019) 36:235-244. DOI:10.1007/s42461-018-0035-5

iv. TEIXEIRA, L.A.V., SILVA, R.G., MAJUSTE, D., CIMINELLI, V.S.T. (2020), Stability of Lanthanum in Sulfate and Phosphate Systems and Implications for Selective Rare Earth Extraction, Minerals Engineering, 155, Elsevier, p.1-11. https://doi.org/10.1016/j.mineng.2020.106440.

v. TEIXEIRA, L.A.V., MAJUSTE, D., CIMINELLI, V.S.T. (2020), Atmosphere Effect on Selective Roasting of Rare Earth Sulfates (Manuscript in Preparation)

vi. TEIXEIRA L.A.V., HORIIKE T., YOSHIKAWA T., CIMINELLI, V.S.T. (2020), Cerium and Neodymium Phosphate Conversion into Sulfate and Chloride by High Temperature Exchanging Reaction (Manuscript in Preparation)

7.4 Contributions to Additional Publications

GONTIJO, V.L., TEIXEIRA, L.A.V., CIMINELLI, V.S.T (2020), Behavior of different types of oxy-hydroxide ores during sulfation. (Submitted to Hydrometallurgy, under review by the authors).

GONTIJO, V.L., TEIXEIRA, L.A.V., CIMINELLI, V.S.T (2020), Review of Thermodynamic Data for Rare Earth and its Impact on Mineral Process Development (Manuscript in Preparation)

7.5 Contributions for Future Investigations

(i) The investigation of selective sulfation before roasting should be explored.

(ii) Alternatives for controlling the P_2O_5 partial pressure to avoid REE sulfate reconversion to phosphate.

(iii) Refining the experimental conditions and measurements tools to better assess the effect of reducing atmosphere on reactions taking place during roasting.

(iv) Possibility of applying chlorination to avoid Ce leaching by the previous transformation to Ce(IV).

(v) Deepen the understanding of the phenomena behind the low performance of roasting to some lithologies.

8 CONSIDERAÇÕES FINAIS

8.1 Considerações Gerais

Os resultados deste trabalho indicaram que os minérios de monazita contendo terras raras podem ser tratados seletivamente para separar ferro e tório dos ETR se submetidos a sulfatação, ustulação a 700°C e lixiviação de água sob pH controlado. Esse processo promove alta extração de terras raras (entre 70-80%), baixa extração de ferro e tório (abaixo de 1%) com baixo consumo de ácido (entre 0,21 a 0,34 kg de ácido por 1 kg de minério), sendo adequado para aplicação em minérios altamente intemperizados. Minérios monazíticos deste tipo representam uma grande quantidade dos recursos disponíveis no mundo, em particular no Brasil.

Houve boa concordância entre a simulação termodinâmica e os resultados experimentais obtidos para a decomposição do sulfato de lantânio. Esses resultados também mostram que o sulfato de lantânio se decompõe em um processo de duas etapas, provavelmente formando $La_2O_2SO_4$ como um composto intermediário, o que não pode ser previsto pela avaliação termodinâmica. O estágio chave da extração seletiva é a ustulação, na qual o sulfato de ferro se decompõe em óxido de ferro e libera gás SO_x. A decomposição do sulfato de ferro é alcançada a 700 ° C, condição na qual terras raras atingem a extração máxima. A quantidade de compostos de terras raras insolúveis aumenta acentuadamente para temperaturas superiores a 750°C, reduzindo a quantidade de ETR recuperável durante a etapa de lixiviação e, portanto, tornando o processo de extração menos eficaz. Esta temperatura é mais baixa do que o esperado para a decomposição dos sulfatos de ETR em óxidos, estando, por sua vez, relacionada à formação de compostos de fosfato.

O excesso de fósforo remanescente no material sulfatado pode causar a reconversão de sulfatos de ETR em fosfatos, assim como a presença de ácido fosfórico levará à formação de compostos do tipo monazita. Altas pressões parciais de P_2O_5 converterão sulfatos de ETR em polifosfatos insolúveis - $ETR(PO_3)_3$. Essa condição pode ser alcançada pela decomposição do ácido fosfórico formado durante a sulfatação do minério ou por compostos de fósforo recém-formados, como o fosfato monocálcico. O mecanismo gás-sólido é preferido, pois a fase gasosa é capaz de promover um melhor contato com todas

as partículas de sulfato de ETR presentes no sistema, possibilitando a redução drástica (conversão em fósforo) observada a 800°C.

Tanto a simulação termodinâmica quanto os experimentos de laboratório em forno rotativo, mostraram que a atmosfera do forno durante a ustulação é fator muito importante tanto na definição da temperatura ótima de extração quanto na solubilização de impurezas, tais como ferro e tório, durante a lixiviação. Experimentos mostraram que quando aplicada uma atmosfera redutora (100% CO) a temperatura ótima de extração foi deslocada de 700°C para 400°C. Após 400°C houve grande redução na extração de ETR. A extração de ETR não foi afetada, e continuou na em torno de 80%. A extração de ferro caiu de 9% sob atmosfera de ar para 7% sob atmosfera redutora. A extração de tório caiu de 10% para 1% a 400°C com atmosfera redutora. A solubilização de ferro aumenta com o aumento de temperatura, chegando a valores superiores a 50%. Isso fenômeno se explica pela conversão de Fe^{3+} para Fe^{2+}, muito mais soluvel nas condições adotadas para lixiviação. Analises químicas indicaram que o percentual de Fe^{2+} no ferro lixiviado chegou a mais de 90%.

Análises termodinâmicas mostram que a reação de dupla troca de fosfato de Ce e Nd e sulfato de Al, Fe ou Mg pode ocorrer espontaneamente. No entanto, nenhuma reação foi detetada para aquecimento sob atmosfera inerte. A análise termodinâmica também mostrou que a cloração de fosfato de Ce e Nd pode ser possível pela reação de dupla troca com $MgCl_2$. Experimentos mostraram que a cloração de fosfatos de Nd e Ce é possível sob atmosfera oxidante. A reação de conversão ocorreu para um intervalo de temperatura entre 720-850°C para Nd e entre 600-850°C para Ce. Os principais produtos foram oxicloreto de neodímio (NdOCl) e CeO_2. A formação de Ce (IV) foi relacionada à forte atmosfera oxidante presente pela combinação de Cl_2 e O_2.

8.2 Contribuições Originais dessa Tese

As principais contribuições científicas do presente trabalho são:

(i) Combinação de avaliações termodinâmicas e experimentais para identificar a temperatura ideal para a ustulação seletiva de monazita present em minérios ricos em ferro contendo tório.

(ii) Os mecanismos diretos e indiretos de reconversão de sulfato de ETR em fosfatos – na forma de monazita e polifosfatos.

(iii) O efeito das condições de redução/oxidação no mecanismo de ustulação de sulfato de ETR.

(iv) Evidências experimentais para a formação de $La_2O_2SO_4$ como um composto intermediário da decomposição do sulfato de lantânio, sob condições de oxidação, mas não sob redução.

(v) Cloração de fosfatos de Nd e Ce sob atmosfera atmosférica produzindo oxicloreto de neodímio (NdOCl) e CeO_2.

Em acréscimo as contribuições científicas, o desenvolvimento de uma rota de processamento seletiva para a extração de ETR sobre ferro e tório é de fundamental importância para permitir o desenvolvimento de vários projetos minerais em todo o mundo. Monazita intemperizada representa uma parte significativa dos projetos não desenvolvidos. Esse tipo de depósito não permite o beneficiamento físico do minério, o que resulta em minério de baixo teor sendo alimentado na planta de extração. Este minério, devido ao intemperismo intenso, também é rico em óxido de ferro. Essa combinação de baixo teor e alta quantidade de ferro resulta em alto consumo de ácido, aumentando o gasto operacional (OPEX) da usina. Quando uma grande quantidade de ácido é usada, também haverá uma grande quantidade de impurezas no licor após a lixiviação, aumentando a complexidade dos processos de purificação, o que resultará em maior OPEX e menor recuperação metalúrgica.

As condições operacionais melhor identificada também possibilitarão a seleção adequada de equipamentos de engenharia, por exemplo o forno correto para operar em uma janela estreita de temperatura. Ao entender o fenômeno por trás do processo, novas adaptações podem ser feitas para evitar a formação precoce de fosfatos insolúveis, aumentando a janela de temperatura operacional da ustulação, o que poderia levar a uma seleção menos sofisticada de equipamentos, reduzindo o investimento e melhorando a extração metalúrgica. O teste de ustulação simplificado usando TGA permite uma análise

geometalúrgica rápida e mais barata para novos depósitos, permitindo que vários litotipos diferentes sejam testados e avaliados em um curto espaço de tempo e com uma quantidade mínima de amostra.

ANEXO A

APLICAÇÃO DE PIRÓLISE SELETIVA PARA MINÉRIOS FERRUGINOSOS CONTENDO TERRAS RARAS[3]

A.1 Introdução

Os processos de extração metalúrgica de elementos terras raras geralmente envolvem etapas de beneficiamento físico e hidrometalúrgico. A etapa de beneficiamento produz um concentrado físico. Esse concentrado precisa ser processado em uma usina hidrometalúrgica para gerar um concentrado químico. O concentrado químico é então alimentado em unidade de tratamento do licor (geralmente por extração por solventes - SX) para que sejam produzidos os elementos individuais de terras raras ou grupos específicos destes (Gupta and Krishnamurthy, 2005). Uma etapa de processamento pirometalúrgico pode ser inserida como preparação para a etapa hidrometalúrgica.

Minérios contendo monazita (fosfato de terras raras) possuem uma maior gama de opções de processamento, talvez devido à grande variação em composição e intemperismo, quando comparados a minérios contendo bastenasita (carbonato de terras raras). As opções de processamento podem ser divididas em dois grupos principais: sulfúrico e hidróxido.

O processo convencional com adição de ácido sulfúrico, consiste na adição de ácido ao minério (em proporções que podem variar largamente), seguindo por aquecimento em forno e dissolução em água (Lucas et al, 2015). O processo de purificação do licor depende de qual tipo de composto de ETR será precipitado (e.g. hidróxido, oxalato, cloreto, carbonato). A razão de massa ácido/minério é muito importante, uma vez que impacta diretamente na economicidade do projeto e na quantidade e tipo de impureza que será carregada para o processamento *downstream*, variando geralmente entre 1/1 e 1/2. Quanto maior a adição de ácido, maior será a dissolução de impurezas. O processo sulfúrico pode ser dividido em baixa temperatura (abaixo de 300°C) ou alta temperatura (acima de 300°C) (Zhang et al., 2016). O processo a baixa temperatura é mais antigo e gera uma solução complexa para ser processada.

[3] Publicação por Leandro, L.A.V. (2017) XXVII Encontro Nacional de Tratamento de Minérios e Metalurgia Extrativa, Belém, ENTMME 2017.

O processo de alta temperatura diminui a quantidade de tório extraída devido à formação de ThP_2O_7 insolúvel (Zhang et al., 2016).

O procedimento estudado neste trabalho segue os procedimentos sugeridos por Teixeira e Silva (2015) e Berni et al., (2013), onde um processo de sulfatação controlada e pirólise seletiva é aplicado. Esse método tem como objetivo reduzir a quantidade de ácido utilizada e diminuir a quantidade de impurezas no licor gerado após a lixiviação em água do produto da pirólise. As reações básicas envolvidas nas etapas de sulfatação do minério de terras raras e pirólise são mostradas nas equações de (A.1) a (A.4).

$$(ETR)PO_{4(s)} + 3H_2SO_{4(l)} \rightarrow 2H_3PO_{4(l)} + (ETR)_2(SO_4)_{3(s)} \quad \text{(A.1)}$$

$$Fe_2O_{3(s)} + 3H_2SO_{4(l)} \rightarrow Fe_2(SO_4)_{3(s)} + 3H_2O_{(l)} \quad \text{(A.2)}$$

$$(ETR)_2(SO_4)_{3(s)} \xrightarrow{\Delta} (ETR)_2O_{3_{(s)}} + 3SO_{3(g)} \quad \text{(A.3)}$$

$$Fe_2(SO_4)_{3(s)} \xrightarrow{\Delta} Fe_2O_{3(s)} + 3SO_{3_{(g)}} \quad \text{(A.4)}$$

Para que o processo funcione com o máximo de eficiência (i.e favorecendo a lixiviação seletiva dos ETR), é necessário que a etapa de pirólise opere em um intervalo restrito de temperatura, onde ocorra a decomposição do sulfato férrico (Eq. (A.4)) mas não ocorra a decomposição dos sulfatos de terras raras (Eq. (A.3)). Esse intervalo depende, entre outros fatores, do nível de deformação da estrutura cristalográfica e do nível de intemperismo do próprio minério, que pode variar. Esse trabalho apresenta um estudo que teve como objetivo correlacionar as diferentes formas obtidas nas análises de termogravimetria com o desempenho da amostra durante nas etapas de pirólise e lixiviação com água.

A.2 Material e Métodos

A.2.1 Reagentes

Foram usados os reagentes ácido sulfúrico (H_2SO_4) com concentração de 97,5% p/p e sulfato férrico P.A ($Fe_2(SO_4)_3.XH_2O$, Fe 22,0%min) fornecido pela Anidrol.

A.2.2 Análises Químicas

As concentrações de alumínio (Al), ferro (Fe), fósforo (P), enxofre (S), lantânio (La), praseodímio (Pr), neodímio (Nd) e samário (Sm) nas amostras líquidas foram determinadas por ICP-OES (Inductively Coupled Plasma – Optical Emission Spectrometry), instrumento da Varian modelo VISTA PRO. Os elementos terras raras restantes e as outras impurezas foram analisadas por ICP-MS (Inductively Coupled Plasma Mass Spectrometry), equipamento da PerkinElmer modelo NexION 300D. Antes das análises, as amostras líquidas foram diluídas em solução de ácido nítrico 2% p/p. A análise da concentração dos íons Fe+2 nos licores foi realizada por titulação com $K_2Cr_2O_7$. As amostras sólidas foram previamente secas em estufa a 100°C por 3 horas, resfriadas até 20°C e pulverizadas até 95% passantes em 74 µm.

A.2.3 Análises de Termo Gravimetria (TGA) e Análise Térmica Diferencial (DTA)

As análises de TG-DTA (Termogravimetria - Análise Térmica Diferencial) foram realizadas em equipamento NETZSCH STA 449F3, sob atmosfera sintética de ar, em cadinho de alumina com taxa de aquecimento de 10K/min até a temperatura limite de 1000°C. Foram utilizados aproximadamente 50 mg de amostra sulfatada do minério contendo terras raras.

A.2.4 Ensaios de extração das terras raras do minério

As etapas envolvidas na extração das terras raras foram (i) separação dos finos naturais (<74 µm) através da escrubagem do minério de terras raras por 15 min em uma polpa contendo 50% p/p de teor de sólidos suspensos e peneiramento a úmido da polpa em peneira com abertura de 74 µm (Testa et al., 2016), (ii) sulfatação ou mistura com ácido sulfúrico 97,5% p/p usando um misturador intensivo da EIRICH, (iii) pirólise em mufla em temperatura de 700°C por 2 horas, (iii) resfriamento da massa reacional até a temperatura de 20°C e (iv) lixiviação em água com teor de sólidos de 10% p/p por 2 horas com agitação mecânica (200 a 300 rpm). A extração das terras raras foi realizada conforme recomendações descritas por Teixeira e Silva (2015), Berni et al., (2013). Ensaios de lixiviação direta foram realizados seguindo o mesmo procedimento acima, entretanto sem passar pela etapa de pirólise em forno.

A.3 Resultados e discussão

A.3.1 Extração das Terras Raras

A composição inicial de uma amostra de minério contendo terras raras é mostrado na Table A.1 (na base óxido – OTR). Essa amostra foi sulfatada através da adição de ácido sulfúrico concentrado e, posteriormente, submetidas a pirólise seletiva. A Figure A.1 mostra o resultado da extração de terras raras, assim como a extração de ferro e tório. Observa-se elevada extração de OTR e reduzida extração de ferro e tório, ilustrando a seletividade do processo.

Table A.1 - Composição do minério de terras raras beneficiado (%)

OTR	CaO	MgO	Fe_2O_3	Al_2O_3	P_2O_5	SiO_2	Mn	ThO_2	U_3O_8	TiO_2
4,86	2,22	1,59	34,39	5,28	4,84	17,43	0,77	0,026	0,0059	16,48

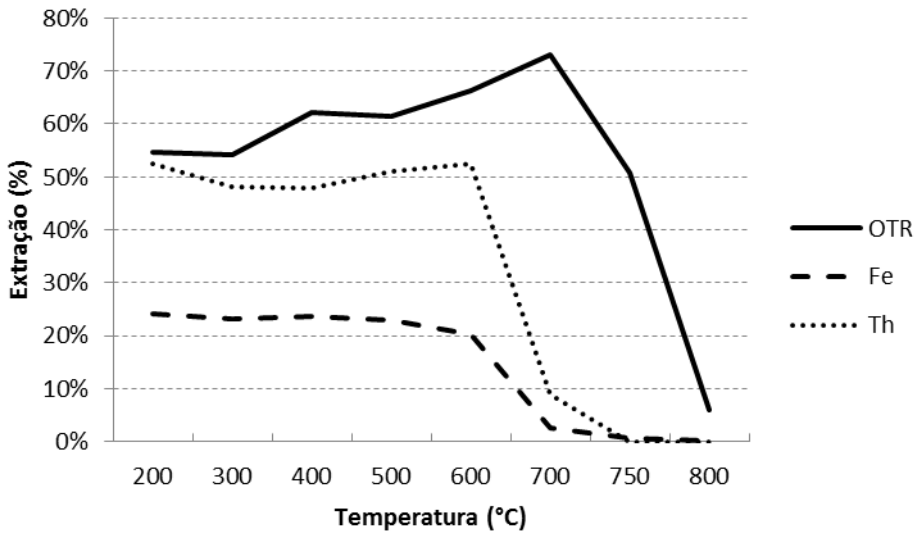

Figure A.1 - Efeito da temperatura na extração de terras raras, ferro e tório após etapa de sulfatação

Simulações termodinâmicas realizadas no software HSC9 (HSC Chemistry, 2015), mostrado na Figure A.2, onde o sulfato de neodímio representa os elementos de terras raras, mostram que é possível esperar uma seletividade na decomposição dos sulfatos. Entretanto, é importante observar que, pelos dados teóricos da simulação, a decomposição do sulfato férrico seria completa em temperaturas próximas de 800°C, enquanto para os sulfatos de terras raras essa temperatura seria próxima de 1000°C. Os resultados dos ensaios mostram que a decomposição do ferro já é quase completa a 700°C e

que as decomposições dos sulfatos de terras raras ocorrem a temperaturas próximas de 800°C, mostrando que, na prática, o intervalo de temperatura de seletividade é bem menor (700 a 800°C) do que o modelado (800 a 1000°C).

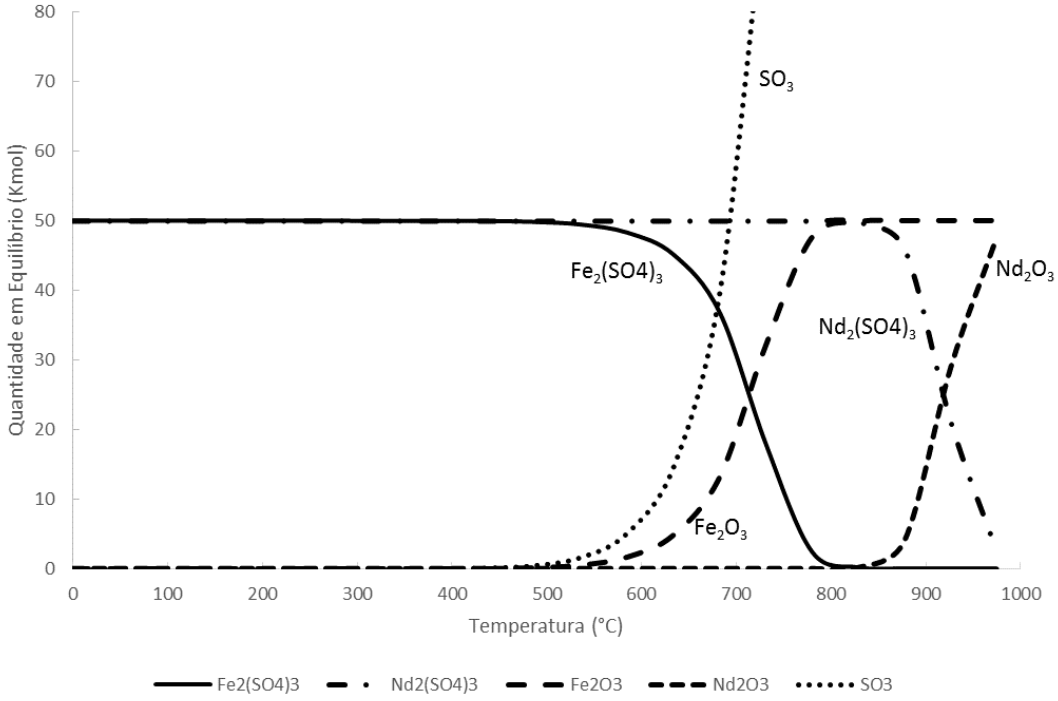

Figure A.2 - Decomposição dos sulfatos férrico e de neodímio a partir da simulação termodinâmica quando submetido a tratamento térmico

Essas temperaturas de decomposições dependem, entre outros fatores, do nível de deformação da estrutura cristalográfica e do nível de intemperismo do próprio minério. Estudos da variabilidade dessa temperatura de decomposição foram realizadas com o suporte de análises de TGA para tentar-se criar uma relação entre o gráfico obtido pela termogravimetria com o resultado a ser esperado quando a amostra fosse submetida a todo o processo de extração seletiva das terras raras envolvendo as etapas de sulfatação, pirólise e lixiviação com água.

O primeiro passo foi levantar qual seria a perda de massa esperada durante a decomposição da amostra a 700°C e saber, desse montante, quanto poderia ser atribuído ao sulfato férrico. Para tal, as amostras sulfatadas e não submetidas a pirólise, foram submetidas a lixiviação direta com água. Considerou-se que todo o sulfato férrico gerado na sulfatação foi lixiviado com água. Dessa forma, foi possível estimar a perda de massa teórica que aquela

amostra deveria perder se apenas o sulfato férrico fosse decomposto termicamente. Esses dados foram confrontados com os resultados do TGA para as amostras. Para realizar tal comparação, o resultado típico de TGA foi dividido em 5 zonas, definidas a seguir:

Z1 (até 200°C) – Umidade livre e/ou adsorvida

Z2 (200-320°C) – Desidratação dos minerais que sofreram intemperismo (por exemplo, goethita)

Z3 (320-600°C) – Outras perdas em geral, não identificadas e de baixa relevância.

Z4 (600-750°C) – Zona de interesse. Decomposição do sulfato férrico.

Z5 (750-900°C) – Outras decomposições (sulfatos de ETR, carbonatos e outros)

A Figure A.3 mostra as razões entre as perdas de massas de SO_3 calculadas a partir da análise da concentração de ferro no licor obtido por lixiviação direta do minério sulfatado e aquela perdida na zona 4 da etapa de pirólise. A perda de massa de SO_3 atribuível à decomposição do sulfato férrico é dada pela equação (A.5).

$$(\%) = \frac{Massa\ de\ SO_3\ calculada\ pela\ lixiviação\ direta\ do\ minério\ sulfatado}{Massa\ de\ SO_3\ perdida\ na\ zona\ 4\ e\ determinada\ por\ TGA}\ x\ 100 \qquad \text{(A.5)}$$

Observa-se, pela Figure A.3, que houve significativa variação nas razões de perda de massa de SO_3. A comparação desses dados com os dados de extração de terras raras é mostrada na Figure A.4. Alguns pontos extrapolam os 100% devido, principalmente, a seleção da curva de decomposição na análise do TGA. Nesses casos, a área adotada pode ter sido menor do que a área real que representa toda a decomposição do sulfato férrico.

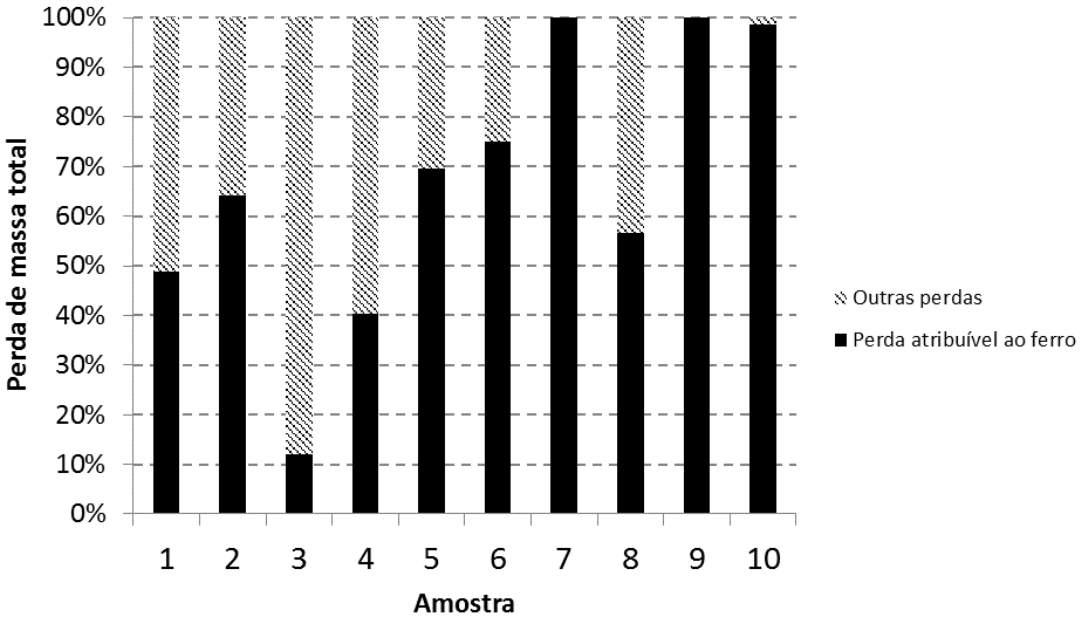

Figure A.3 - Perda de massa atribuível à decomposição do sulfato férrico no intervalo de temperatura de 600 a 700°C

Observa-se uma certa correção entre a perda de massa atribuível ao ferro e a extração de terras raras. Isso ocorre porque, quando a perda de massa é maior do que a atribuível ao ferro, provavelmente existe perda de massa por liberação de SO_3 proveniente dos sulfatos de terras raras. Esses sulfatos são convertidos em óxidos, que são insolúveis em água, resultando em menor extração de terras raras. Podemos dividir os resultados obtidos em 3 grupos:

GI – Amostras que apresentam perda de massa atribuível ao ferro entre 80 e 100%

GII – Amostras que apresentam perda de massa atribuível ao ferro entre 40 e 80%

GIII - Amostras que apresentam perda de massa atribuível ao ferro abaixo de 40%.

Tem-se como objetivo conseguir prever esses resultados a partir das análises de TGA do minério sulfatado. A Figure A.5 mostra resultados de TGA para amostras dos 3 grupos citados acima e do sulfato férrico P.A.

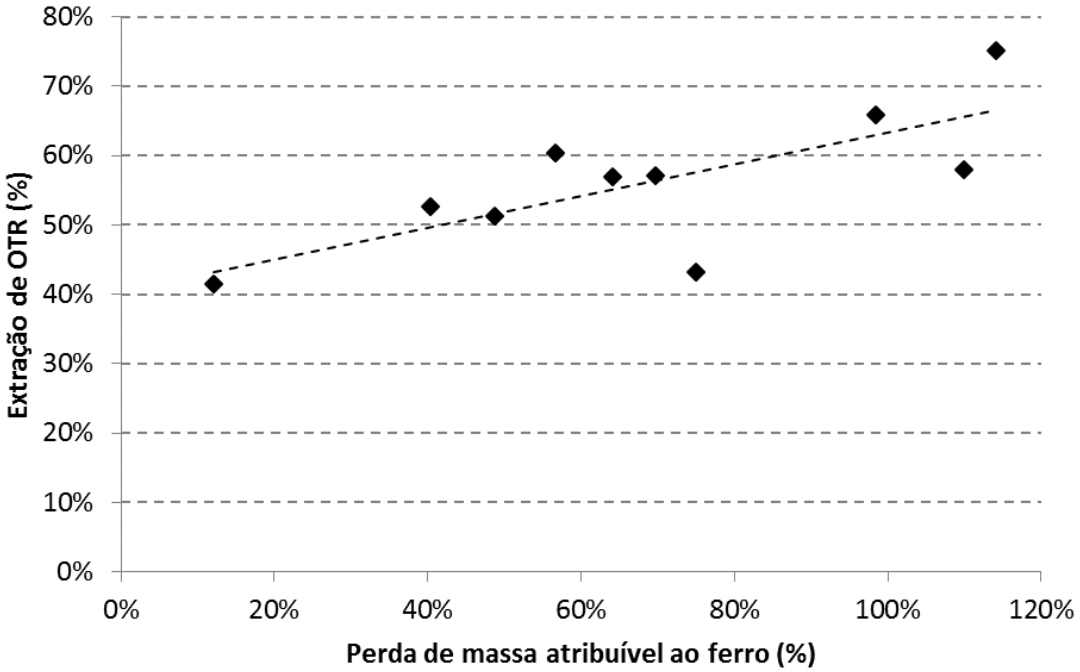

Figure A.4 - Relação entre a porcentagem de perda de massa obtida através da lixiviação direta e das análises de TGA atribuível à decomposição do sulfato férrico e os valores de extração dos OTR obtidos para essas amostras

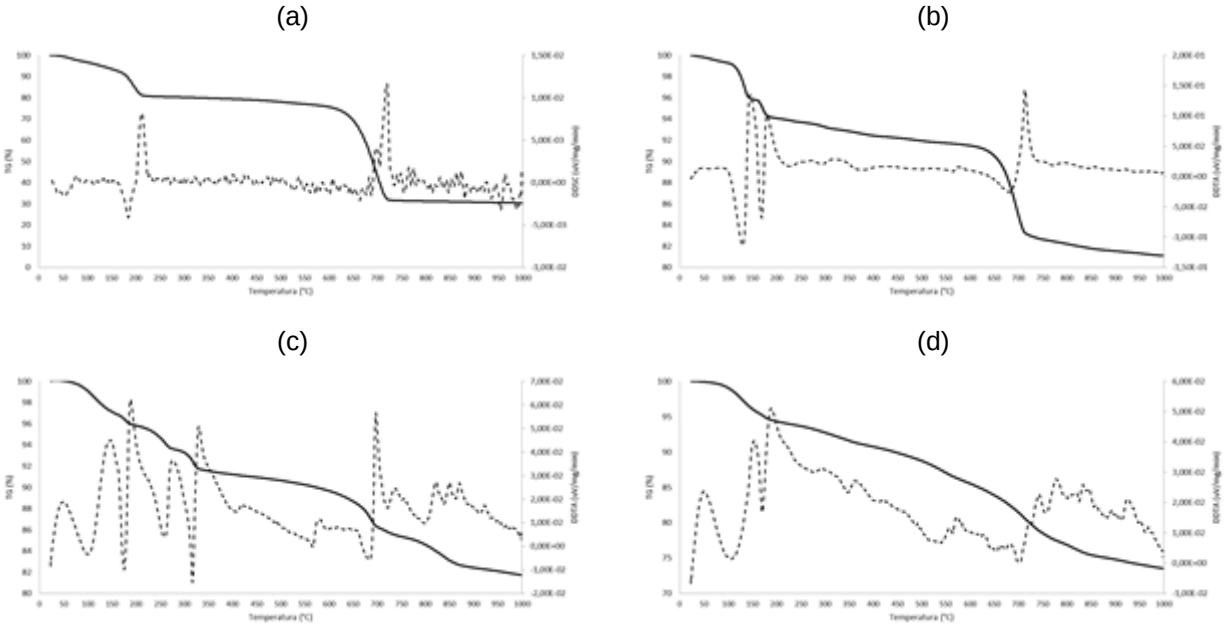

Figure A.5 - Resultado de TGA para sulfato férrico P.A e amostras de minério de terras raras sulfatadas de 3 grupos distintos: (a) Amostra de sulfato férrico P.A., (b) Amostra do Grupo I, (c) Amostra do Grupo II e (d) Amostra do Grupo III

Observa-se que as amostras do Grupo I apresentam zona de perda de massa bem definida, com pico de decomposição entre 700 e 750°C. As amostras do Grupo II apresentam outro evento próximo a 750°C, mas ainda existe um pico característico da decomposição do sulfato férrico. As amostras do Grupo III não apresentam mais o pico característico de decomposição do sulfato férrico. Existe uma série de eventos ocorrendo a partir de 700°C que não podem mais ser separados, ocorrendo, entre esses eventos, a decomposição dos sulfatos de terras raras. Essa decomposição é refletida como baixa extração nos ensaios de lixiviação.

A.4 Conclusão

A técnica de pirólise seletiva para sulfatos de terras raras foi aplicada com êxito para minérios ferruginosos contendo terras raras. O intervalo de temperatura de decomposição do sulfato férrico mostrou-se mais estreito do que o esperado frente aos resultados obtidos por simulações termodinâmicas para o sistema. Esse restrito intervalo irá afetar diretamente a extração das terras raras e a seletividade do processo. Variações estruturais presentes nos minérios, entre outros fatores, podem alterar esse intervalo de seletividade, mas é possível

antecipar o desempenho das amostras sulfatadas na etapa de pirólise através da interpretação dos resultados da análise termogravimétrica das mesmas.

A.5 Referências

Berni, T.V., Pereira, A. C., Mendes, F.D., Rude, A.L. (2013). System and Method for Rare Earth Extraction. Patent US 2013/0336856 A1.

Gupta, C. K. and Krishnamurthy, N. (2005) Extractive Metallurgy of Rare Earths, CRC Press, Nova York.

HSC Chemistry 9, (2015), Equilibrium Calculations, Outotec, Pori, Finland.

Lucas J., Lucas P., Le Mercier T., Rollat A. and Davenport, W. G.I, (2015) Rare Earth: Science, Technology, Production and Use, Elsevier.

Teixeira, L. A. V., Silva, R. G. (2015). System and Process For Selective Rare Earth Extraction With Sulphur Recovery. Patent US 2015/0329940 A1.

Testa, F. G., Avelar, A. N., Silva, R. G., Souza, C. C. (2016). Mineralogical Characterization and Alternative to Concentrate the Rare Earth Lithotypes From Alcaline Complex of Catalão – GO. Associação Brasileira de Metalurgia, Materiais e Mineração, São Paulo, http://dx.doi.org/10.4322/2176-1523.1064.

Zhang J., Zhao B. and Schereiner B., (2016), Separation Hydrometallurgy of Rare Earth Elements, Springer, Switzerland.